Asymptotic theory for Rayleigh and Rayleigh-type waves.

J.Kaplunov and D.A. Prikazchikov

School of Computing and Mathematics,

Keele University, Keele, ST5 5BG, UK

Abstract:

Explicit asymptotic formulations are derived for Rayleigh and Rayleigh-type interfacial and edge waves. The hyperbolic-elliptic duality of surface and interfacial waves is established, along with the parabolic-elliptic duality of the dispersive edge wave on a Kirchhoff plate. The effects of anisotropy, piezoelectricity, thin elastic coatings, and mixed boundary conditions are taken into consideration. The advantages of the developed approach are illustrated by steady-state and transient problems for a moving load on an elastic half-space.

Keywords:

surface wave, interfacial wave, edge wave, asymptotic, moving load, near-resonant.

1 Introduction

A time-harmonic surface wave on a linearly elastic isotropic half-space was discovered by Lord Rayleigh (1885). This pioneering piece of work was inspired by the needs of seismology, including earthquake prediction. Later on, similar Rayleigh-type waves were found for solid-solid and fluid-solid interfaces, see Stoneley (1924), Gogoladze (1948), Schölte (1949), as well as for the edge of a thin Kirchhoff plate, investigated by Konenkov (1960). We also mention a piezoelastic surface wave studied by Bleustein (1968) and Gulyaev (1969), important for various applications, see Campbell (1998) and references therein. Nowadays surface waves are

also widely used in the theory and practice of non-destructive evaluation, see e.g. Gudra & Stawiski (2000). Another recent application is associated with cloaking of surface waves and seismic metamaterials, see Brulé et al. (2014) and Colombi et al. (2016).

Current trends in this area include taking into consideration inhomogeneity, anisotropy, and pre-stress with one of the main focuses on the existence and uniqueness of localised time-harmonic eigensolutions, see references in the introductory sections 2 and 3, which also recall the standard derivations of well-known dispersion relations along with elementary proofs of existence and uniqueness. However, in spite of a substantial interest in the topic, the Rayleigh wave for a long time seemed to be somehow hidden within the classical elasticity model. In particular, the related Lamé wave potentials, e.g. see Achenbach (1973), govern the bulk waves but not the surface one. At the same time the Rayleigh wave contribution often dominates in the overall dynamic response, including the case of a resonant surface excitation. It also usually prevails over a far-field zone near the surface. These observations motivate the derivation of a specialised formulation oriented to the Rayleigh wave.

In section 4 we develop a multiscale perturbation procedure for an elastic half-space subject to prescribed surface stresses. The peculiarities of the procedure are clarified in Appendix A by a simple example of a single degree of freedom linear oscillator. In subsection 4.1 the 2D dynamic equations of the plane strain problem are perturbed around the eigensolution for a surface wave of arbitrary profile obtained in Chadwick (1976b), see also earlier papers of Friedlander (1948) and Sobolev (1937), as well as more recent publications, including Achenbach (1998); Kiselev (2004); Parker & Kiselev (2009); Kiselev & Parker (2010); Rousseau & Maugin (2011); Prikazchikov (2013); Parker (2013), and Kiselev (2015), treating homogeneous Rayleigh and Rayleigh-type waves in a more general setup. It appears that this eigensolution can be expressed in terms of a single harmonic function. As a result, we arrive at a hyperbolic-elliptic theory. This involves a wave equation for one of the Lamé potentials that governs propagation of surface disturbances along with pseudo-static elliptic equations for calculating the Lamé potentials over the interior. The derived model is extended to the general 3D case in subsection 4.2 using the integral Radon transform.

The proposed formulation reflects a duality of the Rayleigh wave. Indeed, hyperbolicity stands for propagation along the surface, whereas ellipticity may be associated with decay into

the interior. At the same time, it should be noted that hyperbolicity is characteristic only for one of the Lamé potentials along the surface, see Erbaş & Şahin (2016) for more detail.

A similar theory is also established in section 5 for several Rayleigh-type waves, including interfacial waves and the surface wave on a coated half-space. For the latter, the hyperbolic equation along the surface is singularly perturbed by a pseudo-differential operator. The effects of anisotropy and mixed boundary conditions are also addressed in this section, along with the extension to piezoelastic surface waves.

The validity of the proposed models is tested in section 6 by comparison with the exact solution of steady-state and transient plane strain moving load problems, given in Appendix B and Kaplunov et al. (2010), respectively. The near-resonant regimes of moving loads apparently present the optimal framework for evaluating the accuracy of the asymptotic approach. In this section we also obtain the explicit solutions of 3D moving load problems for a homogeneous and coated half-space in terms of elementary functions.

Finally, in section 7 we derive a parabolic-elliptic model for a dispersive bending wave propagating along the edge of a thin elastic plate. In this case the adapted asymptotic procedure also perturbs in slow time the eigensolution corresponding to an edge wave of general shape expressed through a single plane harmonic function. This eigenfunction is obtained starting from an implicit ansatz, for which the counterpart for the Rayleigh wave is the classical wave equation.

The material in this chapter originates from the publications Kaplunov & Kossovich (2004); Kaplunov et al. (2004, 2006); Dai et al. (2010); Kaplunov et al. (2010); Erbaş et al. (2013); Kaplunov & Prikazchikov (2013); Kaplunov et al. (2013); Prikazchikov (2013); Erbaş et al. (2014); Kaplunov et al. (2014); Ege et al. (2015); Kaplunov & Nobili (2015); Kaplunov et al. (2016). We express our sincere gratitude to all the co-authors in the publications mentioned above, and also acknowledge fruitful discussions with P. Chadwick, Y. Fu, A.P. Kiselev, D.F. Parker, and A. Pichugin. We also thank P. Wootton for reading the final version of the manuscript and making several valuable comments.

2 Time-harmonic Rayleigh wave on an elastic half-space

In this section we present some basic results for surface waves, including the derivation of the classical Rayleigh equation as well as analysis of a surface wave of arbitrary profile, preceding the development of the explicit hyperbolic-elliptic formulation for the Rayleigh wave field.

2.1 Elementary derivation

Let us first derive the original surface wave equation discovered by Lord Rayleigh (1885). Consider a linearly elastic isotropic half-space

$$\mathcal{H}_3^+ = \left\{(x_1; x_2; x_3) \,\middle|\, -\infty < x_1 < \infty, \quad -\infty < x_2 < \infty, \quad 0 \le x_3 < \infty\right\}.$$

The equations of motion in linear elastodynamics are given by

$$\sigma_{ij,j} = \rho u_{i,tt}, \qquad i, j = 1, 2, 3, \tag{2.1}$$

e.g. see Achenbach (1973). Here σ_{ij} and u_i are the components of the Cauchy stress tensor $\boldsymbol{\sigma}$ and the displacement vector $\mathbf{u}$, respectively, ρ denotes mass volume density, and comma indicates differentiation with respect to spatial or time variables. Einstein's summation convention is adopted throughout this chapter, unless otherwise stated. The stress-strain relations for an isotropic solid are given by

$$\sigma_{ij} = \lambda u_{k,k}\delta_{ij} + 2\mu\varepsilon_{ij}, \qquad i, j = 1, 2, 3, \tag{2.2}$$

with λ and μ being the Lamé elastic moduli, δ_{ij} standing for the Kronecker delta, and the kinematic relations for the components of the strain tensor $\boldsymbol{\varepsilon}$ being expressed as

$$\varepsilon_{ij} = \frac{1}{2}\left(u_{i,j} + u_{j,i}\right). \tag{2.3}$$

On substituting the constitutive relations (2.2) into the equations of motion (2.1) and taking into consideration the relations (2.3), we have the wave equation

$$(\lambda + \mu)\, u_{j,ji} + \mu\, u_{i,jj} = \rho u_{i,tt}. \tag{2.4}$$

Let us now decompose the displacement field according to the Helmholtz theorem as

$$\mathbf{u} = \operatorname{grad}\phi + \operatorname{curl}\boldsymbol{\Psi}, \tag{2.5}$$

where ϕ and $\mathbf{\Psi} = (\psi_1, \psi_2, \psi_3)$ are scalar longitudinal and vector transverse elastic potentials, respectively, allowing separation of extensional and shear motions for an isotropic solid. In addition, the constraint

$$\operatorname{div} \mathbf{\Psi} = 0, \tag{2.6}$$

is required. This condition is not unique, e.g. see Miklowitz (1978). On substituting the Helmholtz decomposition (2.5) into (2.4), we have

$$\phi_{,tt} - c_1^2 \Delta \phi = 0, \qquad \mathbf{\Psi}_{,tt} - c_2^2 \Delta \mathbf{\Psi} = 0, \tag{2.7}$$

where Δ is the 3D Laplace operator in x_1, x_2 and x_3, and

$$c_1 = \sqrt{\frac{\lambda + 2\mu}{\rho}}, \qquad c_2 = \sqrt{\frac{\mu}{\rho}} \tag{2.8}$$

are the longitudinal and transverse wave speeds, respectively.

The stress-free boundary conditions are imposed on the surface $x_3 = 0$, i.e.

$$\sigma_{3i} = 0, \quad i = 1, 2, 3, \tag{2.9}$$

or, in terms of the elastic potentials,

$$\begin{aligned} 2\phi_{,13} - \psi_{1,12} + \psi_{2,11} - \psi_{2,33} + \psi_{3,23} &= 0, \\ 2\phi_{,23} - \psi_{1,22} + \psi_{1,33} + \psi_{2,12} - \psi_{3,13} &= 0, \\ \lambda\left(\phi_{,11} + \phi_{,22}\right) + \left(\lambda + 2\mu\right)\phi_{,33} + 2\mu\left(\psi_{2,13} - \psi_{1,23}\right) &= 0. \end{aligned} \tag{2.10}$$

The solutions of (2.7) and (2.10) are now sought in the form of the travelling harmonic wave

$$(\phi, \psi_1, \psi_2, \psi_3) = (A_1, A_2, A_3, A_4)\, e^{ik(x_1 \cos\theta + x_2 \sin\theta - ct) - kqx_3}, \tag{2.11}$$

where A_i, $i = \overline{1,4}$, are arbitrary constants, k is the wave number, q is the attenuation factor to be determined and c is the sought-for phase speed; the condition $\Re(q) > 0$ is assumed, ensuring decay of the surface wave field as $x_3 \to \infty$. On substituting (2.11) into the equations of motion (2.7), we obtain

$$\phi = A_1\, e^{ik(x_1 \cos\theta + x_2 \sin\theta - ct) - k\alpha x_3}, \tag{2.12}$$

and

$$(\psi_1, \psi_2, \psi_3) = (A_2, A_3, A_4)\, e^{ik(x_1 \cos\theta + x_2 \sin\theta - ct) - k\beta x_3}, \tag{2.13}$$

with the attenuation orders

$$\alpha = \sqrt{1 - \frac{c^2}{c_1^2}}, \qquad \beta = \sqrt{1 - \frac{c^2}{c_2^2}}. \tag{2.14}$$

Then, on inserting (2.12) and (2.13) into the boundary conditions (2.10) and using the constraint (2.6), we obtain a set of linear algebraic equations in respect of the constants A_i, namely

$$\begin{aligned} -2i\alpha \cos\theta A_1 + \sin\theta\cos\theta A_2 - (\cos^2\theta + \beta^2)A_3 - i\beta \sin\theta A_4 = 0, \\ -2i\alpha \sin\theta A_1 + (\sin^2\theta + \beta^2)A_2 - \sin\theta\cos\theta A_3 + i\beta \cos\theta A_4 = 0, \\ (1+\beta^2)A_1 + 2i\beta \sin\theta A_2 - 2i\beta \cos\theta A_3 = 0, \\ i\cos\theta A_2 + i\sin\theta A_3 + \beta A_4 = 0. \end{aligned} \tag{2.15}$$

The determinant of (2.15) equals zero provided that

$$(1+\beta^2)^2 - 4\alpha\beta = 0. \tag{2.16}$$

The latter is the well-known Rayleigh equation. It is often presented as

$$R(r) = 0, \tag{2.17}$$

where

$$R(r) = (2-r)^2 - 4\sqrt{1-r}\sqrt{1-\kappa^2 r}, \tag{2.18}$$

with

$$r = \frac{c^2}{c_2^2}, \qquad \kappa = \frac{c_2}{c_1} < 1. \tag{2.19}$$

The first proof of the existence and uniqueness of the solution of (2.17) was seemingly presented by Sobolev (1937), see also Babich & Kiselev (2014). A similar proof is given below, showing that the Rayleigh equation (2.17) has a unique solution for the phase speed $c = c_R$ over the interval $0 < r < 1$. First, note that

$$R(0) = 0, \qquad R(1) = 1, \tag{2.20}$$

while the derivative

$$R'(0) = 2(\kappa^2 - 1) < 0. \tag{2.21}$$

In addition, the second derivative

$$R''(r) = 2 + \frac{(1-\kappa^2)^2}{[(1-r)(1-\kappa^2 r)]^{3/2}} \tag{2.22}$$

is positive for $0 < r < 1$, so the function $R(r)$ is concave upwards over the interval. Thus, the conditions (2.20) and (2.21) imply the existence of a zero of $R(r)$ in the interval $0 < r < 1$, with (2.22) ensuring uniqueness of solution. A typical behaviour of $R(r)$ is shown in Fig.1 for $\kappa = \frac{1}{3}$ $\left(\nu = \frac{1}{4}\right)$.

It is obvious that the solution of (2.17) for a given Poisson ratio ν is a constant, i.e. the Rayleigh wave is non-dispersive. A variation of the scaled Rayleigh wave speed c_R/c_2 versus the Poisson ratio is shown in Fig. 2.

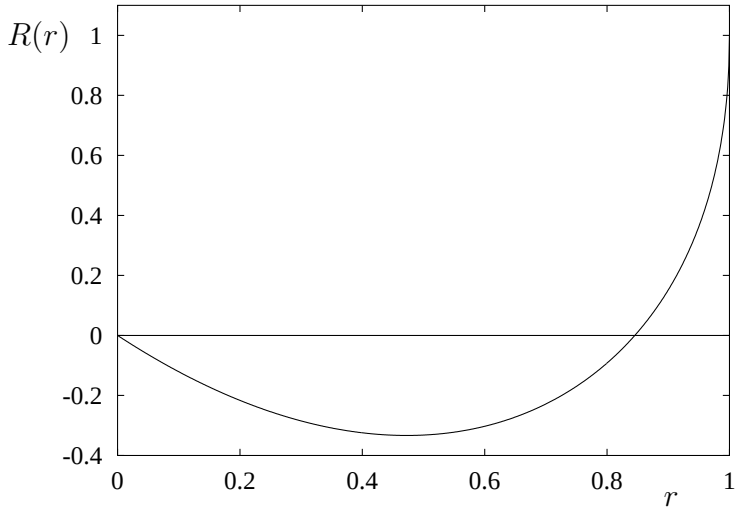

Figure 1: Variation of $R(r)$ along the interval $0 < r < 1$ for $\nu = \frac{1}{4}$.

It is also well-known from the original paper of Lord Rayleigh (1885) that (2.17) may be transformed to the cubic equation

$$r^3 - 8(r-1)\left(r - 2(1-\kappa^2)\right) = 0. \tag{2.23}$$

The solution of this equation may be obtained through Cardano's formula, see e.g. Malischewsky (2000) and Vinh & Ogden (2004). It should be noted that existence and uniqueness of the Rayleigh wave have been also proved for anisotropic materials, e.g. see Barnett & Lothe (1974) and Kamotskii & Kiselev (2009). Obviously, the evaluation of the surface wave speed becomes more difficult in anisotropic medium. In this case the so-called surface-impedance

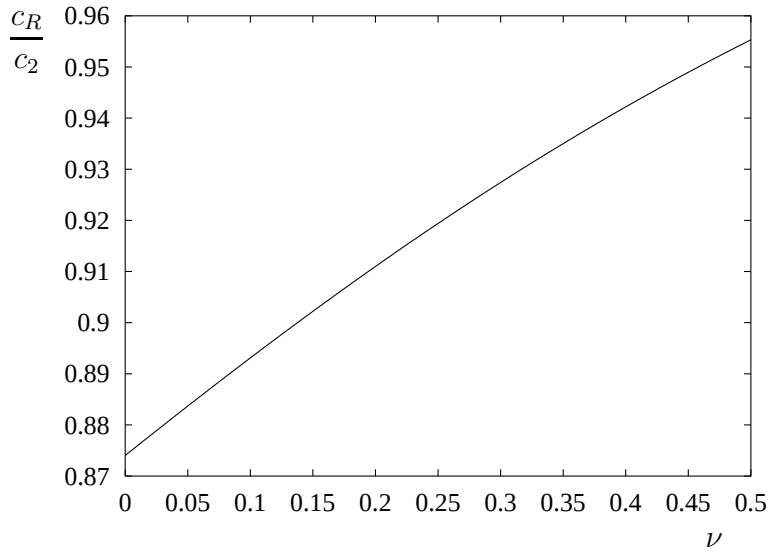

Figure 2: The Rayleigh wave speed vs. the Poisson ratio ν.

matrix technique, leading to a matrix Ricatti equation, see Fu & Mielke (2002), proved to be robust. We also mention contributions studying surface waves in media with more sophisticated properties, see e.g. Hayes & Rivlin (1961); Alenitsyn (1963); Agarwal (1978); Ivanov (1988); Dowaikh & Ogden (1990); Rogerson (1998); Destrade (2004, 2007); Steigmann & Ogden (2007); Kiselev & Rogerson (2009); Dockrey et al. (2013); Vinh et al. (2014), and many others.

2.2 Rayleigh wave of arbitrary profile

In the previous section the solution was sought in the form of a travelling time-harmonic plane wave. Below we generalise it to a wave of general time-dependence, relying on the key contribution of Chadwick (1976b), see also the earlier works of Friedlander (1948) and Sobolev (1937). Following these papers, we consider a plane strain problem, assuming

$$u_2 = 0, \qquad u_i = u_i(x_1, x_3, t), \quad i = 1, 3, \tag{2.24}$$

for the half-plane

$$\mathcal{H}_2^+ = \left\{ (x_1; x_3) \,\middle|\, -\infty < x_1 < \infty, \quad 0 \le x_3 < \infty \right\}. \tag{2.25}$$

In this case the displacement field is conventionally expressed through the 2D elastic potentials ϕ and ψ as

$$u_1 = \frac{\partial \phi}{\partial x_1} - \frac{\partial \psi}{\partial x_3}, \qquad u_3 = \frac{\partial \phi}{\partial x_3} + \frac{\partial \psi}{\partial x_1}, \tag{2.26}$$

satisfying the wave equations

$$\phi_{,tt} - c_1^2\,(\phi_{,11} + \phi_{,33}) = 0, \qquad\qquad \psi_{,tt} - c_2^2\,(\psi_{,11} + \psi_{,33}) = 0. \tag{2.27}$$

together with the boundary conditions

$$\begin{aligned} 2\phi_{,13} + \psi_{,11} - \psi_{,33} &= 0, \\ (\kappa^{-2} - 2)\,\phi_{,11} + \kappa^{-2}\phi_{,33} + 2\psi_{,13} &= 0, \end{aligned} \tag{2.28}$$

along the stress-free surface $x_3 = 0$, where, as before,

$$\kappa = \frac{c_2}{c_1} = \sqrt{\frac{1-2\nu}{2-2\nu}}.$$

Let us study the elastic potentials of the form

$$\phi = \phi(x_1 - ct, x_3), \qquad \psi = \psi(x_1 - ct, x_3), \tag{2.29}$$

corresponding to a wave of arbitrary shape propagating at a speed c. Using (2.29), the equations of motion (2.27) are reduced to the elliptic equations

$$\phi_{,33} + \alpha^2\phi_{,11} = 0, \qquad\qquad \psi_{,33} + \beta^2\psi_{,11} = 0, \tag{2.30}$$

where α and β are defined by (2.14). Thus, the eigensolutions for the elastic potentials are

$$\phi = \phi(x_1 - ct, \alpha x_3), \qquad \psi = \psi(x_1 - ct, \beta x_3), \tag{2.31}$$

being plane harmonic functions. In the subsequent analysis we employ the Cauchy-Riemann identities

$$f_{,3} = -\gamma f^*_{,1}, \qquad f_{,1} = \frac{1}{\gamma} f^*_{,3}, \qquad f^{**} = -f, \tag{2.32}$$

for a harmonic function $f(x_1, \gamma x_3)$, being a solution of the equation

$$f_{,33} + \gamma^2 f_{,11} = 0, \qquad \gamma = (\alpha, \beta),$$

where the asterisk denotes a harmonic conjugate function, see e.g. Titchmarch (1939).

After straightforward manipulations involving the aforementioned Cauchy-Riemann identities (2.32), the boundary conditions (2.28) at $x_3 = 0$ may be rearranged as

$$\begin{aligned} -2\alpha\,\phi^*_{,11} + (1+\beta^2)\,\psi_{,11} &= 0, \\ (1+\beta^2)\,\phi_{,11} + 2\beta\,\psi^*_{,11} &= 0, \end{aligned} \tag{2.33}$$

Then, on taking conjugate of the first equation, we deduce from the solvability of (2.33) that

$$(1+\beta^2)^2 - 4\alpha\beta = 0, \tag{2.34}$$

which is the Rayleigh equation, see (2.16). Therefore $c = c_R$, hence, the sought for harmonic eigenfunctions are

$$\phi = \phi(x_1 - ct, \alpha_R x_3), \qquad \psi = \psi(x_1 - ct, \beta_R x_3), \tag{2.35}$$

where

$$\alpha_R = \sqrt{1 - \frac{c_R^2}{c_1^2}}, \qquad \beta_R = \sqrt{1 - \frac{c_R^2}{c_2^2}}. \tag{2.36}$$

In addition, we obtain the relations between the potentials along the surface $x_3 = 0$, following from (2.28), namely

$$\psi_{,1} = -\frac{2}{1+\beta_R^2}\phi_{,3}, \qquad \psi_{,3} = \frac{1+\beta_R^2}{2}\phi_{,1}. \tag{2.37}$$

Moreover, the maximum principle for harmonic functions implies a condition relating the potentials ϕ and ψ not only along the surface $x_3 = 0$, but over the entire half-plane. Thus,

$$\psi(x_1 - c_R t, \beta_R x_3) = \frac{2\alpha_R}{1+\beta_R^2}\,\phi^*(x_1 - c_R t, \beta_R x_3), \tag{2.38}$$

and

$$\phi(x_1 - c_R t, \alpha_R x_3) = -\frac{2\beta_R}{1+\beta_R^2}\,\psi^*(x_1 - c_R t, \alpha_R x_3), \tag{2.39}$$

for more details see Chadwick (1976b). This allows expressing the displacements in terms of a single plane harmonic function, say in terms of the potential ϕ, as

$$\begin{aligned} u_1(x_1, x_3, t) &= \phi_{,1}(x_1 - c_R t, \alpha_R x_3) - \frac{1+\beta_R^2}{2}\,\phi_{,1}(x_1 - c_R t, \beta_R x_3), \\ u_3(x_1, x_3, t) &= \phi_{,3}(x_1 - c_R t, \alpha_R x_3) - \frac{2}{1+\beta_R^2}\,\phi_{,3}(x_1 - c_R t, \beta_R x_3). \end{aligned} \tag{2.40}$$

The obtained representation (2.40) extends the class of decaying eigensolutions, in particular, allowing a non-periodic behaviour along the surface. In fact, the potentials ϕ and ψ generally may not decay at infinity. As an example, we take

$$\phi(s_R, x_3) = \tan^{-1}\frac{s_R}{\alpha_R x_3 + a}, \qquad \psi(s_R, x_3) = \frac{\alpha_R}{1+\beta_R^2}\,\ln\left[s_R^2 + (\beta_R x_3 + a)^2\right], \tag{2.41}$$

where $a > 0$ is a parameter chosen in order to smooth discontinuities at the origin and $s_R = x_1 - c_R t$ is a moving coordinate. The potentials (2.41) correspond to the following decaying displacement components

$$\begin{aligned} u_1(x_1, x_3, t) &= \frac{\alpha_R x_3 + a}{s_R^2 + (\alpha_R x_3 + a)^2} - \frac{1 + \beta_R^2}{2} \frac{\beta_R x_3 + a}{s_R^2 + (\beta_R x_3 + a)^2}, \\ u_3(x_1, x_3, t) &= -\frac{\alpha_R s_R}{s_R^2 + (\alpha_R x_3 + a)^2} + \frac{2}{1 + \beta_R^2} \frac{\beta_R s_R}{s_R^2 + (\beta_R x_3 + a)^2}. \end{aligned} \tag{2.42}$$

Variation of the displacements (2.42) on s_R at several depths is shown in Fig. 3 for $a = 0.1$ and the Poisson's ratio $\nu = \frac{1}{3}$. An example of non-decaying displacements is studied in subsection 6.1.

It is clear that similar derivation may be performed for a surface wave travelling in the opposite direction, when the argument $x_1 - ct$ in (2.11) is replaced by $x_1 + ct$. Moreover, it is also possible to take into account simultaneously surface waves propagating along both directions. To this end, we should assume an *implicit travelling wave ansatz* given by

$$\phi_{,tt} - c^2 \phi_{,11} = 0, \qquad \psi_{,tt} - c^2 \psi_{,11} = 0, \tag{2.43}$$

where $\phi = \phi(x_1, x_3, t)$ and $\psi = \psi(x_1, x_3, t)$. It is easily verified that on employing the last assumptions, the wave equations (2.27) become the elliptic equations (2.30), with all the following derivations above being perfectly valid and leading to the eigensolution of arbitrary profile (2.40).

To conclude this subsection, we note that the obtained representation of the Rayleigh wave field in terms of a single harmonic function may be generalised to the 3D case. More details on the subject may be found in the recent contribution by Kiselev & Parker (2010). The same results also follow from a more general analysis in Dai et al. (2010).

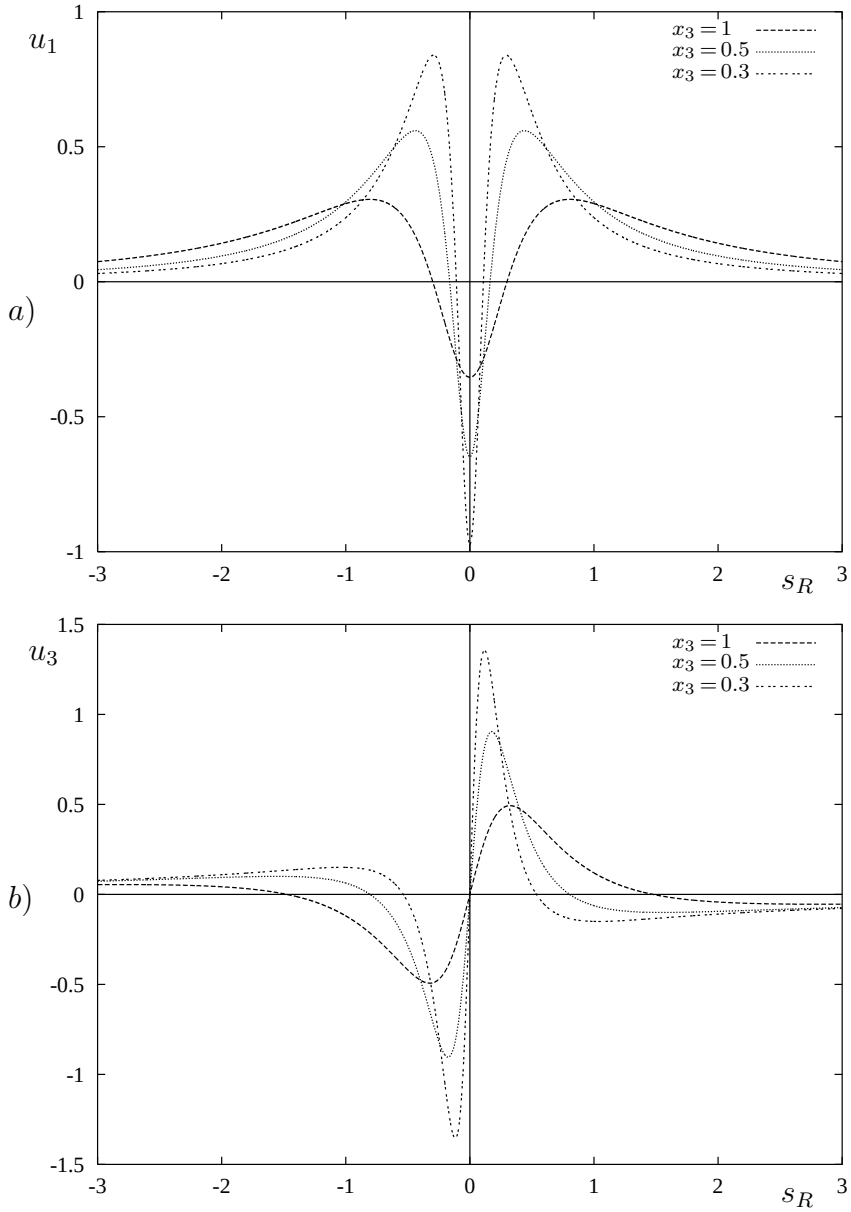

Figure 3: The profiles of a) horizontal and b) vertical displacements (2.42) vs. the moving coordinate s_R.

3 Rayleigh-type interfacial and edge elastic waves

In this section we discuss several extensions of the Rayleigh elastic wave, including the waves localised at solid-fluid and solid-solid interfaces. In addition, we derive the dispersion relation for the bending wave propagating along the edge of a semi-infinite thin elastic plate. All of these waves were originally referred to as Rayleigh-type waves, see Stoneley (1924), Schölte (1949), Gogoladze (1948), and Konenkov (1960).

3.1 Schölte-Gogoladze wave

Let us consider the half-plane $\mathcal{H}_2^+$ composed of a linearly elastic isotropic material, see (2.25), contacting with the half-plane

$$\mathcal{H}_2^- = \left\{(x_1; x_3) \,\middle|\, -\infty < x_1 < \infty, \quad -\infty < x_3 \leq 0\right\},$$

occupied by an ideal fluid. We concentrate on the wave propagating along the interface $x_3 = 0$ and decaying away from it. This wave was discovered independently by Schölte (1949) and Gogoladze (1948) and is usually named after these authors.

The equations of motion for the elastic medium are given by (2.27), whereas the fluid motion is governed by the wave equation

$$\chi_{,tt} - c_f^2 \left(\chi_{,11} + \chi_{,33}\right) = 0, \tag{3.1}$$

where χ is the displacement potential and c_f is the sound wave speed. The interfacial conditions at $x_3 = 0$ are written as

$$\sigma_{31} = 0, \qquad u_3 = v, \qquad \sigma_{33} = p_f, \tag{3.2}$$

where v and p_f are the vertical displacement and pressure in the fluid, respectively, given by

$$v = \chi_{,3}, \qquad p_f = \rho_f \, \chi_{,tt},$$

with ρ_f denoting the fluid volume density.

The conditions (3.2) may be presented as

$$\begin{aligned} 2\phi_{,13} - \psi_{,11} + \psi_{,33} &= 0, \\ \phi_{,3} + \psi_{,1} - \chi_{,3} &= 0, \\ \mu\left[\left(\kappa^{-2} - 2\right)\phi_{,11} + \kappa^{-2}\phi_{,33} - 2\psi_{,13}\right] - \rho_f \chi_{,tt} &= 0. \end{aligned} \tag{3.3}$$

The solution for the potentials are found from the wave equations (2.27) and (3.1) in the form of a travelling harmonic wave ensuring decay away from the interface into the interior, namely

$$(\phi, \psi, \chi) = \left(A_1\, e^{-k\alpha x_3}, A_2\, e^{-k\beta x_3}, A_3\, e^{k\gamma x_3}\right) e^{ik(x_1 - ct)}, \tag{3.4}$$

where, as before, k is the wave number, c is the sought for phase speed, the attenuation orders α and β are defined by (2.14), and

$$\gamma = \sqrt{1 - \frac{c^2}{c_f^2}}. \tag{3.5}$$

Substitution of (3.4) into (3.3) results in a set of linear algebraic equations in respect of the constants A_1, A_2, and A_3. The solvability of the latter implies the related determinant being zero, giving

$$\left(1 + \beta_{SG}^2\right)^2 - 4\alpha_{SG}\beta_{SG} + \frac{\rho_f}{\rho}\,\frac{\alpha_{SG}}{\gamma_{SG}}\left(1 - \beta_{SG}^2\right)^2 = 0, \tag{3.6}$$

where

$$\alpha_{SG} = \sqrt{1 - \frac{c_{SG}^2}{c_1^2}}, \qquad \beta_{SG} = \sqrt{1 - \frac{c_{SG}^2}{c_2^2}}, \qquad \gamma_{SG} = \sqrt{1 - \frac{c_{SG}^2}{c_f^2}}, \tag{3.7}$$

with c_{SG} denoting the Schölte-Gogoladze wave speed. It is may be shown that the sought for solution always exists in the interval $0 < c_{SG} < c_f$ provided that $c_f < c_2 < c_1$, see e.g. Gogoladze (1948), and also Viktorov (1981), tackling a more general setup. Indeed, let us denote the left hand side of (3.6) by

$$SG(r) = (2 - r)^2 - 4\sqrt{1 - r}\sqrt{1 - \kappa^2 r} + \frac{\rho_f}{\rho}\,\frac{\sqrt{1 - \kappa^2 r}}{\sqrt{1 - \kappa_f^2 r}}\, r^2 \tag{3.8}$$

where

$$\kappa_f = c_2/c_f > 1, \tag{3.9}$$

with r and κ defined by (2.19). It is then clear that

$$SG(0) = 0, \qquad \lim_{r \to \kappa_f^{-2} - 0} SG(r) = +\infty, \qquad SG'(0) = 2(\kappa^2 - 1) < 0, \tag{3.10}$$

guaranteeing existence of the solution over the interval $0 < r < \kappa_f^{-2}$. It is also known that leaky interfacial waves are possible, see e.g. Zhu et al. (2004) and references therein.

Similarly to the surface wave of arbitrary profile considered in subsection 2.2, the eigensolution for the Schölte-Gogoladze wave of general time dependence may be derived, as shown by Kiselev & Parker (2010) and Parker (2012).

3.2 Stoneley wave

Let us now consider the wave propagating along the interface of two elastic half-planes $\mathcal{H}_2^-$ and $\mathcal{H}_2^+$. This wave was first discovered by Stoneley (1924). Unlike the Rayleigh wave, it only exists for a restricted range of material parameters. The existence conditions for two bonded isotropic half-spaces have been obtained by Schölte (1947). It is also known from Barnett et al. (1985), that the Stoneley wave speed exceeds the smaller of the Rayleigh wave speeds for the two half-spaces. The cited contribution of Barnett et al. (1985) also contains rigorous results on existence of the Stoneley wave on the interface of two anisotropic half-spaces. Similarly to the Rayleigh wave, the surface-impedance matrix method may be used for robust computations of the Stoneley wave speed, see Destrade & Fu (2006). We also mention contributions dealing with Stoneley waves in media with more sophisticated properties, see e.g. Dowaikh & Ogden (1991); Goda (1992); Vinh & Seriani (2010).

For the sake of simplicity, we once again restrict ourselves to the framework of the plane strain assumption. The equations of motion are written in terms of the elastic wave potentials as

$$\phi_{n,tt} - c_{1n}^2\left(\phi_{n,11} + \phi_{n,33}\right) = 0, \qquad \psi_{n,tt} - c_{2n}^2\left(\psi_{n,11} + \psi_{n,33}\right) = 0, \tag{3.11}$$

where the suffix $n = 1, 2$ corresponds to the elastic media occupying $\mathcal{H}_2^+$ and $\mathcal{H}_2^-$, respectively, and c_{1n} and c_{2n} denote the longitudinal and transverse wave speeds in these media. The interfacial conditions at $x_3 = 0$ for perfectly bonded half-spaces are given by

$$\begin{aligned}
\phi_{1,1} - \phi_{2,1} + \psi_{1,3} - \psi_{2,3} &= 0,\\
\phi_{1,3} - \phi_{2,3} - \psi_{1,1} + \psi_{2,1} &= 0\\
2\mu_1\phi_{1,13} - 2\mu_2\phi_{2,13} + \mu_1\left(\psi_{1,33} - \psi_{1,11}\right) - \mu_2\left(\psi_{2,33} - \psi_{2,11}\right) &= 0,\\
\lambda_1\phi_{1,11} + \left(\lambda_1 + 2\mu_1\right)\phi_{1,33} - \lambda_2\phi_{2,11} - \left(\lambda_2 + 2\mu_2\right)\phi_{2,33} - 2\mu_1\psi_{1,13} + 2\mu_2\psi_{2,13} &= 0,
\end{aligned} \tag{3.12}$$

where λ_n and μ_n, $n = 1, 2$, are the Lamé elastic moduli.

As usual, the potentials are found from (3.11) in the form of a travelling harmonic wave decaying away from the interface, namely

$$\left(\phi_1, \psi_1, \phi_2, \psi_2\right) = \left(A_1\, e^{-k\alpha_1 x_3}, A_2\, e^{-k\beta_1 x_3}, A_3\, e^{k\alpha_2 x_3}, A_4\, e^{k\beta_2 x_3}\right) e^{ik(x_1 - ct)}, \tag{3.13}$$

where

$$\alpha_n = \sqrt{1 - \frac{c^2}{c_{1n}^2}}, \qquad \beta_n = \sqrt{1 - \frac{c^2}{c_{2n}^2}}, \qquad n = 1, 2. \tag{3.14}$$

On substituting (3.13) into (3.12), we deduce the well-known equation

$$c_S^4\left((\rho_1-\rho_2)^2-a_1a_2\right)+2c_S^2m_{12}(\rho_2b_1-\rho_1b_2)+m_{12}^2b_1b_2=0, \tag{3.15}$$

in which c_S is the Stoneley wave speed and

$$\begin{gathered} a_1=\rho_1\alpha_{2S}+\rho_2\alpha_{1S}, \qquad a_2=\rho_1\beta_{2S}+\rho_2\beta_{1S}, \\ b_n=1-\alpha_n\beta_n, \qquad m_{12}=2\left(\mu_1-\mu_2\right), \end{gathered} \tag{3.16}$$

with

$$\alpha_{nS}=\sqrt{1-\frac{c_S^2}{c_{1n}^2}}, \qquad \beta_{nS}=\sqrt{1-\frac{c_S^2}{c_{2n}^2}}, \qquad n=1,2. \tag{3.17}$$

An interfacial Stoneley wave of arbitrary profile have been investigated by Chadwick (1976b), resulting in the representation of the displacement field in terms of a single plane harmonic function, similarly to the Rayleigh wave. These results have been recently generalised to three dimensions by Kiselev & Parker (2010). The cited papers allow reduction of a vector problem in linear elasticity for both surface and interfacial waves to a scalar Dirichlet problem for the Laplace equation. Thus, the analysis of interfacial waves turns out to be not much different compared to that of the Rayleigh waves.

3.3 Bending edge wave on a thin plate

Consider now the Rayleigh-type bending wave on a semi-infinite elastic plate of thickness $2h$ occupying the region $-\infty<x_1<\infty$, $0\leq x_2<\infty$, $-h\leq x_3\leq h$. This wave has been originally discovered by Konenkov (1960), however, clear hints may already be seen in the earlier work of Ishlinsky (1954) studying stability of a thin plate. It is peculiar that this wave was rediscovered several times, for more detail see Norris et al. (2000) and Lawrie & Kaplunov (2012).

Within the framework of the classical Kirchhoff plate theory, the deflection of the midplane $W=W(x_1,x_2,t)$ is governed by

$$D\Delta^2W+2\rho hW_{,tt}=0, \tag{3.18}$$

where ρ is volume mass density, Δ is the Laplacian in the variables x_1 and x_2, and the bending stiffness D is given by

$$D=\frac{2Eh^3}{3\left(1-\nu^2\right)}, \tag{3.19}$$

with E and ν denoting the Young's modulus and the Poisson ratio, respectively.

In the absence of bending moments and modified shear forces the boundary conditions at the edge $x_2 = 0$ are written as

$$\begin{aligned} W_{,22} + \nu W_{,11} = 0, \\ W_{,222} + (2-\nu)\, W_{,112} = 0. \end{aligned} \tag{3.20}$$

The solution of (3.18) is found in the form of a travelling harmonic wave as

$$W(x_1, x_2, t) = \sum_{j=1}^{2} A_j e^{i(kx_1 - \omega t) - k\gamma_j x_2}, \tag{3.21}$$

where the attenuation coefficients γ_j are given by ($\Re(\gamma_j) > 0$)

$$\gamma_j = \sqrt{1 + (-1)^j \sqrt{\frac{2\rho h}{D}} \frac{\omega}{k^2}}, \qquad j = 1, 2. \tag{3.22}$$

On substituting (3.21) into (3.20), we arrive at the set of linear algebraic equations

$$\begin{aligned} (\gamma_1^2 - \nu))A_1 + (\gamma_2^2 - \nu))A_2 = 0, \\ ((2-\nu)\gamma_1 - \gamma_1^3)\, A_1 + ((2-\nu)\gamma_2 - \gamma_2^3)\, A_2 = 0. \end{aligned} \tag{3.23}$$

Then, on employing the solvability condition, we deduce the dispersion relation

$$D k^4 \gamma_e^4 = 2\rho h \omega^2, \tag{3.24}$$

as first shown by Konenkov (1960). Here the coefficient

$$\gamma_e = \left[(1-\nu) \left(3\nu - 1 + 2\sqrt{2\nu^2 - 2\nu + 1} \right) \right]^{1/4} \tag{3.25}$$

depends on the Poisson's ratio only, see Fig. 3. In view of (3.24), we have for the attenuation coefficients

$$\gamma_j = \sqrt{1 + (-1)^j \gamma_e^2}, \qquad j = 1, 2. \tag{3.26}$$

Thus, the bending edge wave is a dispersive analogue of the Rayleigh surface wave. It should also be noted that such a wave may be considered within the framework of refined plate theories, see e.g. Zakharov (2004), and may be generalised to a plate with a curved contour as in Cherednichenko (2007). The effect of anisotropy may also be addressed, see e.g. Norris (1994), Thompson et al. (2002). The aspects of existence and uniqueness of bending

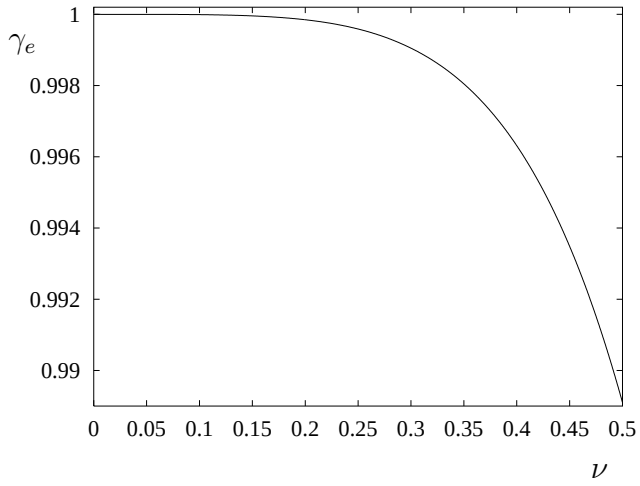

Figure 4: The coefficient γ_e vs. the Poisson's ratio ν.

edge waves in a generally anisotropic thin elastic plate were studied by Fu (2003) by using the edge-impedance matrix. Recent developments in the theory of bending edge waves involve incorporating the effect of an elastic foundation, see Kaplunov et al. (2014), Kaplunov & Nobili (2015), and Kaplunov et al. (2016). The recent contribution by Destrade et al. (2016) on a closely related problem of edge wrinkling opens the path for bending edge waves in pre-stressed plates.

In addition to bending edge waves in thin elastic plates, we also mention extensional waves, see Pichugin & Rogerson (2012), and related 3D edge waves, see e.g. Kaplunov et al. (2005), Zernov & Kaplunov (2008), and Kryshynska (2011).

4 Hyperbolic-elliptic model for the Rayleigh wave induced by surface stresses

In this section we present the derivation of an asymptotic formulation for the near-surface wave field in an elastic half-space, induced by prescribed surface stresses. This formulation was first reported in Kaplunov & Kossovich (2004), starting from the symbolic Lourier method, e.g. see Kaplunov et al. (1998) and references therein. The subject was further developed in Kaplunov et al. (2006), using a slow time perturbation procedure applied to the self-similar eigensolution in Chadwick (1976b), followed by extension to the 3D case in Dai et al. (2010) and other contributions. Below we present an improved perturbation scheme based on the implicit travelling wave ansatz (2.43).

4.1 Plane strain problem

In the plane strain setup the equations of motion of the elastic isotropic half-plane $\mathcal{H}_2^+$ are taken in the form (2.27), with the boundary conditions along the surface $x_3 = 0$ given by

$$\sigma_{31} = Q(x_1, t), \qquad \sigma_{33} = P(x_1, t), \tag{4.1}$$

where $P(x_1, t)$ and $Q(x_1, t)$ are prescribed surface stresses. The conditions (4.1) may be expressed in terms of the wave potentials as

$$\begin{aligned} 2\phi_{,13} + \psi_{,11} - \psi_{,33} &= \frac{Q}{\mu}, \\ \left(\kappa^{-2} - 2\right)\phi_{,11} + \kappa^{-2}\phi_{,33} + 2\psi_{,13} &= \frac{P}{\mu}, \end{aligned} \tag{4.2}$$

where, as previously, μ is the Lamé elastic shear modulus and $\kappa = c_2/c_1$.

In what follows we consider separately the effects of vertical ($Q(x_1, t) = 0$) and horizontal ($P(x_1, t) = 0$) loads. First, we analyse the near-resonant regimes of the vertical load

$$P = P(x_1 \pm ct), \tag{4.3}$$

see Fig. 5, where the load speed c is close to the Rayleigh wave speed c_R, i.e.

$$c = c_R(1 \pm \varepsilon), \tag{4.4}$$

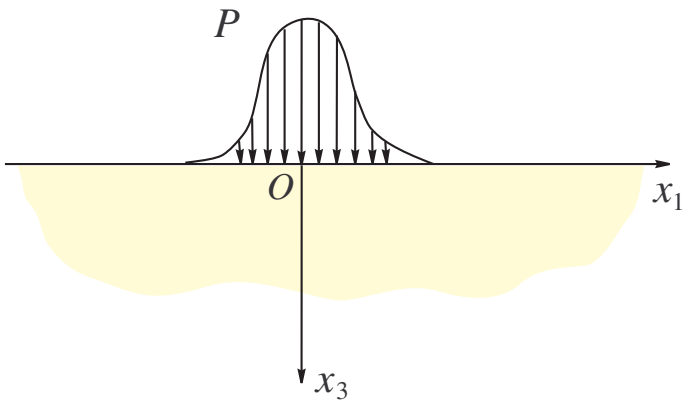

Figure 5: An elastic half-plane subject to a vertical load.

with a small parameter $0 < \varepsilon \ll 1$.

We proceed with a multiple scale perturbation scheme, see e.g. Cole (1968) and Nayfeh (2000), introducing the the fast and slow time variables, τ_f and τ_s, respectively, as

$$\tau_f = t, \qquad \tau_s = \varepsilon t. \tag{4.5}$$

The concept of slow time is essential for modelling of the near-resonant phenomena caused by the load of the form, see (4.3),

$$P = P(x_1 \pm c_R \tau_f, \tau_s). \tag{4.6}$$

The simplest example of a near-resonant excitation is presented in Appendix A for a single degree of freedom linear oscillator.

On taking into account the symbolic identity

$$\frac{\partial}{\partial t} = \frac{\partial}{\partial \tau_f} + \varepsilon \frac{\partial}{\partial \tau_s}, \tag{4.7}$$

the equations of motion (2.27) become

$$\begin{aligned} \phi_{,\tau_f\tau_f} + 2\varepsilon\phi_{,\tau_f\tau_s} + \varepsilon^2\phi_{,\tau_s\tau_s} - c_1^2\left(\phi_{,11} + \phi_{,33}\right) = 0, \\ \psi_{,\tau_f\tau_f} + 2\varepsilon\psi_{,\tau_f\tau_s} + \varepsilon^2\psi_{,\tau_s\tau_s} - c_2^2\left(\psi_{,11} + \psi_{,33}\right) = 0. \end{aligned} \tag{4.8}$$

We now employ the implicit travelling wave ansatz (2.43) having

$$\phi_{,\tau_f\tau_f} - c_R^2\phi_{,11} = 0, \qquad \psi_{,\tau_f\tau_f} - c_R^2\psi_{,11} = 0. \tag{4.9}$$

It is obvious that the load (4.6) satisfies (2.43) with respect to fast time, i.e.

$$P_{,\tau_f\tau_f} - c_R^2 P_{,11} = 0. \tag{4.10}$$

Then, the equations (4.8) take the form

$$\begin{aligned} \phi_{,33} + \alpha_R^2 \phi_{,11} - 2\frac{\varepsilon}{c_1^2}\phi_{,\tau_f\tau_s} - \frac{\varepsilon^2}{c_1^2}\phi_{,\tau_s\tau_s} = 0, \\ \psi_{,33} + \beta_R^2 \psi_{,11} - 2\frac{\varepsilon}{c_2^2}\psi_{,\tau_f\tau_s} - \frac{\varepsilon^2}{c_2^2}\psi_{,\tau_s\tau_s} = 0. \end{aligned} \tag{4.11}$$

Next, we expand the potentials in asymptotic series as

$$\begin{aligned} \phi(x_1, x_3, \tau_f, \tau_s) = \varepsilon^{-1}\left(\phi_0(x_1, x_3, \tau_f, \tau_s) + \varepsilon\phi_1(x_1, x_3, \tau_f, \tau_s) + \dots\right), \\ \psi(x_1, x_3, \tau_f, \tau_s) = \varepsilon^{-1}\left(\psi_0(x_1, x_3, \tau_f, \tau_s) + \varepsilon\psi_1(x_1, x_3, \tau_f, \tau_s) + \dots\right), \end{aligned} \tag{4.12}$$

where the factor ε^{-1} is due to a near-resonant excitation, see also a similar asymptotic expansion in Appendix A.

Below we present in detail the perturbation procedure for the potential ϕ, which, in view of the ansatz (4.9), at leading order satisfies the equation

$$\phi_{0,33} + \alpha_R^2 \phi_{0,11} = 0, \tag{4.13}$$

with the solution given by a plane harmonic function in the first two arguments, i.e.

$$\phi_0 = \phi_0(x_1, \alpha_R x_3, \tau_f, \tau_s). \tag{4.14}$$

At next order

$$\phi_{1,33} + \alpha_R^2 \phi_{1,11} = \frac{2}{c_1^2}\,\phi_{0,\tau_f\tau_s}, \tag{4.15}$$

so the first order correction can be written as

$$\phi_1 = \phi_{10} + x_3\phi_{11}, \tag{4.16}$$

where $\phi_{10} = \phi_{10}(x_1, \alpha_R x_3, \tau_f, \tau_s)$ and $\phi_{11} = \phi_{11}(x_1, \alpha_R x_3, \tau_f, \tau_s)$ are plane harmonic functions. On substituting the solution (4.16) into (4.15) and using the Cauchy-Riemann identities, we arrive at

$$\phi_{11,1} = \frac{1}{\alpha_R c_1^2}\,\phi^*_{0,\tau_f\tau_s}, \tag{4.17}$$

where, as previously, the asterisk denotes a harmonic conjugate function. The derivation for the transverse potential ψ is very similar to that presented above. Thus, the two-term expansions for the derivatives of the potentials are

$$\begin{aligned}\phi_{,1} &= \frac{1}{\varepsilon}\left[\phi_{0,1} + \varepsilon\left(\phi_{10,1} + \frac{x_3}{\alpha_R c_1^2}\,\phi^*_{0,\tau_f\tau_s}\right) + \dots\right] \quad , \\ \psi_{,1} &= \frac{1}{\varepsilon}\left[\psi_{0,1} + \varepsilon\left(\psi_{10,1} + \frac{x_3}{\beta_R c_2^2}\,\psi^*_{0,\tau_f\tau_s}\right) + \dots\right].\end{aligned} \tag{4.18}$$

It may be readily observed that the obtained expansion is essentially a slow time perturbation of the eigensolution for the Rayleigh wave of arbitrary profile discussed in subsection 2.2.

On substituting (4.18) into (4.2) at $Q = 0$ and making use of the Cauchy-Riemann identities, we obtain at leading order

$$\begin{aligned}2\alpha_R\phi_{0,11} + (1+\beta_R^2)\,\psi^*_{0,11} &= 0, \\ (1+\beta_R^2)\,\phi_{0,11} + 2\beta_R\psi^*_{0,11} &= 0,\end{aligned} \tag{4.19}$$

implying the Rayleigh equation

$$\left(1+\beta_R^2\right)^2 - 4\alpha_R\beta_R = 0 \tag{4.20}$$

as a solvability condition. In addition, we recover the relations (2.37) between the leading order potentials ϕ_0 and ψ_0.

At next order we deduce

$$\begin{aligned}2\phi_{10,113} + \psi_{10,111} - \psi_{10,133} &= -\frac{2}{\alpha_R c_1^2}\,\phi^*_{0,1\tau_f\tau_s} + \frac{2}{\beta_R c_2^2}\,\psi^*_{0,3\tau_f\tau_s}, \\ (\kappa^{-2}-2)\phi_{10,111} + \kappa^{-2}\phi_{10,133} + 2\psi_{10,113} &= -\frac{2}{\alpha_R\kappa^2 c_1^2}\,\phi^*_{0,3\tau_f\tau_s} - \frac{2}{\beta_R c_2^2}\,\psi^*_{0,1\tau_f\tau_s} + \frac{P_{,1}}{\mu}\,.\end{aligned} \tag{4.21}$$

Then, on using the Cauchy-Riemann identities along with (2.37), these equations may be simplified to

$$\begin{aligned}2\alpha_R\phi_{10,111} + (1+\beta_R^2)\,\psi^*_{10,111} &= \left(\frac{2}{\alpha_R c_1^2} - \frac{1+\beta_R^2}{\beta_R c_2^2}\right)\phi_{0,1\tau_f\tau_s}, \\ (1+\beta_R^2)\phi_{10,111} + 2\beta_R\psi^*_{10,111} &= \left(\frac{2}{c_2^2} - \frac{1+\beta_R^2}{\beta_R^2 c_2^2}\right)\,\phi_{0,1\tau_f\tau_s} - \frac{P_{,1}}{\mu}\,.\end{aligned} \tag{4.22}$$

The solvability of the latter implies

$$\phi_{0,\tau_f\tau_s} = -\frac{(1+\beta_R^2)c_R^2}{4\mu B}\,P, \tag{4.23}$$

where

$$B = \frac{\alpha_R}{\beta_R}\,(1-\beta_R^2) + \frac{\beta_R}{\alpha_R}\,(1-\alpha_R^2) - 1 + \beta_R^4 \tag{4.24}$$

is a dimensionless constant. On taking into account the leading order approximation $\phi = \varepsilon^{-1}\phi_0$ and the ansatz (4.9), the relation (4.23) may be rewritten as

$$\phi_{,\tau_f\tau_f} + 2\varepsilon\phi_{,\tau_f\tau_s} - c_R^2\phi_{,11} = -\frac{(1+\beta_R^2)\,c_R^2\,P}{2\mu B}. \tag{4.25}$$

Now, employing the approximate symbolic formula

$$\frac{\partial^2}{\partial t^2} = \frac{\partial^2}{\partial \tau_f^2} + 2\varepsilon\frac{\partial^2}{\partial\tau_s\partial\tau_f} + O(\varepsilon^2), \tag{4.26}$$

we restate (4.25) in terms of the original variables as

$$\phi_{,11} - \frac{1}{c_R^2}\,\phi_{,tt} = \frac{(1+\beta_R^2)\,P}{2\mu B}. \tag{4.27}$$

Thus, the asymptotic formulation for the Rayleigh wave involves a scalar problem for the pseudo-static elliptic equation

$$\phi_{,33} + \alpha_R^2\phi_{,11} = 0, \tag{4.28}$$

subject to the Dirichlet boundary condition at $x_3 = 0$ in the form of the 1D wave equation (4.27). The transverse potential ψ may then be restored from (2.38).

We also note that the hyperbolic equation (4.27) can be transformed to an equation for the horizontal displacement u_1. Indeed, on differentiating (4.27) with respect to x_1 and using (2.40) at $x_3 = 0$, we get

$$u_{1,11} - \frac{1}{c_R^2}u_{1,tt} = \frac{1-\beta_R^4}{4\mu B}\,P_{,1}. \tag{4.29}$$

Consider now the boundary conditions (4.2) for a horizontal load, when $P = 0$. A very similar procedure leads to the same two-term expansions (4.18). The analysis of the boundary conditions gives the Rayleigh equation (4.20) at leading order, along with the relations (2.37) between the potentials ϕ_0 and ψ_0. Finally, we arrive at a 1D wave equation for the potential ψ which can be written as

$$\psi_{,11} - \frac{1}{c_R^2}\psi_{,tt} = -\frac{(1+\beta_R^2)\,Q}{2\mu B}. \tag{4.30}$$

Its solution provides a Dirichlet boundary condition for the elliptic equation given by

$$\psi_{,33} + \beta_R^2\psi_{,11} = 0. \tag{4.31}$$

In this case the potential ϕ follows from (2.39). Similarly to (4.29), we also have

$$u_{3,11} - \frac{1}{c_R^2} u_{3,tt} = -\frac{1-\beta_R^4}{4\mu B}\, Q_{,1}. \tag{4.32}$$

The asymptotic formulations (4.27), (4.28) and (4.30), (4.31) reveal a dual *hyperbolic-elliptic* nature of the Rayleigh wave. Indeed, the elliptic equations (4.28) and (4.31) characterise decay of a wide range of surface disturbances into the interior, whereas the 1D wave equations (4.27) and (4.30) govern the wave propagation along the surface with a finite speed c_R. At the same time, it should be emphasized that a hyperbolic wave-like behaviour is only typical for one of the potentials along the surface, see (4.27) and (4.30).

Finally, it should be noted that the applicability of the developed explicit formulations for the surface wave field is not restricted only to near-resonant loading as in (4.6). In fact, it may be shown, using the integral transform technique, that they approximate the contribution of the Rayleigh wave to the overall dynamic response for an arbitrary surface load as well. For example, in case of the vertical load $P = P(x_1, t)$ the transformed solution of the problem (4.27) and (4.28) is given by

$$\phi^{FL} = -\frac{(1+\beta_R^2)\, c_R^2\, e^{-\alpha_R |p| x_3}}{2\mu B\, (p^2 + c_R^2 k^2)}\, P^{FL}, \tag{4.33}$$

where k and p are the Fourier and Laplace transform parameters, respectively, and the superscript FL denotes Fourier-Laplace transforms. The formula (4.33) coincides with the local behaviour of the transformed exact solution of the original plane problem near the Rayleigh wave poles, see consideration in subsection 4.3.1 ensuring identical surface wave patterns.

4.2 3D problem

Let us generalise the analysis in the previous subsection to the 3D setup, in which the equations of motion are taken in the form (2.4), with the boundary conditions at $x_3 = 0$ written as

$$\sigma_{3i} = Q_i(x_1, x_2, t), \qquad \sigma_{33} = P(x_1, x_2, t), \qquad i = 1, 2. \tag{4.34}$$

4.2.1 Vertical load

Consider a vertical load, see Fig. 6, when $Q_1 = Q_2 = 0$ in (4.34). First, we specify the Radon

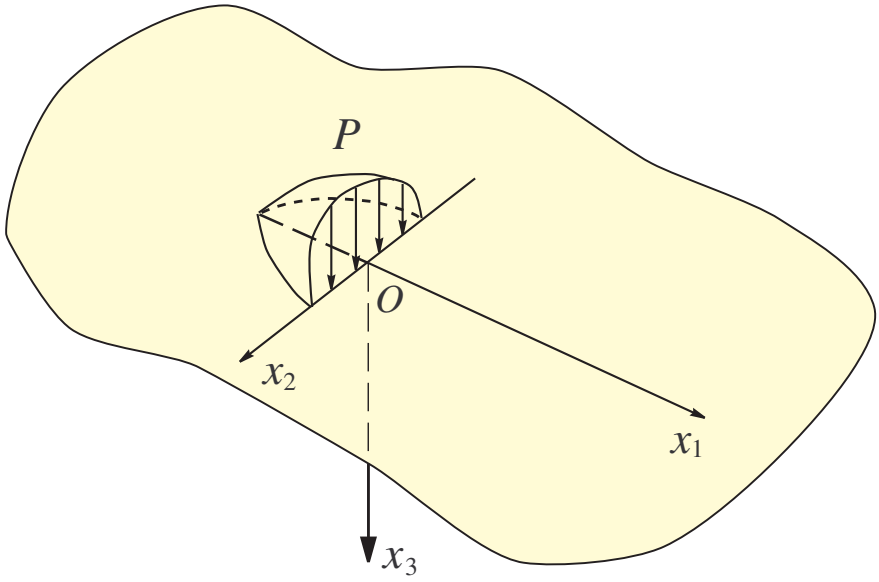

Figure 6: An elastic half-space under a vertical load.

integral transform

$$f^{(\alpha)}(\chi, \alpha, x_3, t) = \int_{-\infty}^{\infty} f(\chi \cos\alpha - \eta \sin\alpha, \chi \sin\alpha + \eta \cos\alpha, x_3, t)\, d\zeta, \tag{4.35}$$

where

$$\chi = x_1 \cos\alpha + x_2 \sin\alpha, \qquad \eta = -x_1 \sin\alpha + x_2 \cos\alpha,$$

with the angle α varying over the interval $0 \le \alpha < 2\pi$; here and below the Radon transforms are supplied with the superscript (α). It is well-known that the Radon transform allows reduction of the original 3D problem in elasticity to a 2D problem for the associated transforms, see Georgiadis & Lykotrafitis (2001).

Let us also define transformed displacements in the Cartesian frame (χ, η) as

$$u_\chi^{(\alpha)} = u_1^{(\alpha)} \cos\alpha + u_2^{(\alpha)} \sin\alpha, \qquad u_\eta^{(\alpha)} = -u_1^{(\alpha)} \sin\alpha + u_2^{(\alpha)} \cos\alpha, \tag{4.36}$$

imposing the assumption

$$u_\eta^{(\alpha)} = 0, \tag{4.37}$$

meaning that anti-plane motion does not induce surface waves.

On taking into account (4.37), the transformed equations of motion (2.4) become, see also

Dai et al. (2010),

$$\begin{aligned}(\lambda+2\mu)u^{(\alpha)}_{\chi,\chi\chi}+\mu u^{(\alpha)}_{\chi,33}+(\lambda+\mu)u^{(\alpha)}_{3,\chi 3}&=\rho u^{(\alpha)}_{\chi,tt},\\ (\lambda+\mu)u^{(\alpha)}_{\chi,\chi 3}+\mu u^{(\alpha)}_{3,\chi\chi}+(\lambda+2\mu)u^{(\alpha)}_{3,33}&=\rho u^{(\alpha)}_{3,tt}.\end{aligned} \tag{4.38}$$

The transformed boundary conditions (4.34) at $Q_1 = Q_2 = 0$ are written as

$$\begin{aligned}\sigma^{(\alpha)}_{\chi 3}&=\mu\left(u^{(\alpha)}_{\chi,3}+u^{(\alpha)}_{3,\chi}\right)=0,\\ \sigma^{(\alpha)}_{33}&=\mu u^{(\alpha)}_{\chi,\chi}+(\lambda+2\mu)\,u^{(\alpha)}_{3,3}=P^{(\alpha)}.\end{aligned} \tag{4.39}$$

The equations (4.38) and (4.39) are formally identical to those in the plane strain problem. Therefore, we can introduce the conventional scalar wave potentials $\phi^{(\alpha)}$ and $\psi^{(\alpha)}$, having

$$u^{(\alpha)}_{\chi}=\frac{\partial\phi^{(\alpha)}}{\partial\chi}-\frac{\partial\psi^{(\alpha)}}{\partial x_3},\qquad u^{(\alpha)}_{3}=\frac{\partial\phi^{(\alpha)}}{\partial x_3}+\frac{\partial\psi^{(\alpha)}}{\partial\chi} \tag{4.40}$$

and follow the multiple scale procedure developed in the previous subsection. In this case the transformed implicit travelling wave ansatz, see (2.43),

$$\phi^{(\alpha)}_{,\tau_f\tau_f}-c_R^2\phi^{(\alpha)}_{,\chi\chi}=0. \tag{4.41}$$

corresponds to the 2D wave equation

$$\phi_{,\tau_f\tau_f}-c_R^2\Delta\phi=0, \tag{4.42}$$

where Δ denotes the 2D Laplace operator in x_1 and x_2.

The analogues of the two-term asymptotic expansions (4.18) become

$$\begin{aligned}\phi^{(\alpha)}_{,\chi}&=\frac{1}{\varepsilon}\left[\phi^{(\alpha)}_{0,\chi}+\varepsilon\left(\phi^{(\alpha)}_{10,\chi}+\frac{x_3}{\alpha_R c_1^2}\,\phi^{(\alpha)*}_{0,\tau_f\tau_s}\right)+\dots\right],\\ \psi^{(\alpha)}_{,\chi}&=\frac{1}{\varepsilon}\left[\psi^{(\alpha)}_{0,\chi}+\varepsilon\left(\psi^{(\alpha)}_{10,\chi}+\frac{x_3}{\beta_R c_2^2}\,\psi^{(\alpha)*}_{0,\tau_f\tau_s}\right)+\dots\right].\end{aligned} \tag{4.43}$$

On substituting these formulae into the boundary conditions (4.39), at leading order we obtain the Rayleigh wave equation and the relations between the potentials mirroring (2.37), whereas at next order the solvability dictates

$$\phi^{(\alpha)}_{0,\tau_f\tau_s}=-\frac{(1+\beta_R^2)c_R^2}{4\mu B}\,P^{(\alpha)}, \tag{4.44}$$

with the material constant B defined by (4.24). Finally, the explicit formulation for the Radon transforms includes the hyperbolic equation

$$\phi^{(\alpha)}_{,\chi\chi}-\frac{1}{c_R^2}\phi^{(\alpha)}_{,tt}=\frac{(1+\beta_R^2)\,P^{(\alpha)}}{2\mu B}, \tag{4.45}$$

along the surface $x_3 = 0$, following from (4.44) and providing the boundary condition for the elliptic equation

$$\phi^{(\alpha)}_{,33} + \alpha_R^2 \phi^{(\alpha)}_{,\chi\chi} = 0 \tag{4.46}$$

over the interior. Now, the transformed potential $\psi^{(\alpha)}$ satisfies the equation

$$\psi^{(\alpha)}_{,33} + \beta_R^2 \psi^{(\alpha)}_{,\chi\chi} = 0, \tag{4.47}$$

being related on the surface to $\phi^{(\alpha)}$ by the formulae

$$\psi^{(\alpha)}_{,\chi} = -\frac{2}{1+\beta_R^2}\, \phi^{(\alpha)}_{,3} \tag{4.48}$$

and

$$\psi^{(\alpha)}_{,3} = \frac{1+\beta_R^2}{2}\, \phi^{(\alpha)}_{,\chi}. \tag{4.49}$$

Next, we introduce a pair of the potentials $\psi_1^{(\alpha)} = \psi^{(\alpha)} \cos\alpha$ and $\psi_2^{(\alpha)} = \psi^{(\alpha)} \sin\alpha$ in order to invert the transforms in (4.46)-(4.49). As a result, we get the elliptic equations

$$\phi_{,33} + \alpha_R^2 \Delta\phi = 0, \qquad \psi_{i,33} + \beta_R^2 \Delta\psi_i = 0, \qquad i = 1, 2, \tag{4.50}$$

governing behaviour over the interior. The boundary conditions at $x_3 = 0$ include a 2D wave equation for the potential ϕ, i.e.

$$\Delta\phi - \frac{1}{c_R^2}\phi_{,tt} = \frac{(1+\beta_R^2)\, P}{2\mu B}, \tag{4.51}$$

along with the relations

$$\phi_{,i} = \frac{2}{1+\beta_R^2}\psi_{i,3}, \qquad \phi_{,3} = -\frac{1+\beta_R^2}{2}\left(\psi_{1,1} + \psi_{2,2}\right), \qquad i = 1, 2. \tag{4.52}$$

The Helmholz representation (2.5) for the displacement vector $\mathbf{u}$ may now be written as

$$\mathbf{u} = \mathrm{grad}\phi + \mathrm{curl}\Psi, \tag{4.53}$$

where $\Psi = (-\psi_2, \psi_1, 0)$, as observed in Kaplunov & Prikazchikov (2013). In view of (4.52) and (4.53), at $x_3 = 0$

$$u_i = \frac{1-\beta_R^2}{2}\, \phi_{,i}, \qquad i = 1, 2. \tag{4.54}$$

Hence, we deduce hyperbolic equations on the surface for the horizontal displacements, u_1 and u_2, namely,

$$\Delta u_i - \frac{1}{c_R^2} u_{i,tt} = \frac{1-\beta_R^4}{4\mu B} P_{,i}, \qquad i = 1, 2, \tag{4.55}$$

corresponding to (4.29) within the plane strain formulation.

4.2.2 Horizontal load

Consider now a horizontal load, setting $P = 0$ in (4.34), see Fig. 7. First, we decompose the

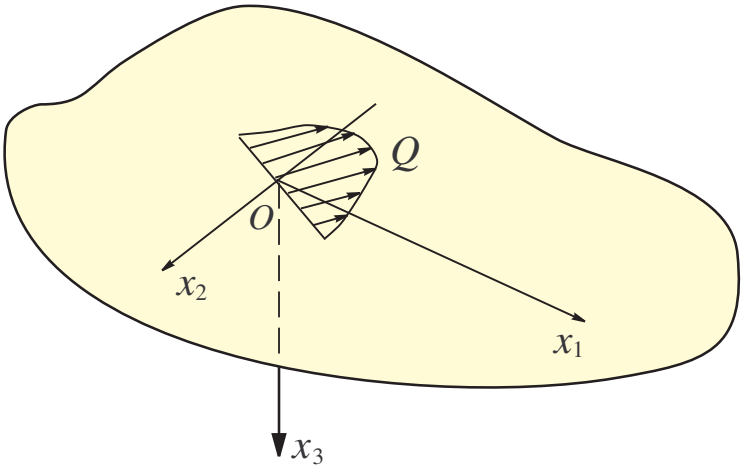

Figure 7: An elastic half-space under a horizontal load.

surface stresses using the Helmholz theorem into the gradient and rotational parts, $Q_g(x_1, x_2, t)$ and $Q_r(x_1, x_2, t)$, respectively, as

$$Q_1 = Q_{g,1} + Q_{r,2}, \qquad Q_2 = Q_{g,2} - Q_{r,1}. \tag{4.56}$$

On applying the Radon transform (4.35) along with the assumption (4.37), we express the boundary conditions (4.34) as

$$\begin{aligned} \mu\left(2\phi^{(\alpha)}_{,\chi 3} + \psi^{(\alpha)}_{,\chi\chi} - \psi^{(\alpha)}_{,33}\right) &= Q^{(\alpha)}_{g,\chi}, \\ \left(\kappa^{-2} - 2\right)\phi^{(\alpha)}_{,\chi\chi} + \kappa^{-2}\phi^{(\alpha)}_{,33} + 2\psi^{(\alpha)}_{,\chi 3} &= 0. \end{aligned} \tag{4.57}$$

Thus, as might be expected, the rotational part of the load does not contribute to the excitation of the Rayleigh wave, see Ege et al. (2015) for further detail.

A slow time perturbation procedure similar to that developed in subsection 4.1, results in a boundary value problem for the elliptic equation

$$\psi^{(\alpha)}_{,33} + \beta_R^2 \psi^{(\alpha)}_{,\chi\chi} = 0. \tag{4.58}$$

Predictably, the surface wave propagation along the boundary $x_3 = 0$ is governed by the hyperbolic equation

$$\psi^{(\alpha)}_{,\chi\chi} - \frac{1}{c_R^2}\psi^{(\alpha)}_{,tt} = -\frac{1+\beta_R^2}{2\mu B}\, Q^{(\alpha)}_{g,\chi}. \tag{4.59}$$

The transformed potential $\phi^{(\alpha)}$ is then found from (4.47) combined with any of the relations (4.48) or (4.49).

On applying the inverse Radon transform to the formulae above, we arrive at the same 3D pseudo-static elliptic equations

$$\phi_{,33} + \alpha_R^2 \Delta\phi = 0, \qquad \psi_{i,33} + \beta_R^2 \Delta\psi_i = 0, \qquad i = 1, 2, \tag{4.60}$$

together with the relations between the potentials at $x_3 = 0$

$$\phi_{,i} = \frac{2}{1+\beta_R^2}\psi_{i,3} \qquad \phi_{,3} = -\frac{1+\beta_R^2}{2}\left(\psi_{1,1} + \psi_{2,2}\right), \qquad i = 1, 2. \tag{4.61}$$

The counterpart of (4.51) now involves a 2D vector hyperbolic equation containing the gradient part of the in-plane load Q_g, namely

$$\Delta\psi_i - \frac{1}{c_R^2}\psi_{i,tt} = -\frac{1+\beta_R^2}{2\mu B}\, Q_{g,i}, \qquad i = 1, 2. \tag{4.62}$$

We also write down the 2D wave equation for the vertical displacement u_3 on the surface $x_3 = 0$, following from (4.52) and (4.53), complementing (4.32)

$$\Delta u_3 - \frac{1}{c_R^2} u_{3,tt} = \frac{1-\beta_R^4}{4\mu B}\Delta Q_g. \tag{4.63}$$

4.3 Examples

This subsection contains a few examples of dynamic surface loading demonstrating the advantages of the explicit formulation for the Rayleigh wave developed in subsections 4.1 and 4.2.

4.3.1 Comparison with 2D exact solution

Let us compare the approximate solution coming from the derived hyperbolic-elliptic formulation with the exact solution of the plane strain problem. For example, for the vertical load $P = P(x_1, t)$ we get by applying the double Fourier-Laplace integral transform in (2.27) and (4.2) at $Q = 0$

$$\phi^{FL}_{,33} - k^2 a_R^2 \phi^{FL} = 0, \qquad \psi^{FL}_{,33} - k^2 b_R^2 \phi^{FL} = 0, \tag{4.64}$$

subject to

$$
\begin{aligned}
2ik\phi^{FL}_{,3} - k^2\psi^{FL} - \psi^{FL}_{,33} = 0,\\
\left(2-\kappa^{-2}\right)k^2\psi^{FL} + \kappa^{-2}\phi^{FL}_{,33} + 2ik\psi^{FL}_{,3} = \frac{P^{FL}}{\mu},
\end{aligned}
\tag{4.65}
$$

at $x_3 = 0$. In the above

$$
a_R = \sqrt{1+\frac{p^2}{c_1^2k^2}}, \qquad b_R = \sqrt{1+\frac{p^2}{c_2^2k^2}},
\tag{4.66}
$$

where k and p are the Fourier and Laplace transform parameters, respectively.

The solution of the problem (4.64) and (4.65) for the transformed potential ϕ^{FL} is given by

$$
\phi^{FL} = -\frac{1+b_R^2}{R}\,\frac{P^{FL}}{\mu}\,\frac{e^{-a_R|k|x_3}}{k^2},
\tag{4.67}
$$

where

$$
R = R\left(\frac{p^2}{k^2}\right) = 4\sqrt{1+\frac{p^2}{c_1^2k^2}}\sqrt{1+\frac{p^2}{c_2^2k^2}} - \left(2+\frac{p^2}{c_2^2k^2}\right)^2.
\tag{4.68}
$$

At the same time, within the framework of the hyperbolic-elliptic model in 4.1, the associated transformed solution takes the form (4.33). It is clear that the Rayleigh poles in (4.67) are given by $p^2 = -c_R^2k^2$. In this case the quantities a_R and b_R defined by (4.66) become α_R and β_R, respectively. Therefore, by expanding the denominator R in (4.67) as a Taylor series around $p^2 = -c_R^2k^2$, we have

$$
R \approx R'(-c_R^2)\left(\frac{p^2}{k^2}+c_R^2\right) = 2B\left(1+\frac{p^2}{c_R^2k^2}\right),
\tag{4.69}
$$

where B is the same as in (4.24).

Thus, the approximation of (4.67) in the vicinity of the Rayleigh poles coincides with (4.33), providing another justification of the validity of the developed model. We remark that the consideration in this subsection is restricted to the loads, which do not generate the poles that are close to the Rayleigh ones, arising from P^{FL} in the transformed solution (4.67).

The proposed approach brings in a significant simplification of the Rayleigh wave analysis, reducing the original problem to a scalar problem for the elliptic equation (4.28) together with a boundary condition in the form of the hyperbolic equation (4.27).

Consider, for example, the Lamb problem, see Lamb (1904), for the vertical point impulse $P = P_0\delta(x_1)\delta(t)$. In this case $P^{FL} = P_0$ in (4.67). On evaluating the residues related to the

Rayleigh poles and taking the inverse Fourier transform, we get

$$\phi = \frac{(1+\beta_r^2)c_R\,P_0}{4\pi\mu B}\left[\tan^{-1}\frac{x_1-c_Rt}{\alpha_R x_3}-\tan^{-1}\frac{x_1+c_Rt}{\alpha_R x_3}\right]. \tag{4.70}$$

The last formula also follows from (4.33). However, the derivation starting from the Rayleigh wave model allows a more straightforward treatment, which does not require double integral transforms. Indeed, we solve the hyperbolic equation

$$\phi_{,11}-\frac{1}{c_R^2}\phi_{,tt}=\frac{(1+\beta_R^2)P_0}{2\mu B}\,\delta(x_1)\delta(t), \tag{4.71}$$

on the surface $x_3=0$, immediately having

$$\phi\big|_{x_3=0}=\frac{(1+\beta_R^2)c_RP_0}{4\mu B}\left[H(x_1-c_Rt)-H(x_1+c_Rt)\right], \tag{4.72}$$

which follows from the fundamental solution of the wave equation, e.g. see Polyanin (2002). Then, the Poisson formula, e.g. see Courant & Hilbert (1989), enables the potential ϕ to be restored over the interior, coinciding with (4.70).

Thus, for the studied 2D problem the approximate approach captures the contribution of the Rayleigh wave, which is usually dominant in the far-field zone, see also a practical example in Chouet (1985).

4.3.2 2D near-resonant time-harmonic excitation

Next, investigate the time-harmonic plane strain problem for the vertical load

$$P=P_0e^{ik(x_1-ct)}, \tag{4.73}$$

where k is the wave number and c is the phase speed (4.4), being close to the Rayleigh wave speed c_R.

The solution for the potential ϕ within the approximate formulation (4.27) and (4.28) is readily obtained in the form

$$\phi=\frac{(1+\beta_R^2)P_0}{2\mu Bk^2}\,\frac{c_R^2}{c^2-c_R^2}\,e^{ik(x_1-ct)-k\alpha_Rx_3}, \tag{4.74}$$

demonstrating a resonant response as $c\to c_R$.

For the sake of definiteness, below we set $c = (1+\varepsilon)c_R$. Then, $c^2 - c_R^2 \approx 2\varepsilon c_R^2$. Hence, the near-resonant behaviour of (4.74) becomes

$$\phi = \frac{(1+\beta_R^2)P_0}{4\varepsilon\mu B k^2}\, e^{ik(x_1-ct)-k\alpha_R x_3}. \tag{4.75}$$

Now, let us study the exact 2D solution for the prescribed near-resonant harmonic loading. The same potential ϕ, satisfying the equations (2.27), subject to the conditions (4.2) with P in the form of (4.73), is written as

$$\phi = \frac{P_0(1+\beta^2)}{\mu k^2 R(c)}\, e^{ik(x_1-ct)-k\alpha x_3}, \tag{4.76}$$

with

$$R(c) = (1+\beta^2)^2 - 4\alpha\beta \tag{4.77}$$

and α and β defined by (2.14). On employing the asymptotic formulae

$$\alpha \sim \alpha_R\left(1 - \varepsilon\frac{1-\alpha_R^2}{\alpha_R^2}\right), \qquad \beta \sim \beta_R\left(1 - \varepsilon\frac{1-\beta_R^2}{\beta_R^2}\right), \tag{4.78}$$

we deduce

$$R(c) \sim (1+\beta_R^2)^2 - 4\alpha_R\beta_R + 4\varepsilon\left[\frac{\alpha_R}{\beta_R}(1-\beta_R^2) + \frac{\beta_R}{\alpha_R}(1-\alpha_R^2) - 1 + \beta_R^4\right] = 4\varepsilon B, \tag{4.79}$$

with B defined by (4.24). Thus, the limiting behaviour of (4.76) coincides with (4.75), since at leading order $\alpha \sim \alpha_R$ and $\beta \sim \beta_R$ as $c \to c_R$.

A comparison of the asymptotic and exact solutions, given by (4.75) and (4.76), respectively, is demonstrated in Fig. 8, where the scaled potential

$$\phi_s = \frac{\varepsilon\mu k^2}{P_0}\, e^{-ik(x_1-ct)}\phi(x_1, 0, t) \tag{4.80}$$

is displayed. Here the solid line shows variation of the exact solution over a range of near-resonant speeds, whereas the dashed line corresponds to the asymptotic model, clearly matching at $\varepsilon = 0$.

In addition to the consideration in subsection 4.3.1 mainly oriented to the far-field analysis, this example highlights another major application of the proposed methodology, associated with a near-resonant excitation.

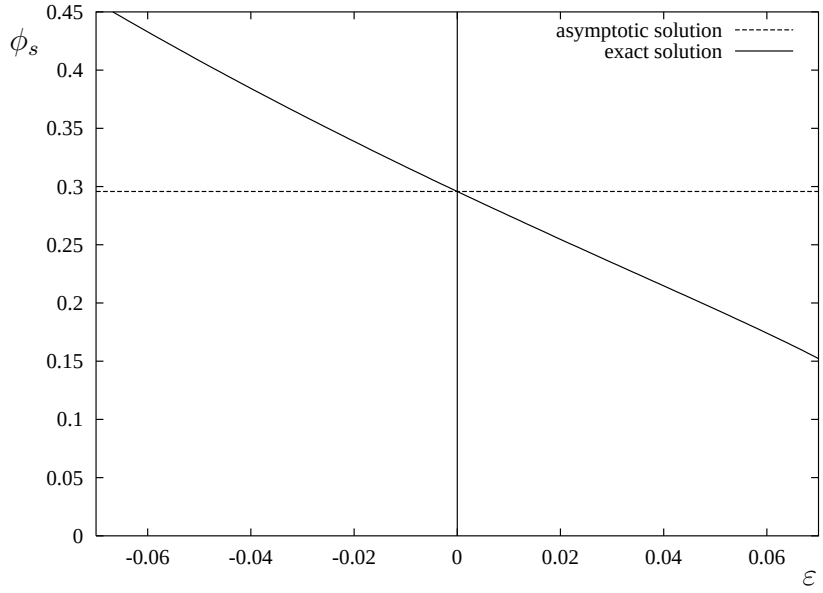

Figure 8: Comparison of exact and asymptotic results for the near-resonant regime.

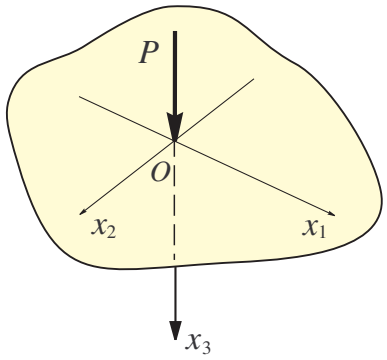

Figure 9: An axisymmetric vertical point load.

4.3.3 Axisymmetric and 3D problems for point impulses

Let us now analyse the effect of a *vertical* point force, setting $P = P_0\delta(x_1)\delta(x_2)\delta(t)$ and $Q_1 = Q_2 = 0$ in (4.34), see Fig. 9.

The longitudinal potential ϕ on the surface is found as the fundamental solution of the wave equation, see e.g. Polyanin (2002). It follows from (4.51), that

$$\phi(x_1, x_2, 0, t) = \frac{(1+\beta_R^2)P_0}{4\pi\mu B c_R} \frac{H\left(c_R t - r\right)}{\sqrt{c_R^2 t^2 - r^2}}, \tag{4.81}$$

where $r = \sqrt{x_1^2 + x_2^2}$ is the polar radius. In order to restore the potential ϕ over the interior, we solve the equation (4.50) with the boundary condition (4.81). On applying the Hankel

transform, we get

$$\frac{\partial^2 \phi^H}{\partial x_3^2} - \alpha_R^2 p^2 \phi^H = 0, \tag{4.82}$$

where

$$\phi^H = \int_0^\infty \phi(r, x_3, t) J_0(pr) r dr. \tag{4.83}$$

Therefore,

$$\begin{aligned}
\phi(x_1, x_2, x_3, t) &= \frac{(1+\beta_R^2)P_0}{4\pi\mu B c_R} \int_0^\infty \sin(c_R p t) \exp(\alpha_R p x_3) J_0(pr)\, dp \\
&= \frac{(1+\beta_R^2)P_0}{4\pi\mu B c_R} \mathrm{Im} \int_0^\infty \exp\left[-(\alpha_R p x_3 - i c_R t)\right] J_0(pr)\, dp, \\
&= \frac{(1+\beta_R^2)P_0}{4\pi\mu B c_R} \mathrm{Im} \left\{ \left[r^2 + (\alpha_R x_3 - i c_R t)^2 \right]^{-1/2} \right\}.
\end{aligned} \tag{4.84}$$

Then, using the relations (4.52), we obtain the potentials ψ_n, $n = 1, 2$, in the form

$$\psi_1(x_1, x_2, x_3, t) = -\frac{\alpha_R P_0}{2\pi\mu c_R B} \mathrm{Re} \left\{ \frac{\cos\theta(\beta_R x_3 - i c_R t)}{r\left[r^2 + (\beta_R x_3 - i c_R t)^2\right]^{1/2}} \right\}. \tag{4.85}$$

and

$$\psi_2(x_1, x_2, x_3, t) = -\frac{\alpha_R P_0}{2\pi\mu B c_R} \mathrm{Re} \left\{ \frac{\sin\theta(\beta_R x_3 - i c_R t)}{r\left[r^2 + (\beta_R x_3 - i c_R t)^2\right]^{1/2}} \right\}, \tag{4.86}$$

where θ is the polar angle. It may also be verified that (4.84)-(4.86) satisfy both (4.50) and (4.52).

The behaviour of the scaled longitudinal potential

$$\phi_*(r_1, z) = \mathrm{Im} \left\{ \left[r_1^2 + (\alpha_R z - i)^2 \right]^{-1/2} \right\},$$

with

$$r_1 = \frac{r}{c_R t}, \qquad z = \frac{x_3}{c_R t},$$

is illustrated in Fig 10. The Rayleigh wave front propagating along the surface is shown by dotted line at $r_1 = 1$. The associated discontinuity becomes smoother with depth as seen from Fig. 10. Graphs for the scaled transverse potential

$$\psi_{1*}(r_1, z) = \mathrm{Re} \left\{ \frac{\cos\theta(\beta_R z - i)}{r_1\left[r_1^2 + (\beta_R z - i)^2\right]^{1/2}} \right\},$$

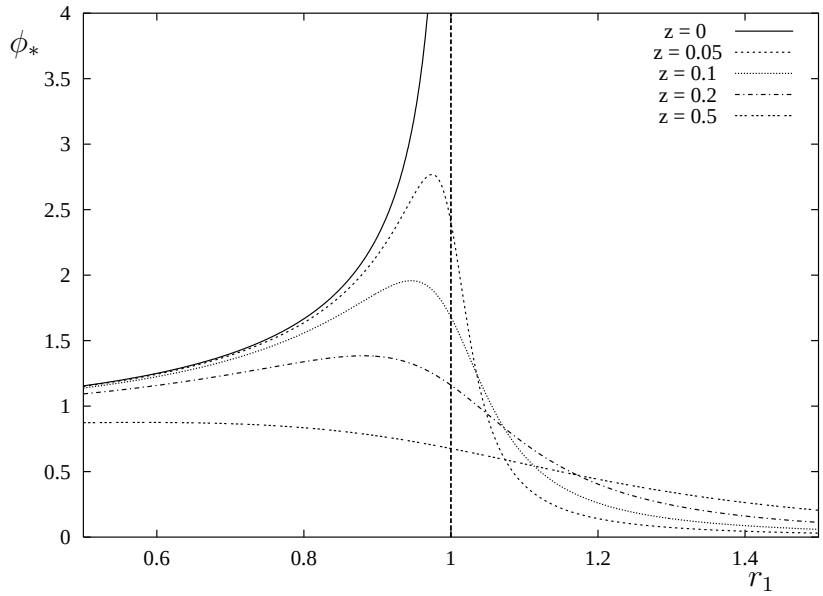

Figure 10: The scaled longitudinal potential ϕ_* vs. the dimensionless polar radius r_1.

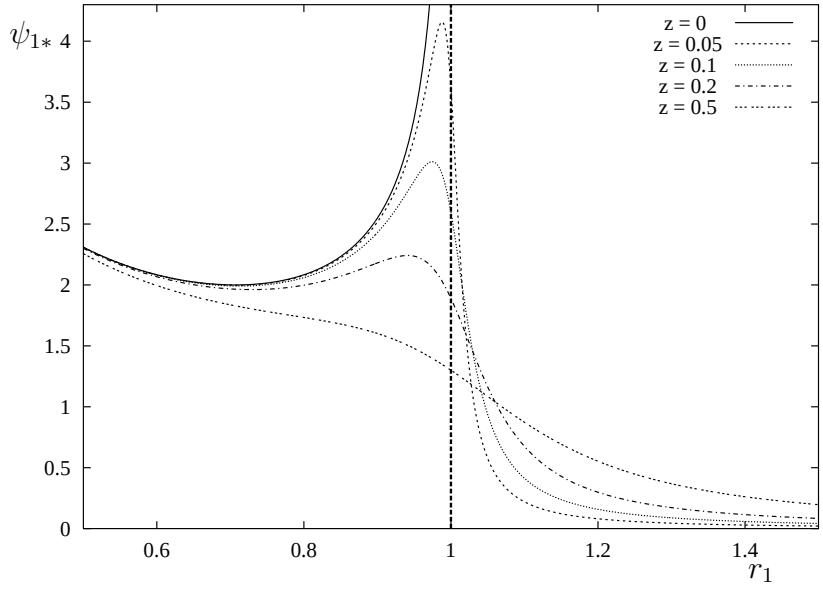

Figure 11: The scaled transverse potential ψ_{1*} vs. the dimensionless polar radius r_1.

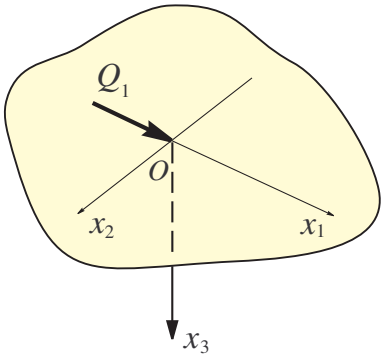

Figure 12: A horizontal point load.

are plotted in Fig. 11 for $\theta = 0$. Obviously, we may expect a similar behaviour of the second component of the transverse potential ψ_2.

Next, we investigate the effect of a *horizontal* point impulse, see Fig. 12, on substituting $Q_1 = Q_0\delta(x_1)\delta(x_2)\delta(t)$, and $Q_2 = P = 0$ into (4.34).

We restrict ourselves to analysis of the surface transverse displacement only. First, we decompose the prescribed in-plane load (Q_1, Q_2) according to (4.56), having

$$\Delta Q_g = Q_0\delta'(x_1)\delta(x_2)\delta(t). \tag{4.87}$$

This allows a straightforward evaluation of the aforementioned displacement governed by (4.63). Indeed, on using (4.87) along with the fundamental solution (4.81), we finally arrive at

$$u_3(x_1, x_2, 0, t) = \frac{c_R Q_0(1-\beta_R^4) r\cos\theta}{8\pi\mu B}\,\frac{H\left(c_R t - r\right)}{\left(c_R^2 t^2 - r^2\right)^{3/2}}. \tag{4.88}$$

5 Generalisations of the hyperbolic-elliptic model

5.1 Coated half-space

The asymptotic formulation derived in the previous section may be extended to a coated half-space at the long-wave limit. Consider an elastic half-space H_3^+ coated by an elastic layer occupying the region $-h \le x_3 \le 0$, see Fig. 13. Throughout this subsection we assume the

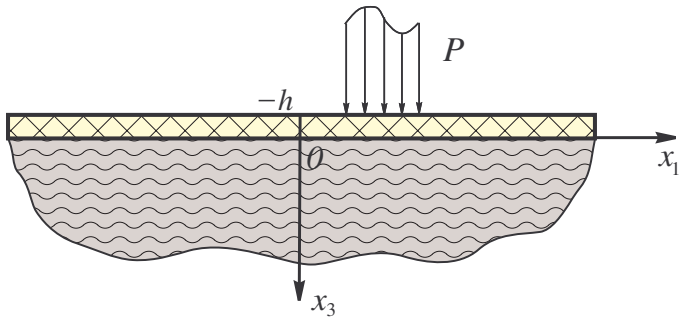

Figure 13: A half-space coated by a thin elastic layer

thickness of the coating h to be small in comparison with a typical wave length L, i.e. $h \ll L$. Similarly to subsection 4.2, we impose the boundary conditions (4.34) on the upper face of the coating $x_3 = -h$. We also assume continuity of all displacements and stresses along the interface $x_3 = 0$ and restrict ourselves to a vertical load only.

A standard asymptotic technique, applied to a thin coating, for more details see Dai et al. (2010) and references therein, results in effective boundary conditions on the interface $x_3 = 0$, namely

$$\begin{aligned} \sigma_{31} &= \rho_0 h \left\{ u_{1,tt} - c_{20}^2 \big[u_{1,22} + 4\left(1-\kappa_0^{-2}\right) u_{1,11} + \left(3-4\kappa_0^{-2}\right) u_{2,12} \big] \right\}, \\ \sigma_{32} &= \rho_0 h \left\{ u_{2,tt} - c_{20}^2 \big[u_{2,11} + 4\left(1-\kappa_0^{-2}\right) u_{2,22} + \left(3-4\kappa_0^{-2}\right) u_{1,12} \big] \right\}, \end{aligned} \tag{5.1}$$

and

$$\sigma_{33} = \rho_0 h\, u_{3,tt} + P.$$

where ρ_0 is density of the coating, c_{10} and c_{20} are associated bulk wave speeds, and $\kappa_0 = c_{10}/c_{20}$.

Thus, the original problem for a coated half-space is reduced to analysis of the homogeneous half-space H_3^+ subject to the boundary conditions (5.1) imposed along its surface $x_3 = 0$. In this case the transformed equations

$$\phi^{(\alpha)}_{,\chi\chi} + \phi^{(\alpha)}_{,33} - \frac{1}{c_1^2}\phi^{(\alpha)}_{,tt} = 0, \qquad \psi^{(\alpha)}_{,\chi\chi} + \psi^{(\alpha)}_{,33} - \frac{1}{c_2^2}\psi^{(\alpha)}_{,tt} = 0, \tag{5.2}$$

following from (4.38) and (4.40), are accompanied by the boundary conditions at $x_3 = 0$

$$\begin{aligned} \mu\left[2\phi^{(\alpha)}_{,\chi 3} + \psi^{(\alpha)}_{,\chi\chi} - \psi^{(\alpha)}_{,33}\right] &= \mu_0 h\left[c_{20}^{-2}\left(\phi^{(\alpha)}_{,\chi tt} - \psi^{(\alpha)}_{,3tt}\right) - 4\left(1-\kappa_0^{-2}\right)\left(\phi^{(\alpha)}_{,\chi\chi\chi} - \psi^{(\alpha)}_{,3\chi\chi}\right)\right], \\ \mu\left[\left(\kappa^2-2\right)\phi^{(\alpha)}_{,\chi\chi} + \kappa^2\phi^{(\alpha)}_{,33} + 2\psi^{(\alpha)}_{,\chi 3}\right] &= \mu_0 h c_{20}^{-2}\left(\phi^{(\alpha)}_{,3tt} + \psi^{(\alpha)}_{,\chi tt}\right) - P^{(\alpha)}. \end{aligned} \tag{5.3}$$

A multiple scale perturbation procedure similar to that in subsection 4.1 results in a singularly perturbed hyperbolic equation on the surface $x_3 = 0$, which can be written as

$$\phi^{(\alpha)}_{,\chi\chi} - \frac{1}{c_R^2}\,\phi^{(\alpha)}_{,tt} + \frac{bh}{\alpha_R}\,\phi^{(\alpha)}_{,3\chi\chi} = \frac{1+\beta_R^2}{2\mu B}\,P^{(\alpha)}, \tag{5.4}$$

where the constant

$$b = \frac{\mu_0}{\mu}\,\frac{(1-\beta_R^2)}{2B}\left[(1-\beta_{R0}^2)(\alpha_R+\beta_R) - 4\beta_R(1-\kappa_0^{-2})\right] \tag{5.5}$$

depends on the properties of both the substrate and the coating, with B defined in (4.24).

In the original variables, we get from (5.4)

$$\Delta\phi - \frac{1}{c_R^2}\,\phi_{,tt} + \frac{bh}{\alpha_R}\Delta\phi_{,3} = \frac{(1+\beta_R^2)\,P}{2\mu B}, \tag{5.6}$$

which is a boundary condition for the elliptic equation (4.60), where, as before, Δ is the 2D Laplace operator in the variables x_1 and x_2.

The perturbed hyperbolic equation (5.6) can also be presented in a pseudo-differential form, i.e.

$$\Delta\phi - \frac{1}{c_R^2}\,\phi_{,tt} - bh\sqrt{-\Delta}\,(\Delta\phi) = \frac{(1+\beta_R^2)\,P}{2\mu B}. \tag{5.7}$$

In the plane strain case it becomes

$$\phi_{,11} - \frac{1}{c_R^2}\,\phi_{,tt} - bh\sqrt{-\partial_{,11}}\phi_{,11} = \frac{(1+\beta_R^2)\,P}{2\mu B}. \tag{5.8}$$

This can also be rewritten using the Hilbert transform as

$$\phi_{,11} - \frac{1}{c_R^2}\,\phi_{,tt} - bh\hat{H}\phi_{,111} = \frac{(1+\beta_R^2)\,P}{2\mu B}, \tag{5.9}$$

where

$$\hat{H}f(x) = \frac{1}{\pi}\int\limits_{-\infty}^{\infty}\frac{f(\xi)}{\xi - x}\,d\xi, \tag{5.10}$$

denotes the Hilbert transform, e.g. see Erdelyi et al. (1954).

Thus, the presence of a coating inevitably leads to a pseudo-differential or an integro-differential formulation.

The derived equation enables a straightforward approximation of the exact dispersion relation, e.g. see Shuvalov & Every (2008). Naturally, we deduce from (5.8) that

$$v^{ph} = \frac{c}{c_R} = 1 - \frac{b}{2}\,|kh| + \ldots, \tag{5.11}$$

demonstrating that the Rayleigh wave speed c_R is a local extremum over the long-wave domain $kh \ll 1$, where, as usual, k denotes the wave number, see Fig. 14.

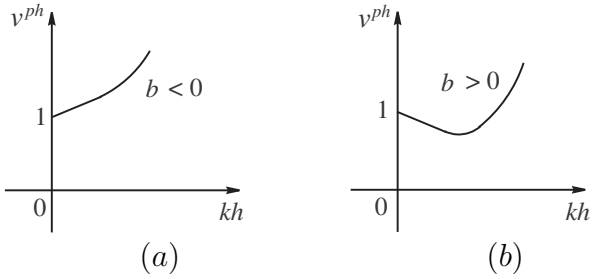

Figure 14: Local extrema of the phase speed.

In order to illustrate the developed approach, let us consider an impulse point load, setting $P = P_0\delta(x_1)\delta(t)$ in the R.H.S. of (5.8) and specify the dimensionless variables as

$$X = \frac{x_1}{L}, \qquad \tau = \frac{c_R t}{L}, \tag{5.12}$$

where L is a chosen linear scale. Then, on introducing the quantities

$$\Theta = -\frac{\phi}{B_0}, \qquad h_L = \frac{h|b|}{L} \ll 1 \tag{5.13}$$

where

$$B_0 = \frac{(1+\beta_R^2)\, c_R P_0}{4\mu B}, \tag{5.14}$$

the equation (5.8) becomes

$$\Theta_{,XX} - \Theta_{,\tau\tau} - h_L \mathrm{sgn}(b)\sqrt{-\partial_{XX}}\,\Theta_{,XX} = -\delta(X)\delta(\tau). \tag{5.15}$$

Below we implement the method of matched asymptotic expansions, see e.g. Cole (1968) and Nayfeh (2000). The inner co-ordinate associated with the boundary layer occurring in the vicinity of the Rayleigh wave front $X = \tau$ is

$$\zeta = \frac{\tau - X}{\sqrt{h_L}}. \tag{5.16}$$

Thus, the width of the boundary layer is $O(h_L^{1/2})$. On substituting (5.16) into the homogeneous equation (5.15), we obtain for the inner region at leading order

$$\Theta^{inn}_{,\tau} - \frac{h_L}{2}\,\mathrm{sgn}(b)\sqrt{-\partial_{,\zeta\zeta}}\Theta^{inn}_{,\zeta} = 0. \tag{5.17}$$

The solution of (5.17) is written as

$$\Theta^{inn} = \frac{1}{2\pi}\int\limits_{-\infty}^{\infty}\left(C(\omega)\exp\left[i\omega\left(\zeta_0 - \frac{h_L|\omega|\tau\,\mathrm{sgn}(b)}{2}\right)\right]\right)d\omega, \tag{5.18}$$

where $\zeta_0 = \tau - X$ and $C(\omega)$ has to be determined from matching with the leading oder outer expansion.

In the outer region (5.15) reduces to the wave equation

$$\Theta^{out}_{,XX} - \Theta^{out}_{,\tau\tau} = -2\delta(X)\delta(\tau), \tag{5.19}$$

from which we have

$$\Theta^{out} = H\left(\zeta_0\right) = \frac{1}{2\pi}\int\limits_{-\infty}^{\infty}\left(\pi\delta(\omega) + \frac{1}{i\omega}\right)\exp\left(i\omega\zeta_0\right)d\omega. \tag{5.20}$$

Matching of the expansions (5.18) and (5.20) yields

$$\Theta^{inn} = \frac{1}{2\pi}\int\limits_{-\infty}^{\infty}\left(\pi\delta(\omega) + \frac{1}{i\omega}\right)\exp\left[i\omega\left(\zeta_0 - \frac{h_L\omega\tau\,\mathrm{sgn}(b)}{2}\right)\right]d\omega, \tag{5.21}$$

resulting in the uniform asymptotic behaviour

$$\Theta = \frac{1}{2} - \frac{1}{\pi}\,\mathrm{sgn}(b)\,I\left(\frac{(X-\tau)\,\mathrm{sgn}(b)}{\sqrt{2h_L\tau}}\right), \tag{5.22}$$

where

$$I(x) = \int\limits_0^{\infty}\frac{\sin\left(t^2+2tx\right)}{t}\,dt = \frac{\pi}{2}\left[\frac{1}{2} + \mathrm{sgn}(x)\left[C(x)+S(x)\right] - C^2(x) - S^2(x)\right], \tag{5.23}$$

and $C(x)$ and $S(x)$ are Fresnel integrals, see e.g. Prudnikov et al. (1986),

$$C(x) = \int\limits_0^x \cos\left(\frac{\pi}{2}t^2\right)dt, \qquad S(x) = \int\limits_0^x \sin\left(\frac{\pi}{2}t^2\right)dt. \tag{5.24}$$

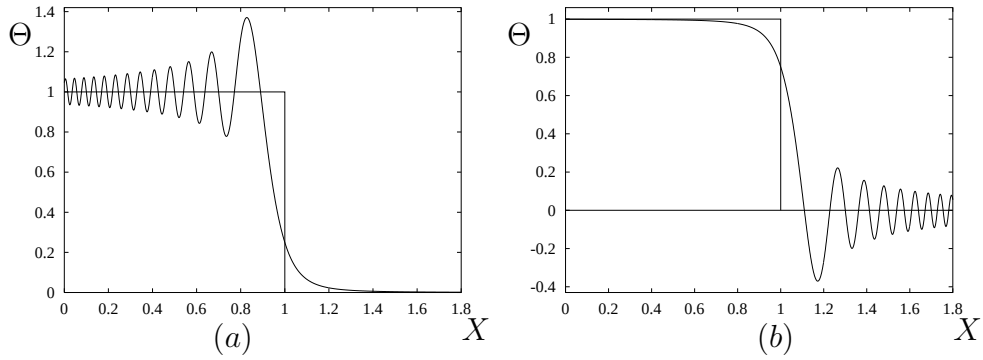

Figure 15: Receding and advancing Rayleigh wave fronts.

Numerical results illustrating the effect of the coating on smoothing the wave front are displayed in Fig. 15 for $\tau = 1$ and $h_L = 0.01$. In case $b > 0$ corresponding to the local maximum of the phase velocity at the Rayleigh wave speed, see Fig. 14(a), we observe a receding front. Another case $b < 0$ is associated with the minimum of the phase velocity leading to an advancing front, see Fig. 14(b). We also remark that similar graphs expressed in terms of Airy functions were observed for receding and advancing fronts in the problem of pre-stressed plate extension, see Kaplunov et al. (2000).

5.2 Mixed boundary value problems

The formulation for the Rayleigh wave developed in subsection 4.1 may also be extended to mixed boundary value problems in linear elasticity. Consider a *vertical stamp* acting on the surface of the elastic half-plane H_2^+, see (2.25). The boundary conditions at $x_3 = 0$ include the normal stress P and vertical displacements U_3 prescribed along the disjoint parts of the surface S_1 and S_2, $(S_1 \cup S_2 = \mathbb{R})$, respectively, see Fig. 16, along with zero tangential stress, i.e.

$$\begin{aligned} \sigma_{33} &= P(x_1, t), \quad \text{at} \quad x_1 \in S_1, \\ u_3 &= U_3(x_1, t), \quad \text{at} \quad x_1 \in S_2, \\ \sigma_{31} &= 0, \quad \text{at} \quad x_1 \in \mathbb{R}. \end{aligned} \tag{5.25}$$

On employing (4.27) and (4.28) along with (2.38), we arrive at a scalar mixed boundary value problem for the elliptic equation

$$\phi_{,33} + \alpha_R^2 \phi_{,11} = 0 \tag{5.26}$$

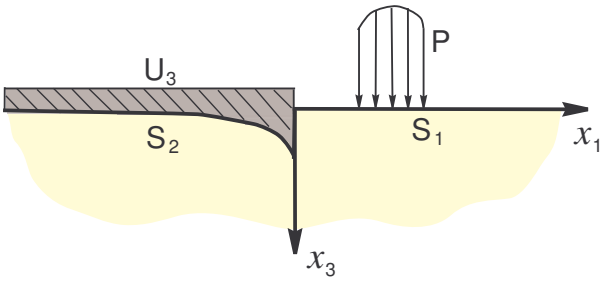

Figure 16: A vertical rigid stamp

subject to the following mixed boundary conditions along the surface $x_3 = 0$

$$\phi_{,11} - \frac{1}{c_R^2}\phi_{,tt} = \frac{1+\beta_R^2}{2\mu B}\,P, \quad \text{at} \quad x_1 \in S_1, \tag{5.27}$$

and

$$\phi_{,3} = \frac{1+\beta_R^2}{1-\beta_R^2}\,U_3, \quad \text{at} \quad x_1 \in S_2, \tag{5.28}$$

see Erbaş et al. (2013) for more detail. The shear potential ψ may then be determined through (2.38).

We stress that the approximate formulation above is meaningful only provided that the contribution of the Rayleigh wave is dominant compared to that of the bulk waves. As an example, consider the near-resonant regime of a stamp, moving steadily at the constant speed c given by (4.4), setting in the above formulae $U_3(x_1, t) = f(x_1 - ct)$ and also assuming for simplicity the absence of normal stresses on S_2, see Fig. 17.

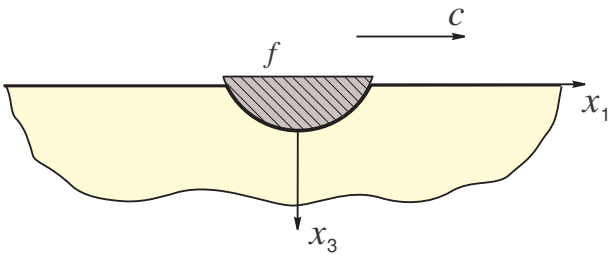

Figure 17: Steady-state motion of a rigid stamp.

On introducing the moving coordinate $s = x_1 - ct$, the problem (5.26) - (5.28) may be reduced to a standard mixed problem for the Laplace equation for the scaled normal derivative

$$\varphi_1(s, z) = \frac{\beta_R^2 - 1}{\beta_R^2 + 1}\,\phi_{,3}, \tag{5.29}$$

where $z = \alpha_R x_3$. Indeed, we have

$$\varphi_{1,zz} + \varphi_{1,ss} = 0, \tag{5.30}$$

with the mixed boundary conditions

$$\varphi_1 = f(s), \quad \text{at} \;\; s \in S_2' \tag{5.31}$$

and

$$\varphi_{1,z} = 0, \quad \text{at} \;\; s \in S_1', \tag{5.32}$$

where and S_1' and S_2' are the traction free and constrained parts of the surface $z = 0$, respectively.

The vertical displacement is expressed in terms of the quantity φ_1 as

$$u_3(s, x_3) = \frac{1}{\beta_R^2 - 1} \left[\left(\beta_R^2 + 1 \right) \varphi_1(s, \alpha_R x_3) - 2\varphi_1(s, \beta_R x_3) \right]. \tag{5.33}$$

This result matches the limiting behaviour of the exact solution (B.6), see also (B.14) and (B.15), as $c \to c_R$, leading to $\alpha \to \alpha_R$ and $\beta \to \beta_R$. It is confirmed by the numerical comparison in Erbaş et al. (2013) for a semi-infinite stamp of an exponential shape $f(s) = be^{-as}$, where $a, b > 0$. For the latter

$$\varphi_1(s, z) = b\mathrm{Re}\left\{ e^{-aq} \left[1 - \mathrm{erf}\left(\sqrt{-aq} \right) \right] \right\}, \tag{5.34}$$

where $q = s + iz$, see Sveshnikov & Tikhonov (2005), and

$$\mathrm{erf}(q) = \frac{2}{\sqrt{\pi}} \int_0^q e^{-x^2} dx$$

is the error function, e.g. see Abramowitz & Stegun (2012).

A resonant nature of the Rayleigh wave is also clearly seen from the formula for the normal stress under the stamp

$$\sigma_{33}(s, 0) = \frac{2\mu B \alpha_R^3 \left(c^2 - c_R^2 \right)}{(\beta_R^2 - 1) c_R^2} \varphi_{1,z}(s, 0) \quad \text{at} \;\; s \in S_2, \tag{5.35}$$

demonstrating that the limit as $c \to c_R$ corresponds to asymptotically vanishing stresses induced by displacements of finite magnitude.

The approach exposed in this subsection can also be adapted for high speed moving cracks and dislocations, see e.g. important contributions by Eshelby (1949), Yoffe (1951), along with the substantial book by Freund (1990). In particular, it would be interesting to apply the hyperbolic-elliptic model for surface waves to analysis of crack front waves, see Willis & Movchan (1995), Morrissey & Rice (1998), Norris & Abrahams (2007), and references therein.

5.3 Interfacial waves

In this subsection we implement the proposed methodology to the Schölte-Gogoladze and Stoneley interfacial waves introduced in section 3. Similarly to the Rayleigh wave, we obtain a scalar formulation for an elliptic equation over the interior, subject to the condition in the form of a hyperbolic equation along the interface.

5.3.1 Schölte-Gogoladse wave

The equations of motion are given by (2.27) and (3.1), respectively. Let us focus on the wave field arising from a vertical interfacial load P, assuming the following contact conditions at $x_3 = 0$

$$\sigma_{31} = 0, \qquad u_3 = v, \qquad \sigma_{33} - p_f = P(x_1, t). \tag{5.36}$$

The relations (5.36) expressed in terms of the potentials ϕ, ψ, and χ become

$$\begin{aligned} 2\phi_{,13} - \psi_{,11} + \psi_{,33} &= 0, \\ \phi_{,3} + \psi_{,1} - \chi_{,3} &= 0, \\ \mu\left[\left(\kappa^{-2} - 2\right)\phi_{,11} + \kappa^{-2}\phi_{,33} - 2\psi_{,13}\right] - \rho_f \chi_{,tt} &= P. \end{aligned} \tag{5.37}$$

Then, similarly to the consideration in subsection 4.1, we establish a multiscale perturbation procedure resulting in an approximate hyperbolic-elliptic formulation for the Schölte-Gogoladze wave. The behaviour over the interior is again governed by the *elliptic* equation

$$\phi_{,33} + \alpha_{SG}^2 \phi_{,11} = 0, \tag{5.38}$$

whereas the wave propagation along the interface is described by the *hyperbolic* equation

$$\frac{\partial^2 \phi}{\partial x_1^2} - \frac{1}{c_{SG}^2}\frac{\partial^2 \phi}{\partial t^2} = \frac{1 + \beta_{SG}^2}{2\mu B_{SG}}\, P, \tag{5.39}$$

where

$$\begin{aligned} B_{SG} = \frac{\beta_{SG}}{\alpha_{SG}}\left(1 - \alpha_{SG}^2\right) + \frac{\alpha_{SG}}{\beta_{SG}}\left(1 - \beta_{SG}^2\right) - 1 + \beta_{SG}^4 \\ - \frac{\rho_f}{\rho}\frac{\left(1 - \beta_{SG}^2\right)^2\left(\gamma_{SG}^2 - \alpha_{SG}^2 - 4\alpha_{SG}^2\gamma_{SG}^2\right)}{4\alpha_{SG}\gamma_{SG}^3}, \end{aligned} \tag{5.40}$$

with α_{SG}, β_{SG}, and γ_{SG} defined by (3.7).

The potentials ψ and χ are related to ϕ as

$$\psi(x_1, \beta_{SG} x_3, t) = \frac{2\alpha_{SG}}{1+\beta_{SG}^2}\, \phi^*(x_1, \beta_{SG} x_3, t), \tag{5.41}$$

and

$$\chi(x_1, \gamma_{SG} x_3, t) = -\frac{1-\beta_{SG}^2}{1+\beta_{SG}^2}\, \phi(x_1, \gamma_{SG} x_3, t). \tag{5.42}$$

5.3.2 Stoneley wave

In case of the wave propagating along a solid-solid interface the statement of the problem includes the equations of motion (3.11), subject to

$$\begin{aligned}
\phi_{1,1} - \phi_{2,1} + \psi_{1,3} - \psi_{2,3} &= 0,\\
\phi_{1,3} - \phi_{2,3} - \psi_{1,1} + \psi_{2,1} &= 0\\
2\mu_1\phi_{1,13} - 2\mu_2\phi_{2,13} + \mu_1\left(\psi_{1,33} - \psi_{1,11}\right) - \mu_2\left(\psi_{2,33} - \psi_{2,11}\right) &= 0,\\
\lambda_1\phi_{1,11} + \left(\lambda_1 + 2\mu_1\right)\phi_{1,33} - \lambda_2\phi_{2,11} - \left(\lambda_2 + 2\mu_2\right)\phi_{2,33} - 2\mu_1\psi_{1,13} + 2\mu_2\psi_{2,13} &= P,
\end{aligned} \tag{5.43}$$

where $P = P(x_1, t)$ is once again a prescribed vertical disturbance.

The asymptotic model for the Stoneley wave arising from the boundary value problem (3.11) and (5.43), contains the *elliptic* equation

$$\phi_{1,33} + \alpha_{1S}^2 \phi_{1,11} = 0, \tag{5.44}$$

governing the behaviour over the interior. The rest of the wave potentials are determined by

$$\begin{aligned}
\psi_2(x_1, \beta_{2S} x_3, t) &= \frac{f_4}{f_1 \beta_{2S}}\, \phi_1^*(x_1, \beta_{2S} x_3, t),\\
\phi_2(x_1, \alpha_{2S} x_3, t) &= \frac{f_2}{f_1}\, \phi_1(x_1, \alpha_{2S} x_3, t),\\
\psi_1(x_1, \beta_{1S} x_3, t) &= \frac{f_3}{f_4}\, \psi_2(x_1, \beta_{1S} x_3, t),
\end{aligned} \tag{5.45}$$

where

$$\begin{aligned}
f_1 &= (m_{12} - \rho_1 c_S^2) b_2 + \rho_2 c_S^2 (1 + \alpha_{2S}\beta_{1S}),\\
f_2 &= (\rho_2 c_S^2 + m_{12}) b_1 - \rho_1 c_S^2 (1 + \alpha_{1S}\beta_{2S}),\\
f_3 &= \rho_2 c_S^2 (\alpha_{1S} + \alpha_{2S}) - m_{12}\alpha_{1S} b_2,\\
f_4 &= \rho_1 c_S^2 (\alpha_{1S} + \alpha_{2S}) - m_{12}\alpha_{2S} b_1,
\end{aligned} \tag{5.46}$$

with the problem parameters introduced in subsection 3.2, see (3.16).

The *hyperbolic* equation for ϕ_1 on the interface $x_3 = 0$ is written as

$$\phi_{1,11} - \frac{1}{c_S^2}\phi_{1,tt} = \frac{f_1 P}{c_S^2 B_S}, \tag{5.47}$$

where the constant B_S is given by

$$\begin{aligned} B_S = &-2c_S^2\left[(\rho_1-\rho_2)^2 - a_1a_2\right] - m_{12}c_S^2\left(\rho_2 l_2 - \rho_1 l_1\right) \\ &-\frac{m_{12}^2}{2}\left(b_2 l_1 + b_1 l_2\right) - \frac{c_S^4}{2}\left(d_1 a_2 + d_2 a_1\right) + 2m_{12}\left(\rho_2 b_1 - \rho_1 b_2\right), \end{aligned} \tag{5.48}$$

with

$$d_n = \frac{\rho_2}{\alpha_{nS}c_{1n}^2} + \frac{\rho_1}{\beta_{nS}c_{2n}^2}, \qquad l_n = \frac{\alpha_{nS}}{\beta_{nS}c_{2n}^2} + \frac{\beta_{nS}}{\alpha_{nS}c_{1n}^2}, \qquad (k = 1, 2).$$

It is remarkable that even though the models for the interfacial Stoneley and Schölte-Gogoladze waves contain rather cumbersome material constants B_{SG} and B_S, the obtained formulations are not more difficult than that for the Rayleigh wave, due to the relations (5.41), (5.42), and (5.45) allowing reduction to a scalar elliptic problem for one of the potentials.

5.4 Bleustein-Gulyaev wave

Next consider the antiplane motion of the transversely isotropic piezoelastic half-plane $\mathcal{H}_2^+$, with the out of plane axis oriented along the direction of the sixfold axis for a crystal in the symmetry class C_{6mm}. The associated surface wave was discovered independently by Bleustein (1968) and Gulyaev (1969), see also Ikeda (1990). The governing equations of motion are written as

$$u_{2,11} + u_{2,33} - c_e^{-2}u_{2,tt} = 0, \qquad \psi_{e,11} + \psi_{e,33} = 0, \tag{5.49}$$

where u_2 is the out of plane displacement, ψ_e is a complementary function related to the electric potential ϕ_e as

$$\psi_e = \phi_e - \frac{e_{15}}{\epsilon_{11}}\,u_2 \tag{5.50}$$

with

$$c_e = \left(\frac{\overline{c}_{44}}{\rho}\right)^{1/2}, \qquad \overline{c}_{44} = c_{44} + \frac{e_{15}^2}{\epsilon_{11}}. \tag{5.51}$$

Here $\overline{c}_{44}$ is the piezoelectrically stiffened elastic constant, ρ is the volume mass density, c_e is the low-frequency limit of the shear horizontal wave speed, and c_{44}, e_{15}, and ϵ_{11} are the elastic, piezoelectric, and dielectric constants, respectively.

In what follows we study two types of boundary conditions along the surface $x_3 = 0$, e.g. see Kaplunov et al. (2006), including a surface coated by an infinitesimally thin perfectly conducting grounded electrode, for which

$$\sigma_{32} = \overline{c}_{44} u_{2,3} + e_{15}\psi_{e,3} = P, \qquad \phi_e = 0, \tag{5.52}$$

and also a surface in contact with a vacuum modelled by

$$\sigma_{32} = P, \qquad \phi_e = \hat{\phi}_e, \qquad e_{15}u_{2,3} - \epsilon_{11}\phi_{e,3} = \hat{\phi}_{e,3}. \tag{5.53}$$

In the above $\hat{\phi}_e$ is the electric potential in a vacuum satisfying

$$\hat{\phi}_{e,11} + \hat{\phi}_{e,33} = 0, \qquad x_3 \le 0, \tag{5.54}$$

and $P = P(x_1, t)$ denotes a prescribed mechanical load along the surface $x_3 = 0$.

First, we derive the eigensolution of arbitrary time-dependence for a surface coated with an electrode, see (5.52) at $P = 0$. The travelling wave ansatz, similar to (2.43), now takes the form

$$u_{2,tt} - c^2 u_{2,11} = 0, \qquad \phi_{e,tt} - c^2 \phi_{e,11} = 0, \tag{5.55}$$

where c is the sought for phase speed. Then, (5.49) implies

$$u_{2,33} + \alpha_e^2 u_{2,11} = 0, \qquad \psi_{e,11} + \psi_{e,33} = 0, \tag{5.56}$$

with

$$\alpha_e^2 = 1 - \frac{c^2}{c_e^2}. \tag{5.57}$$

The solution of (5.56) may be expressed in terms of plane harmonic functions as

$$u_2 = u_2(x_1, \alpha_e x_3, t), \qquad \psi_e = \psi_e(x_1, x_3, t). \tag{5.58}$$

On substituting the latter into (5.52) and employing the Cauchy-Riemann identities, we have at $x_3 = 0$

$$\begin{aligned} \alpha_e \overline{c}_{44} u_{2,1} + e_{15}\psi_{e,1} = 0, \\ e_{15}u_2 + \epsilon_{11}\psi_e = 0. \end{aligned} \tag{5.59}$$

Hence, we get from the solvability

$$c = c_{BG} = c_e\sqrt{1 - \alpha_{BG}^2}, \tag{5.60}$$

coinciding with Bleustein (1968), where α_{BG} is the electromechanical coupling factor

$$\alpha_{BG} = \frac{e_{15}^2}{\epsilon_{11}\overline{c}_{44}}. \tag{5.61}$$

The eigenfunctions u_2 and ψ_e are related as

$$u_2(x_1, \alpha_{BG}x_3, t) = -\frac{e_{15}}{\overline{c}_{44}\alpha_{BG}}\,\psi_e(x_1, \alpha_{BG}x_3, t), \tag{5.62}$$

being a counterpart of (2.37) for the Rayleigh wave.

In the same manner, for a surface contacting with a vacuum we insert (5.58) together with the implicit ansatz

$$\hat{\phi}_{e,tt} - c^2\hat{\phi}_{e,11} = 0 \tag{5.63}$$

into (5.53), having the following boundary conditions at $x_3 = 0$

$$\begin{aligned} \alpha_e\overline{c}_{44}u_{2,1} + e_{15}\psi_{e,1} &= 0, \\ e_{15}u_2 + \epsilon_{11}(\psi_e - \hat{\phi}_e) &= 0, \\ \epsilon_{11}\psi_{e,3} + \hat{\phi}_{e,3} &= 0. \end{aligned} \tag{5.64}$$

These formulae lead to the same expression (5.60), with the coupling factor

$$\alpha_{BG} = \frac{e_{15}^2}{\epsilon_{11}(1+\epsilon_{11})\,\overline{c}_{44}}. \tag{5.65}$$

Finally, in addition to (5.62), the electrical potential in a vacuum is given by

$$\hat{\phi}_e(x_1, x_3, t) = \epsilon_{11}\,\psi_e(x_1, -x_3, t). \tag{5.66}$$

In case of a non-zero mechanical forcing P in (5.52) and (5.53) a hyperbolic-elliptic formulation extracting the contribution of the piezoelastic surface wave to the overall dynamic response may be derived, for more detail see Kaplunov et al. (2006). For a coated surface (5.52) it contains the elliptic equation

$$u_{2,33} + \alpha_{BG}^2 u_{2,11} = 0, \tag{5.67}$$

where α_{BG} is defined by (5.61), with the boundary condition at $x_3 = 0$ arising from the hyperbolic equation

$$\chi_{e,11} - \frac{1}{c_{BG}^2}\chi_{e,tt} = \frac{2\alpha_{BG}^2}{\rho c_{BG}^2}\,P_{,11}, \tag{5.68}$$

where $\chi_e = u_{2,3}$. The function ψ_e is then determined from (5.58). For a surface contacting with a vacuum we get the same relations (5.67), (5.68), and (5.58), with α_{BG} now given by (5.65). The electrical potential in a vacuum $\hat{\phi}_e$ may be obtained from (5.66).

5.5 Effect of anisotropy

The described methodology may also be adapted for anisotropic media. The surface wave eigensolution in terms of a single harmonic function has been recently derived in Parker (2013) for arbitrary anisotropy by means of the Stroh formalism. Here we present briefly a more explicit result obtained by Prikazchikov (2013) for an orthorhombic half-plane.

The equations of motion are written as

$$\begin{aligned} c_{11}u_{1,11} + c_{55}u_{1,33} + (c_{13} + c_{55})\, u_{3,13} = \rho\ddot{u}_1, \\ (c_{13} + c_{55})\, u_{1,13} + c_{55}u_{3,11} + c_{33}u_{3,33} = \rho\ddot{u}_3, \end{aligned} \tag{5.69}$$

where c_{11}, c_{13}, c_{33}, and c_{55} are the stiffness components satisfying the conditions

$$c_{11} > 0, \qquad c_{11}c_{33} - c_{13}^2 > 0, \qquad c_{55} > 0, \tag{5.70}$$

ensuring the positive definiteness of the strain-energy density, see Chadwick (1976a). The stress-free boundary conditions along the surface $x_3 = 0$ of the half-plane $\mathcal{H}_2^+$ are expressed in terms of the displacements as

$$u_{1,3} + u_{3,1} = 0, \qquad c_{13}u_{1,1} + c_{33}u_{3,3} = 0. \tag{5.71}$$

As in subsection 2.2, we start from the implicit travelling wave ansatz

$$u_{j,tt} - c^2 u_{j,11} = 0, \qquad j = 1, 3, \tag{5.72}$$

where, as usual, c is the sought for surface wave speed, see also (2.43). Substitution of the latter into the equations (5.69) gives

$$\begin{aligned} \left(c_{11} - \rho c^2\right) u_{1,11} + c_{55}u_{1,33} + \beta u_{3,13} = 0, \\ \beta u_{1,13} + \left(c_{55} - \rho c^2\right) u_{3,11} + c_{33}u_{3,33} = 0, \end{aligned} \tag{5.73}$$

with $\beta = c_{13} + c_{55}$.

On eliminating one of the displacements, (5.73) may be transformed to a fourth order partial differential equation. For example, we obtain in terms of u_1

$$u_{1,1111} + \delta u_{1,1133} + \gamma u_{1,3333} = 0, \tag{5.74}$$

where

$$\delta = \frac{c_{55}^2 + c_{11}c_{33} - \beta^2 - (c_{33} + c_{55})\rho c^2}{c_{33}c_{55}}, \qquad \gamma = \frac{(c_{11} - \rho c^2)(c_{55} - \rho c^2)}{c_{33}c_{55}} \tag{5.75}$$

throughout this subsection.

It it not difficult to verify that the equation (5.74) is elliptic, with δ and γ coinciding with the coefficients in the related secular equation for the attenuation orders, see e.g. Royer & Dieulesaint (1996). It may therefore be rewritten in an operator form as

$$\left[\partial_{33} + \Lambda_1^2 \partial_{11}\right]\left[\partial_{33} + \Lambda_2^2 \partial_{11}\right] u_1 = 0, \tag{5.76}$$

where

$$\Lambda_1^2 + \Lambda_2^2 = \delta, \qquad \Lambda_1^2 \Lambda_2^2 = \gamma. \tag{5.77}$$

Hence, the solution of (5.76) is

$$u_1 = \sum_{n=1}^{2} U_n\left(x_1, \Lambda_n x_3, t\right), \tag{5.78}$$

where U_n are arbitrary plane harmonic functions in the first two arguments. Then, on employing the Cauchy-Riemann identities, it is possible to express the remaining displacement from (5.73) as

$$u_3 = \sum_{n=1}^{2} T(\Lambda_n, \rho c^2) U_n^*\left(x_1, \Lambda_n x_3, t\right), \tag{5.79}$$

with the asterisk, as before, denoting a harmonic conjugate and

$$T(\Lambda_n, \rho c^2) = \frac{c_{55}\Lambda_n^2 - c_{11} + \rho c^2}{\beta \Lambda_n}. \tag{5.80}$$

The solutions (5.78) and (5.79) are now substituted into the boundary conditions (5.71), giving

$$\begin{aligned} &\sum_{n=1}^{2} \left(T\left(\Lambda_n, \rho c^2\right) - \Lambda_n\right) U_{n,1}\left(x_1, 0, t\right) = 0, \\ &\sum_{n=1}^{2} \left(c_{13} + c_{33}\Lambda_n T(\Lambda_n, \rho c^2)\right) U_{n,1}\left(x_1, 0, t\right) = 0. \end{aligned} \tag{5.81}$$

The solvability dictates

$$c_{33}c_{55}\rho^2 c^4 \left(c_{11} - \rho c^2\right) - \left(c_{55} - \rho c^2\right)\left[c_{33}\left(c_{11} - \rho c^2\right) - c_{13}^2\right]^2 = 0, \tag{5.82}$$

coinciding with the surface wave equation in an orthorhombic half-plane, see again Royer & Dieulesaint (1996). Then, as in subsection 2.2, we express the displacements in terms of a single harmonic function. Indeed, as follows from (5.81), the functions U_1 and U_2 are related as

$$U_2(x_1, \Lambda_2 x_3, t) = -Y(\rho c_R^2)\, U_1(x_1, \Lambda_2 x_3, t), \tag{5.83}$$

where $c = c_R$ is the unique real root of (5.82) and

$$Y(\rho c_R^2) = \frac{T(\Lambda_1, \rho c_R^2) - \Lambda_1}{T(\Lambda_2, \rho c_R^2) - \Lambda_2}.$$

Therefore, the representation of the surface wave field through the plane harmonic function U_1 is given by

$$\begin{aligned} u_1(x_1, x_3, t) &= U_1(x_1, \Lambda_1 x_3, t) - Y(\rho c_R^2)\, U_1(x_1, \Lambda_2 x_3, t), \\ u_2(x_1, x_3, t) &= T(\Lambda_1, \rho c_R^2) U_1^*(x_1, \Lambda_1 x_3, t) - T(\Lambda_2, \rho c_R^2)\, Y(\rho c_R^2)\, U_1^*(x_1, \Lambda_2 x_3, t). \end{aligned} \tag{5.84}$$

This eigensolution is a key preliminary step for deriving a hyperbolic-elliptic model for the surface wave in anisotropic media.

6 Moving load problems

This is seemingly the optimal setup for validating the asymptotic considerations in the subsections 4.1, 4.2 and 5.1. First of all, a near-resonant moving load obeys the basic assumption (4.4). At the same time there are several benchmark exact solutions available in literature, including the famous paper by Cole & Huth (1958). In addition, a further insight into near-resonant regimes of moving loads is inspired by the needs of modern high-speed transport, e.g. see Dieterman & Metrikine (1996), de Hoop (2002), Cao et al. (2012), and also experimental data in Madshus & Kaynia (2000).

6.1 Plane strain steady-state problem

We begin with the plane strain problem for a steadily moving vertical line force, see Fig. 18, using the hyperbolic-elliptic model derived in subsection 4.1, with $P = P_0\delta(x_1 - ct)$ in the wave equation (4.27) along the surface $x_3 = 0$. Here c is a constant speed of the load, which is assumed to be close to the Rayleigh wave speed, see (4.4).

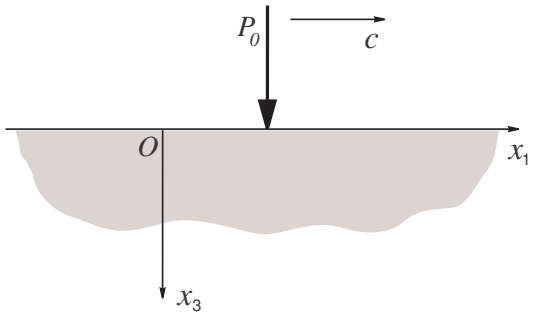

Figure 18: A line force travelling along the surface of a half-space.

Then, (4.27) reduces to

$$\phi_{,ss}(s,0) = \frac{(1+\beta_R^2)c_R^2 P_0}{2\mu B\,(c_R^2 - c^2)}\,\delta(s), \tag{6.1}$$

where $s = x_1 - ct$ is a moving coordinate. Remarkably, the resonant effect at $c = c_R$ follows immediately from an elementary analysis of the surface behaviour (6.1). On integrating the last equation with respect to s, we deduce

$$\phi_{,s}(s,0) = \frac{(1+\beta_R^2)c_R^2 P_0}{2\mu B\,(c_R^2 - c^2)}\left[H(s) - \frac{1}{2}\right], \tag{6.2}$$

where H denotes the Heaviside function and a constant of integration is chosen because of symmetry.

Let us focus on the derivative $\varphi = \phi_{,s}$, for which

$$\varphi_{,33} + \alpha_R^2 \varphi_{,ss} = 0, \tag{6.3}$$

following from (4.28), subject to the boundary condition (6.2). On employing the Poisson formula, e.g. see Courant & Hilbert (1989), we obtain

$$\begin{aligned} \phi_{,s}(s,x_3) = \frac{(1+\beta_R^2)c_R^2 P_0}{2\mu B\,(c_R^2-c^2)} \int\limits_{-\infty}^{\infty} \frac{\alpha_R x_3}{(r-s)^2+\alpha_R^2 x_3^2} \left[H(r)-\frac{1}{2}\right] dr \\ = \frac{(1+\beta_R^2)P_0 c_R^2}{2\pi\mu B\,(c_R^2-c^2)}\, \tan^{-1}\frac{s}{\alpha_R\, x_3}. \end{aligned} \tag{6.4}$$

The derivative of the transverse potential ψ is restored through the relations (2.38), giving

$$\psi_{,s}(s,x_3) = -\frac{\alpha_R P_0 c_R^2}{4\pi\mu B\,(c_R^2-c^2)}\, \ln\left(s^2+\beta_R^2\, x_3^2\right). \tag{6.5}$$

On using the Cauchy-Riemann identities, the steady-state displacements are written as

$$\begin{aligned} u_1^{st}(\xi) &= \frac{(1+\beta_R^2)P_0 v_R^2}{2\mu\pi B(v_R^2-v^2)}\left[\tan^{-1}\frac{\xi}{\alpha_R} - \frac{1+\beta_R^2}{2}\tan^{-1}\frac{\xi}{\beta_R}\right], \\ u_2^{st}(\xi) &= -\frac{(1+\beta_R^2)P_0 v_R^2 \alpha_R}{4\mu\pi B(v_R^2-v^2)}\left[\ln(\xi^2+\alpha_R^2) - \frac{2}{1+\beta_R^2}\ln(\xi^2+\beta_R^2)\right], \end{aligned} \tag{6.6}$$

with the following dimensionless quantities

$$\xi = \frac{s}{x_3}, \qquad v = \frac{c}{c_2}, \qquad v_R = \frac{c_R}{c_2}.$$

It is worth noting that the displacements (6.6) do not decay at infinity in contrast to the Rayleigh wave eigensolutions in subsection 2.2. At the same time, it is possible to show that (6.6) is the leading order Taylor expansion of the exact solution around the Rayleigh speed $c = c_R$ presented in Appendix B, see (B.11).

In Fig. 19 we present the graphs of the scaled stresses

$$S_{33} = \frac{\pi\sigma_{33}x_3}{P_0}, \tag{6.7}$$

against the speed v at $\xi = 0.1$ and $\nu = \frac{1}{4}$ corresponding to $v_R \approx 0.9194$.

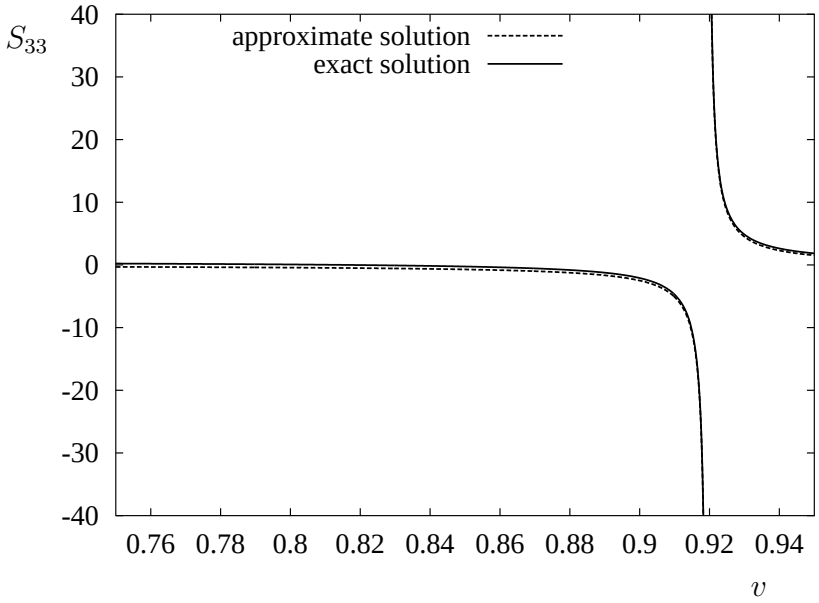

Figure 19: The near-resonant stresses (6.8) and (6.9).

The exact solution

$$S_{33} = \frac{\alpha}{R(c)} \left[\frac{(1+\beta^2)^2}{\xi^2+\alpha^2} - \frac{4\beta^2}{\xi^2+\beta^2} \right] \tag{6.8}$$

corresponding to the displacements (B.11) is shown by the solid line, whereas the asymptotic formula

$$S_{33} = \frac{2\alpha_R\beta_R v_R^2}{(v_R^2-v^2)B} \left[-\frac{\alpha_R}{\xi^2+\alpha_R^2} + \frac{\beta_R}{\xi^2+\beta_R^2} \right] \tag{6.9}$$

following from (6.6), is depicted by the dashed line. It may be easily shown that over the near-resonant region, as the speed c is defined by (4.4), the limiting behaviour of (6.8) agrees with (6.9), since

$$\alpha \sim \alpha_R, \qquad \beta \sim \beta_R, \qquad R(c) \sim 4\varepsilon B, \qquad \frac{v_R - v^2}{v_R^2} \sim -2\varepsilon, \tag{6.10}$$

with B defined in (4.24).

6.2 Transient plane strain problem

Next, we address the associated transient problem. In this case the boundary condition for (6.3) at $x_3 = 0$ is written as

$$\phi_{,ss} - \frac{1}{c_R^2}\,\phi_{,tt} = \frac{(1+\beta_R^2)\,P_0}{2\mu B}\delta(s). \tag{6.11}$$

On calculating the convolution of the moving impulse with the fundamental solution, see

(4.72), we have for the potential ϕ along the surface, see Kaplunov et al. (2010) for more detail,

$$\phi(s,0,t) = B_0 \int\limits_0^t \left[H\left(s+(c-c_R)r\right) - H\left(s+(c+c_R)r\right)\right] dr, \tag{6.12}$$

where B_0 has been introduced in (5.14). Then, we immediately derive from (6.12)

$$\phi(s,0,t) = \begin{cases} B_0 \dfrac{s-s_1}{c_R-c}, & 0 \le s < s_1; \\ B_0 \dfrac{s-s_2}{c_R+c}, & s_2 < s < 0; \\ 0, & \text{otherwise}, \end{cases} \tag{6.13}$$

and

$$\phi(s,0,t) = \begin{cases} 2B_0 \dfrac{c_R s}{c^2-c_R^2}, & s_1 \le s \le 0; \\ -B_0 \dfrac{s-s_2}{c_R+c}, & s_2 < s < s_1; \\ 0, & \text{otherwise}. \end{cases} \tag{6.14}$$

for the *sub-Rayleigh* ($c < c_R$) and *super-Rayleigh* ($c > c_R$) regimes, respectively. In the above the values s_1 and s_2 are

$$s_1 = t(c_R - c), \qquad \text{and} \qquad s_2 = -t(c_R + c). \tag{6.15}$$

For the *resonant regime* ($c = c_R$) we have

$$\phi(s,0,t) = \begin{cases} -B_0 \dfrac{s-s_2}{2c_R}, & s_2 \le s \le 0; \\ 0, & \text{otherwise}, \end{cases} \tag{6.16}$$

with $s_2 = -2c_R t$.

Analysis of the 1D problem along the surface, resulting in the solutions (6.13), (6.14), and (6.16), provides an immediate insight into the peculiarities of the near-resonant transient phenomena. The plots of the function $\phi(s,0,t)$ at a fixed time instance t in Fig. 20 show that the resonant regime is clearly distinctive from the two others. If $c \neq c_R$, the solution in question is continuous in s, see Figs 20(a) and 20(b). At the same time, the limiting resonant solution in Fig. 20(c) demonstrates a discontinuity under the force ($s = 0$), which grows linearly in time. As a result, we should not expect a steady-state regime at $c = c_R$. Thus, a

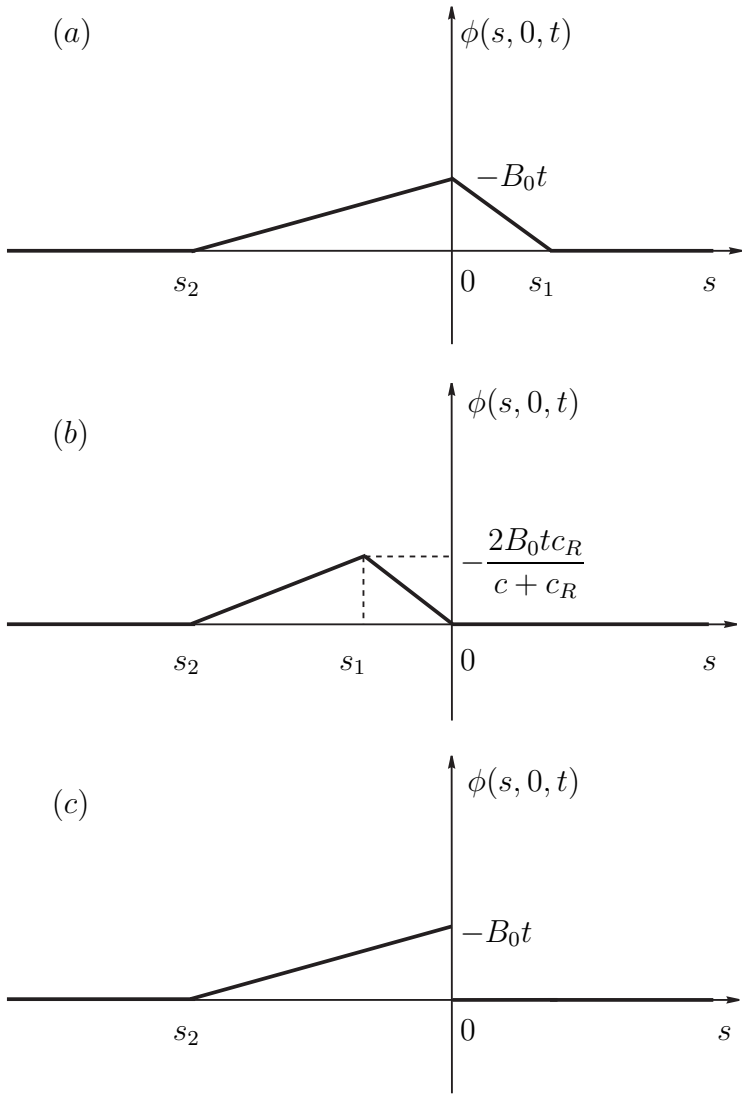

Figure 20: The longitudinal wave potential ϕ vs. the moving co-ordinate s along the surface $x_3 = 0$: (a) sub-Rayleigh regime ($c < c_R$); (b) super-Rayleigh regime ($c > c_R$); (c) resonant regime ($c = c_R$).

rather trivial analysis of the 1D moving load problem (6.11) for an infinite string reveals the resonant phenomena associated with the Rayleigh wave.

Once the potential ϕ is determined along the surface $x_3 = 0$, it may then be restored over the interior through the Poisson formulae, as in the previous subsection. In the *sub-Rayleigh*

and *super-Rayleigh* regimes the displacement components are given by

$$
\begin{aligned}
u_1(\xi,\tau) = {} & \frac{2B_0\, v_R}{\pi c_2(v_R^2 - v^2)}\left[\arctan\frac{\xi}{\alpha_R} - \frac{1+\beta_R^2}{2}\arctan\frac{\xi}{\beta_R}\right] \\
& - \frac{B_0}{\pi c_2(v_R + v)}\left[\arctan\frac{\xi-\xi_2}{\alpha_R} - \frac{1+\beta_R^2}{2}\arctan\frac{\xi-\xi_2}{\beta_R}\right] \\
& - \frac{B_0}{\pi c_2(v_R - v)}\left[\arctan\frac{\xi-\xi_1}{\alpha_R} - \frac{1+\beta_R^2}{2}\arctan\frac{\xi-\xi_1}{\beta_R}\right],
\end{aligned}
\tag{6.17}
$$

and

$$
\begin{aligned}
u_3(\xi,\tau) = {} & \frac{B_0\,\alpha_R}{2\pi c_2(v_R+v)}\left[\ln\frac{(\xi-\xi_2)^2+\alpha_R^2}{\xi^2+\alpha_R^2} - \frac{2}{1+\beta_R^2}\ln\frac{(\xi-\xi_2)^2+\beta_R^2}{\xi^2+\beta_R^2}\right] \\
& + \frac{B_0\,\alpha_R}{2\pi c_2(v_R-v)}\left[\ln\frac{(\xi-\xi_1)^2+\alpha_R^2}{\xi^2+\alpha_R^2} - \frac{2}{1+\beta_R^2}\ln\frac{(\xi-\xi_1)^2+\beta_R^2}{\xi^2+\beta_R^2}\right],
\end{aligned}
\tag{6.18}
$$

with

$$
\tau = \frac{c_2 t}{x_3}, \qquad \xi_1 = \frac{s_1}{x_3} = (v_R - v)\tau, \qquad \xi_2 = \frac{s_2}{x_3} = -(v + v_R)\tau, \tag{6.19}
$$

and s_1 and s_2 defined by (6.15). For the *resonant* regime we obtain

$$
\begin{aligned}
u_1(\xi,\tau) = {} & \frac{B_0\alpha_R\tau}{\pi c_2}\left[\frac{1}{\xi^2+\alpha_R^2} - \frac{2\beta_R^2}{(1+\beta_R^2)(\xi^2+\beta_R^2)}\right] \\
& + \frac{\beta}{2\pi c_2 v_R}\left[\arctan\frac{\xi}{\alpha_R} - \arctan\frac{\xi-\xi_2}{\alpha_R}\right] \\
& - \frac{B_0(1+\beta_R^2)}{4\pi c_2 v_R}\left[\arctan\frac{\xi}{\beta_R} - \arctan\frac{\xi-\xi_2}{\beta_R}\right],
\end{aligned}
\tag{6.20}
$$

and

$$
\begin{aligned}
u_3(\xi,\tau) = {} & \frac{B_0\alpha_R\xi\tau}{\pi c_2}\left[\frac{2}{(1+\beta_R^2)(\xi^2+\beta_R^2)} - \frac{1}{\xi^2+\alpha_R^2}\right] \\
& + \frac{B_0\alpha_R}{4\pi c_2 v_R}\left[\ln\frac{(\xi-\xi_2)^2+\alpha_R^2}{\xi^2+\alpha_R^2} - \frac{2}{1+\beta_R^2}\ln\frac{(\xi-\xi_2)^2+\beta_R^2}{\xi^2+\beta_R^2}\right],
\end{aligned}
\tag{6.21}
$$

with $\xi_2 = -2v_R\tau$.

The obtained displacements (6.17)-(6.21) are expressed in terms of elementary functions in contrast to the integral exact solution of the problem presented in Appendix of Kaplunov et al. (2010). The approximate solution also captures all of the key features of the studied problem. In particular, a large time limiting behaviour as $\tau \to \infty$ is immediately deduced from the formulae above. In the sub-Rayleigh regime we have

$$
u_i(\xi,\tau) \sim u_i^{\infty}(\xi,\tau), \qquad u_i^{\infty}(\xi,\tau) = u_i^{st}(\xi) + u_i^{r}(\tau), \qquad i = 1, 2, \tag{6.22}
$$

where u_i^{st} are the steady-state displacements calculated in the previous subsection, see (6.6), whereas

$$u_1^r(\tau) = u_1^{r0}, \qquad u_2^r(\tau) = u_2^{r0} + u_2^{r\tau}(\tau), \tag{6.23}$$

with

$$\begin{aligned} u_1^{r0} &= \frac{B_0 v\,(1-\beta_R^2)}{2c_2(v_R^2 - v^2)}, \\ u_2^{r0} &= -\frac{B_0\alpha_R(1-\beta_R^2)}{\pi c_2(1+\beta_R^2)}\left[\frac{\ln(v_R+v)}{v_R+v} + \frac{\ln|v_R-v|}{v_R-v}\right], \end{aligned} \tag{6.24}$$

and

$$u_2^{r\tau}(\tau) = -\frac{2B_0 v_R \alpha_R(1-\beta_R^2)}{\pi c_2(v_R^2 - v^2)(1+\beta_R^2)}\ln\tau.$$

Here u_i^r $(i = 1, 2)$ are the components of the rigid body motion of the half-space. It is remarkable that the rigid body motion along the vertical axis demonstrates a logarithmic growth in time according to (6.23) and (6.24), which was first noted in Kaplunov (1986). This means that the steady-state regime for the vertical displacement established in subsection 5.1, cannot be reached at a large time limit.

The formulae (6.22)-(6.24) are also valid for the super-Rayleigh case, except the expression for the rigid body motion component along the horizontal axis, which is now given by

$$u_1^{r0} = -\frac{B_0 v_R\,(1-\beta_R^2)}{2c_2(v_R^2 - v^2)}. \tag{6.25}$$

In the resonant case the limiting behaviour as $\tau \to \infty$ is

$$u_i(\xi,\tau) \sim u_i^{\infty}(\xi,\tau) \qquad (i = 1, 2), \tag{6.26}$$

with

$$u_1^{\infty}(\xi,\tau) = \frac{B_0\alpha_R\tau}{\pi c_2}\left[\frac{1}{\xi^2+\alpha_R^2} - \frac{2\beta_R^2}{(1+\beta_R^2)(\xi^2+\beta_R^2)}\right], \tag{6.27}$$

and

$$\begin{aligned} u_2^{\infty}(\xi,\tau) = {} & \frac{B_0\alpha_R\xi\tau}{\pi c_2}\left[\frac{2}{(1+\beta_R^2)(\xi^2+\beta_R^2)} - \frac{1}{\xi^2+\alpha_R^2}\right] \\ & + \frac{B_0\alpha_R(\beta_R^2-1)}{4\pi c_2 v_R(\beta_R^2+1)}\ln\tau. \end{aligned} \tag{6.28}$$

Thus, the displacements exhibit a linear growth in time, except for the vertical displacement at $\xi = 0$, which increases as $\ln\tau$.

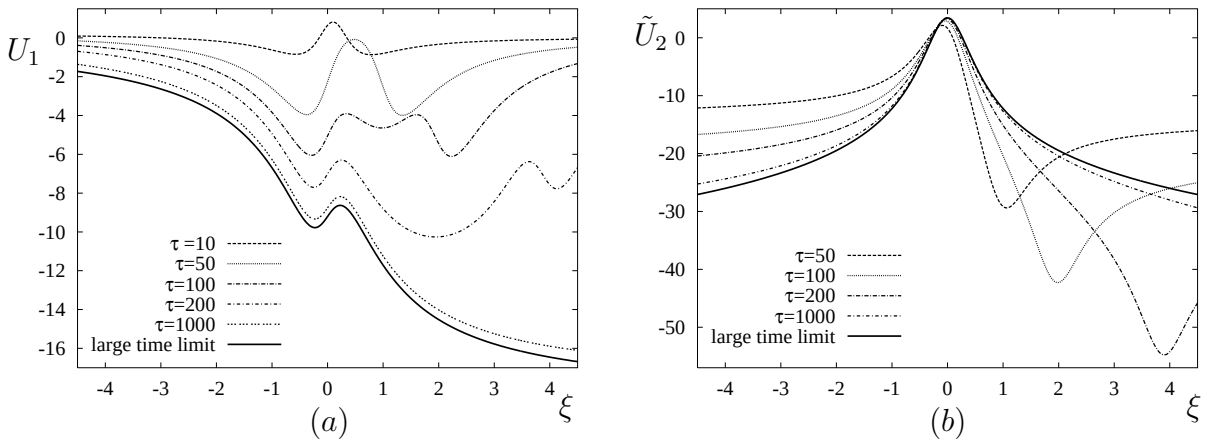

Figure 21: The sub-Rayleigh (a) horizontal and (b) vertical displacements (6.17) and (6.18) and their large time limits for $v = 0.9$.

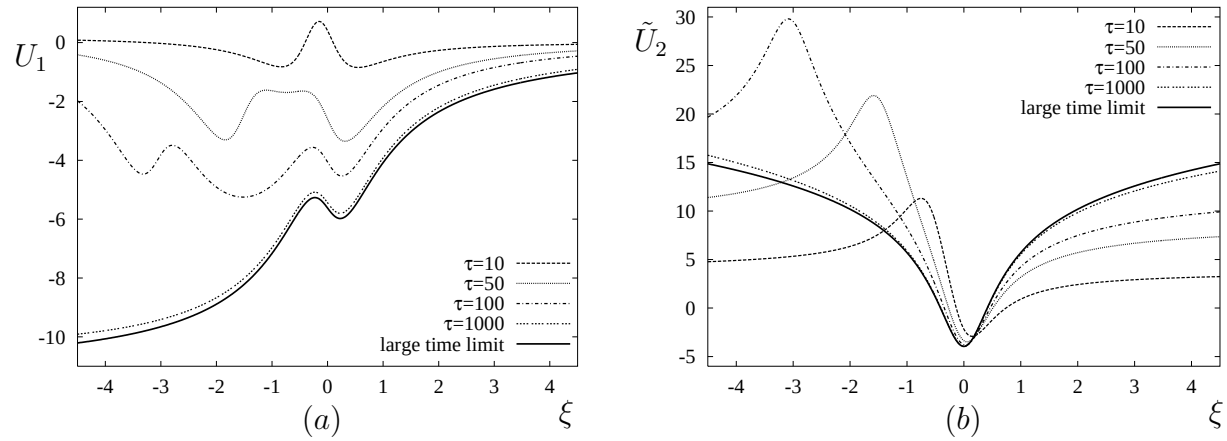

Figure 22: The super-Rayleigh (a) horizontal and (b) vertical displacements (6.17) and (6.18) and the large time limits (6.22) for $v = 0.95$.

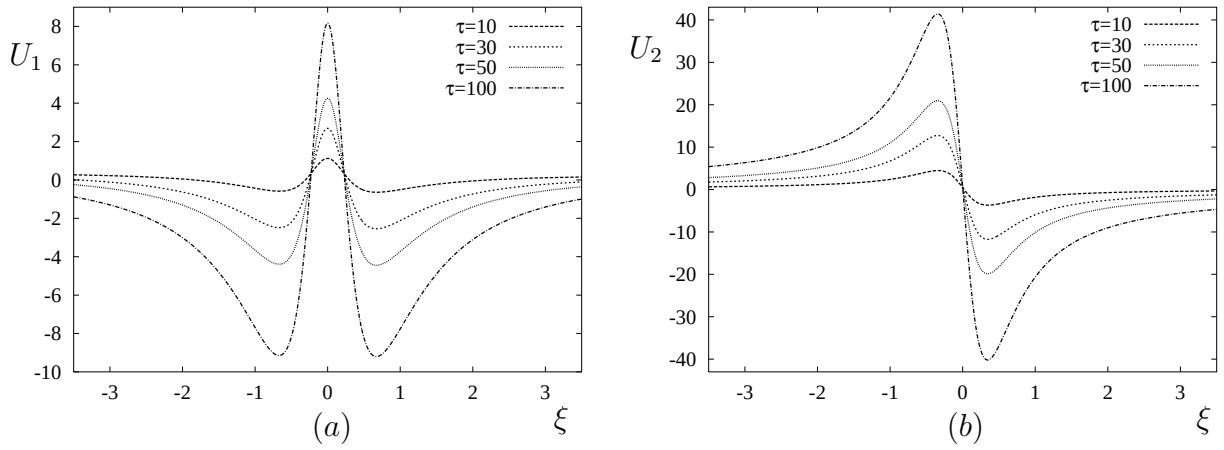

Figure 23: The resonant (a) horizontal and (b) vertical displacements (6.20) and (6.21) for $v = v_R$.

Numerical examples in Figs. 21-23 were produced taking the Poisson's ratio $\nu = \frac{1}{4}$, which corresponds to $v_R \approx 0.9194$. We plot the dimensionless quantities

$$U_i = \frac{\pi \mu u_i}{P_0}, i = 1, 2,$$

and also

$$\tilde{U}_2 = \frac{\pi \mu}{P_0} \left(u_2(\xi, \tau) - u_2^{r\tau}(\tau) \right),$$

subtracting from the vertical displacement $u_2(\xi, \tau)$ the function $u_2^{r\tau}(\tau)$ which has a logarithmic growth in time, see (6.23) and (6.24). In this case we depict only a bounded in time component in order to achieve convergence at a large time limit.

The sub-Rayleigh displacements of the half-space (6.17) and (6.18) are plotted in Fig. 21 for $v = 0.9$ and several values of time τ. Similar results for the super-Rayleigh regime are given in Fig. 22 at $v = 0.95$. The limiting behaviours (6.22) are shown by solid lines. As might be expected, the transient displacements tend to their large time values as time increases. The resonant displacements (6.20) and (6.21) are displayed in Fig. 23 for $\tau = 10$, 30, 50 and 100. They demonstrate a linear growth in time according to the formulae (6.20) and (6.21).

Fig. 24 illustrates a comparison of the horizontal displacement obtained from the asymptotic model with that arising from the exact solution of the associated plane strain problem presented in Appendix of Kaplunov et al. (2010). The computations are performed for $v = 0.9$, $\xi = 0$, and $\nu = \frac{1}{4}$. It is readily observed from Fig. 24 that the use of the asymptotic solution is

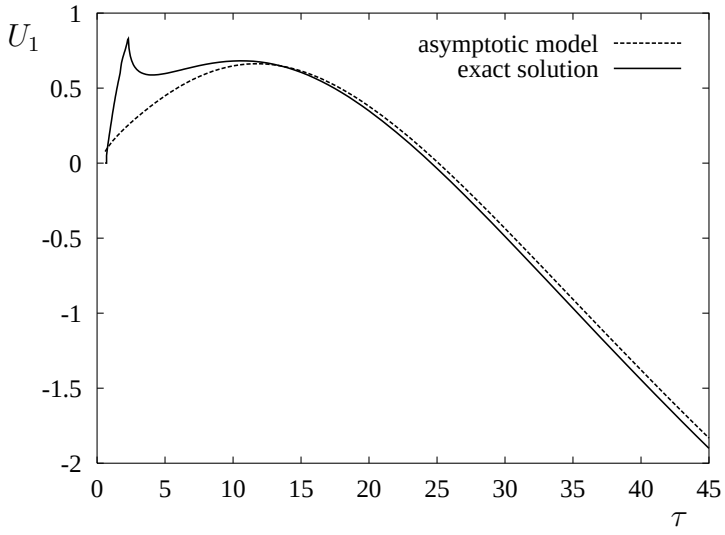

Figure 24: Comparison of approximate and exact solutions

justified once the effect of the bulk waves can be neglected, say, at $\tau \geqslant 10$. This observation is in agreement with the validity of the formula (6.17), which fails at small times, when the arguments of $\tan^{-1}$ become small. This results in the absence of the pole $v = v_R$ violating the original assumption of the Rayleigh wave dominance.

Another interesting example is concerned with the resonant regime of a moving semi-infinite strip, for which $P = P_0 H(x_1 - c_R t)$, see Fig. 25. In this case the asymptotic model for the

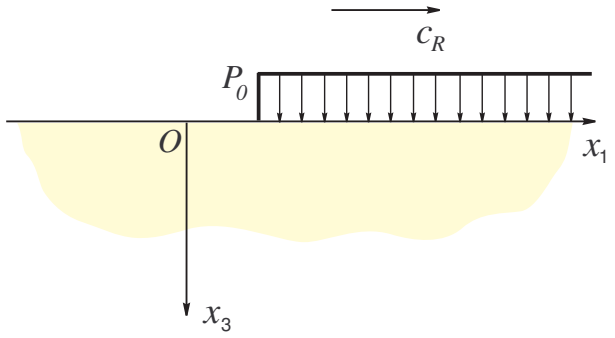

Figure 25: A moving step load.

Rayleigh wave recovers a rather technical result in Goldstein (1965), but with much less effort. Indeed, the derivative of the step load P corresponds to a moving impulse. Thus, the sought for displacements may be obtained by straightforward integration of (6.20) and (6.21).

In the latter case we have for the stresses at $\tau \to \infty$

$$\begin{aligned}
\sigma_{11} &\sim \frac{(1+\beta_R^2)v_r P_0}{4\mu\pi B}\left[\frac{2\alpha_R^2+\beta_R^2-1}{\xi^2+\alpha_R^2}-\frac{\beta_R(1+\beta_R^2)}{\xi^2+\beta_r^2}\right]\tau,\\
\sigma_{22} &\sim \frac{\alpha_R\beta_R v_r P_0}{\mu\pi B}\left[\frac{\beta_R}{\xi^2+\beta_R^2}-\frac{\alpha_R}{\xi^2+\alpha_R^2}\right]\tau,\\
\sigma_{12} &\sim \frac{(1+\beta_R^2)\alpha_R v_r P_0}{2\mu\pi B}\,\frac{\alpha_R^2-\beta_R^2}{(\xi^2+\beta_R^2)(\xi^2+\alpha_R^2)}\,\xi\tau,
\end{aligned} \tag{6.29}$$

for more detail see Kaplunov et al. (2010). Note that the expression for σ_{11} coincides with the formula (2.4) presented in Goldstein (1965).

6.3 3D steady-state problem

Let us now study the steady-state near-resonant regimes of a point vertical force

$$P = -P_0\delta(x_2)\delta(x_1 - ct),$$

travelling along the Ox_1 axis at a constant speed c, see Fig. 26. From the very beginning

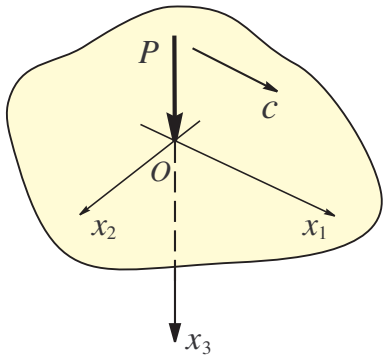

Figure 26: A moving vertical point load.

we distinguish between the sub-Rayleigh and super-Rayleigh regimes, having from (4.51) the elliptic equation

$$\phi_{,22} + \epsilon^2\phi_{,ss} = \frac{(1+\beta_R^2)P_0}{2\mu B}\,\delta(s)\delta(x_2) \tag{6.30}$$

for the sub-Rayleigh case, and the hyperbolic equation

$$\phi_{,22} - \epsilon^2\phi_{,ss} = \frac{(1+\beta_R^2)P_0}{2\mu B}\,\delta(s)\delta(x_2) \tag{6.31}$$

for the super-Rayleigh one. Here and below in this section the small parameter ϵ is defined as

$$\epsilon = \left| 1 - \frac{c^2}{c_R^2} \right|^{1/2}. \tag{6.32}$$

Let us introduce the scaling

$$\eta_1 = \frac{s}{\epsilon}, \qquad \eta_2 = x_2, \qquad \eta_3 = \frac{x_3}{\epsilon}. \tag{6.33}$$

and rewrite the equations (6.30) and (6.31) as

$$\phi_{,22} + \phi_{,11} = \frac{(1+\beta_R^2)P_0}{2\mu B\epsilon}\,\delta(\eta_1)\delta(\eta_2) \tag{6.34}$$

and

$$\phi_{,22} - \phi_{,11} = \frac{(1+\beta_R^2)P_0}{2\mu B\epsilon}\,\delta(\eta_1)\delta(\eta_2) \tag{6.35}$$

with the subscript $_{,i}$ indicating differentiation along the variable η_i, $\;i = 1, 2, 3$.

The elliptic equations (4.60) and relations (4.61) now take the form

$$\phi_{,33} + \alpha_R^2\phi_{,11} = 0, \qquad \psi_{i,33} + \beta_R^2\psi_{i,11} = 0, \qquad i = 1, 2. \tag{6.36}$$

and

$$\psi_{1,3} = \frac{1+\beta_R^2}{2}\,\phi_{,1}, \qquad \psi_{2,3} = \frac{(1+\beta_R^2)\epsilon}{2}\phi_{,2}. \tag{6.37}$$

6.3.1 Sub-Rayleigh regime

For the sub-Rayleigh speeds $c < c_R$ the solution along the surface is

$$\phi\,(\eta_1, \eta_2, 0) = \frac{(1+\beta_R^2)P_0}{8\pi\mu B\epsilon}\ln(\eta_1^2 + \eta_2^2), \tag{6.38}$$

see e.g. Polyanin (2002). Then, we restore the potential ϕ over the interior from (6.36), using the Poisson formula. The result is

$$\phi(\eta_1, \eta_2, \eta_3) = \frac{(1+\beta_R^2)P_0}{8\pi\mu B\epsilon}\ln\left[\eta_1^2 + (\alpha_R\eta_3 + |\eta_2|)^2\right]. \tag{6.39}$$

This solution is formally not differentiable with respect to η_2 along the plane $\eta_2 = 0$ due to the omitted $O(\varepsilon^2)$ terms in the equation (6.36). Now, using (6.36) for the transverse wave potentials ψ_1 and ψ_2 together with (6.37), we have

$$\psi_1(\eta_1, \eta_2, \eta_3) = \frac{\alpha_R P_0}{2\pi\mu B\epsilon}\tan^{-1}\frac{\beta_R\eta_3 + |\eta_2|}{\eta_1}, \tag{6.40}$$

and

$$\psi_2(\eta_1,\eta_2,\eta_3)=\frac{\alpha_R P_0}{4\pi\mu B\epsilon}\,\mathrm{sgn}(\eta_2)\,\ln\left[\eta_1^2+(\beta_R\eta_3+|\eta_2|)^2\right]. \tag{6.41}$$

The leading order displacements are found from (4.53) as

$$u_1=\frac{(1+\beta_R^2)P_0\eta_1}{8\mu\pi B\epsilon^2}\left[\frac{2}{\eta_1^2+(\alpha_R\eta_3+|\eta_2|)^2}+\frac{1+\beta_R^2}{\eta_1^2+(\beta_R\eta_3+|\eta_2|)^2}\right], \tag{6.42}$$

$$u_2=\frac{(1+\beta_R^2)P_0\mathrm{sgn}(\eta_2)}{8\mu\pi B\epsilon}\left[\frac{2(\alpha_R\eta_3+|\eta_2|)}{\eta_1^2+(\alpha_R\eta_3+|\eta_2|)^2}+\frac{(1+\beta_R^2)\,(\beta_R\eta_3+|\eta_2|)}{\eta_1^2+(\beta_R\eta_3+|\eta_2|)^2}\right], \tag{6.43}$$

and

$$u_3=\frac{(1+\beta_R^2)P_0}{8\mu\pi B\epsilon^2}\left[\frac{2\alpha_R(\alpha_R\eta_3+|\eta_2|)}{\eta_1^2+(\alpha_R\eta_3+|\eta_2|)^2}-\frac{(1+\beta_R^2)\,(\beta_R\eta_3+|\eta_2|)}{\beta_R\,(\eta_1^2+(\beta_R\eta_3+|\eta_2|)^2)}\right]. \tag{6.44}$$

We note that the asymptotically secondary displacement u_2 has a discontinuity at $\eta_2=0$ coming from differentiation of (6.39) with respect to η_2.

Numerical results for the scaled displacements

$$U_i=\frac{\mu\,u_i}{P_0}\,,\qquad i=1,2,3,$$

are presented in Figs. 27-29. The graphs in these figures show no discontinuities, with the

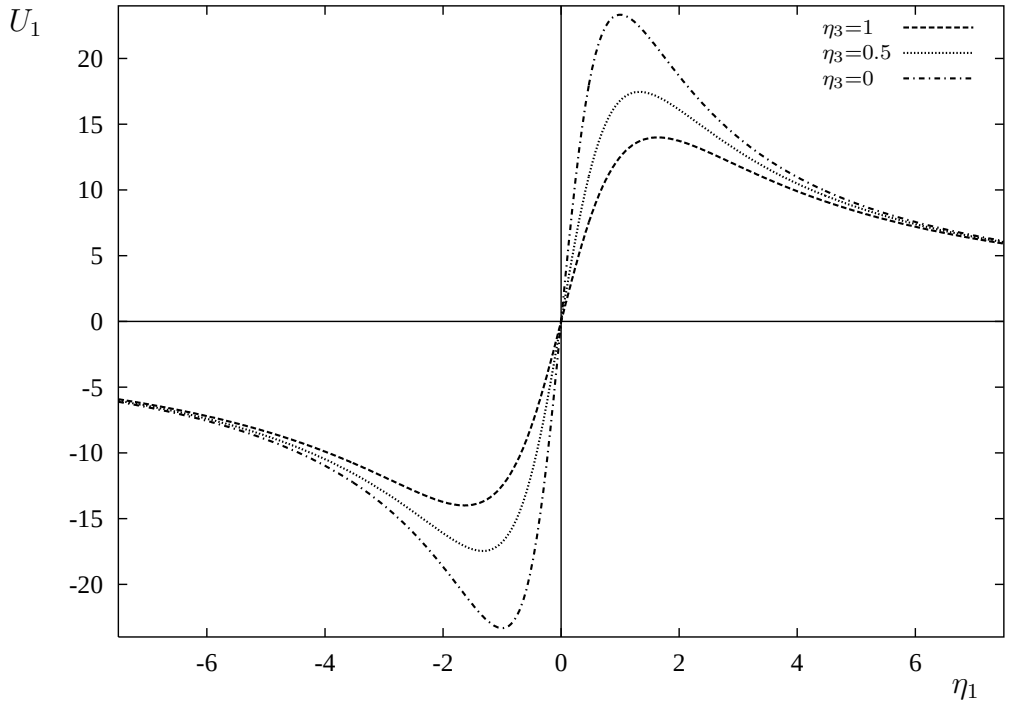

Figure 27: The sub-Rayleigh diplacement U_1 vs. η_1 at $|\eta_2|=1$ and $\eta_3=0,0.5,1.0$.

displacement amplitudes increasing slightly while getting closer to the surface.

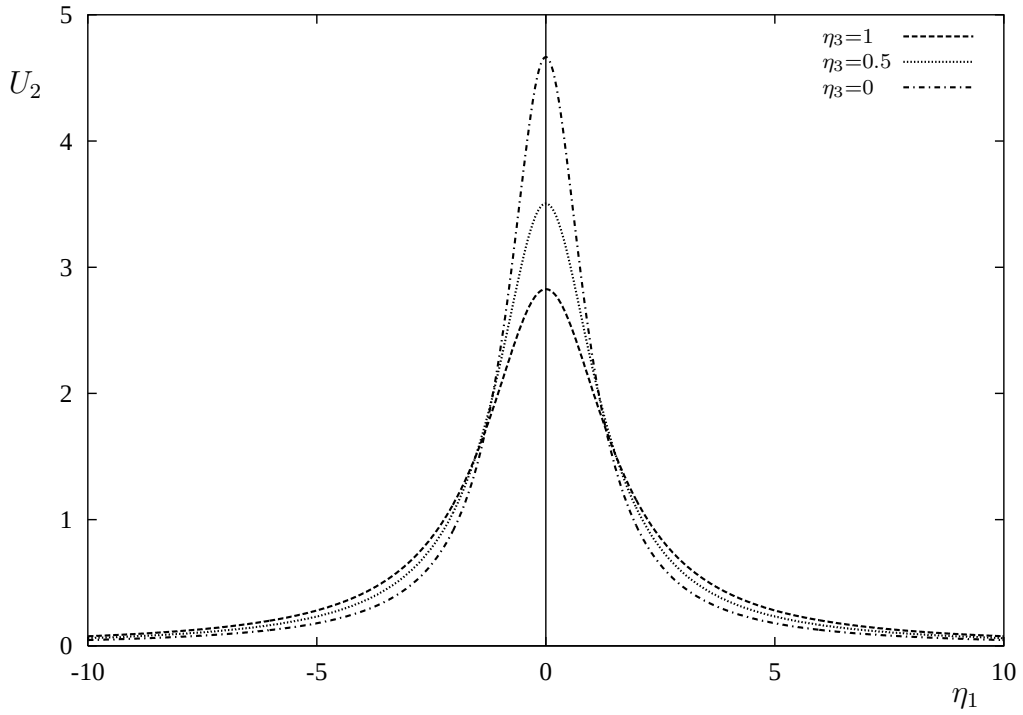

Figure 28: The sub-Rayleigh diplacement U_2 vs. η_1 at $|\eta_2| = 1$ and $\eta_3 = 0, 0.5, 1.0$.

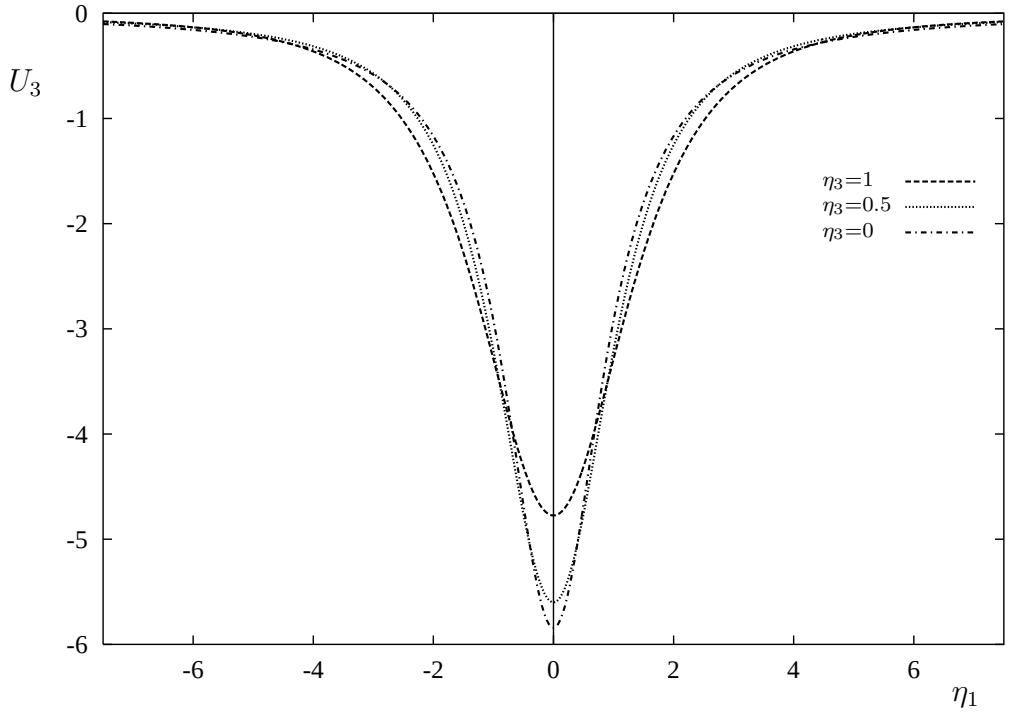

Figure 29: The sub-Rayleigh diplacement U_3 vs. η_1 at $|\eta_2| = 1$ and $\eta_3 = 0, 0.5, 1.0$.

6.3.2 Super-Rayleigh regime

Inspection of the hyperbolic equation (6.35) along the surface $\eta_3 = 0$ immediately suggests a Mach cone associated with the Rayleigh wave, see Fig. 30. Then, on employing the causality

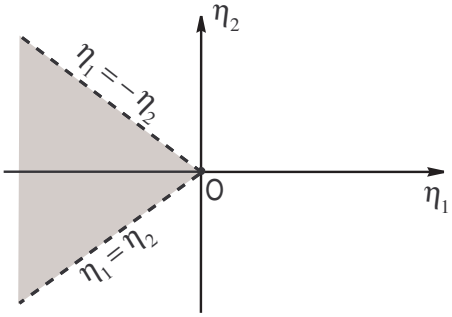

Figure 30: A Mach cone.

principle, i.e. assuming absence of surface disturbances in front of a travelling load, we obtain, see Erbaş & Şahin (2016) for further detail,

$$\phi\left(\eta_1, \eta_2, 0\right) = \frac{(1+\beta_R^2)P_0}{2\mu B\epsilon}\, H(-\eta_1)\left[H(\eta_2-\eta_1) - H(\eta_2+\eta_1)\right]. \tag{6.45}$$

The potential ϕ over the interior is determined from (6.36), giving

$$\phi\left(\eta_1, \eta_2, \eta_3\right) = \frac{(1+\beta_R^2)P_0}{4\pi\mu B\epsilon}\, \cot^{-1}\frac{\eta_1 + |\eta_2|}{\alpha_R \eta_3}. \tag{6.46}$$

The potentials ψ_1 and ψ_2 are then found from (6.36) and (6.37) as

$$\psi_1\left(\eta_1, \eta_2, \eta_3\right) = -\frac{P_0\alpha_R^2}{4\pi\mu B\beta_R\epsilon}\, \ln\left[(\eta_1 + |\eta_2|)^2 + \alpha_R^2\eta_3^2\right] \tag{6.47}$$

and

$$\psi_2\left(\eta_1, \eta_2, \eta_3\right) = -\frac{P_0\alpha_R^2 \mathrm{sgn}(\eta_2)}{4\pi\mu B\beta_R}\, \ln\left[(\eta_1 + |\eta_2|)^2 + \alpha_R^2\eta_3^2\right]. \tag{6.48}$$

Finally, the leading order displacement components corresponding to (6.46)-(6.48) are obtained from (4.53). They are

$$u_1 = -\frac{(1+\beta_R^2)P_0\alpha_R\eta_1}{8\mu\pi B\epsilon^2}\left[\frac{2}{(\eta_1+|\eta_2|)^2 + \alpha_R^3\eta_3^2} + \frac{1+\beta_R^2}{(\eta_1+|\eta_2|)^2 + \beta_R^3\eta_3^2}\right], \tag{6.49}$$

$$u_2 = -\frac{(1+\beta_R^2)P_0\,\alpha_R\eta_3\,\mathrm{sgn}(\eta_2)}{8\mu\pi B\epsilon}\left[\frac{2}{(\eta_1+|\eta_2|)^2 + \alpha_R^3\eta_3^2} + \frac{1+\beta_R^2}{(\eta_1+|\eta_2|)^2 + \beta_R^3\eta_3^2}\right], \tag{6.50}$$

and

$$u_3 = \frac{(1+\beta_R^2)P_0(\eta_1+|\eta_2|)\alpha_R}{8\mu\pi B\epsilon^2}\left[\frac{2}{(\eta_1+|\eta_2|)^2+\alpha_R^3\eta_3^2}-\frac{1+\beta_R^{-2}}{(\eta_1+|\eta_2|)^2+\beta_R^3\eta_3^2}\right]. \tag{6.51}$$

The discontinuities along the surface $\eta_3 = 0$ associated with the Mach cone $\eta_1 + |\eta_2| = 0$, can be seen from the formulae (6.49)-(6.51).

Numerical results are displayed in Figs. 31-33. In contrast to the sub-Rayleigh case, the analysed super-Rayleigh displacements increase significantly near the surface $\eta_3 = 0$. The discontinuities occurring on the surface at $\eta_1 = -1$ are shown by solid line.

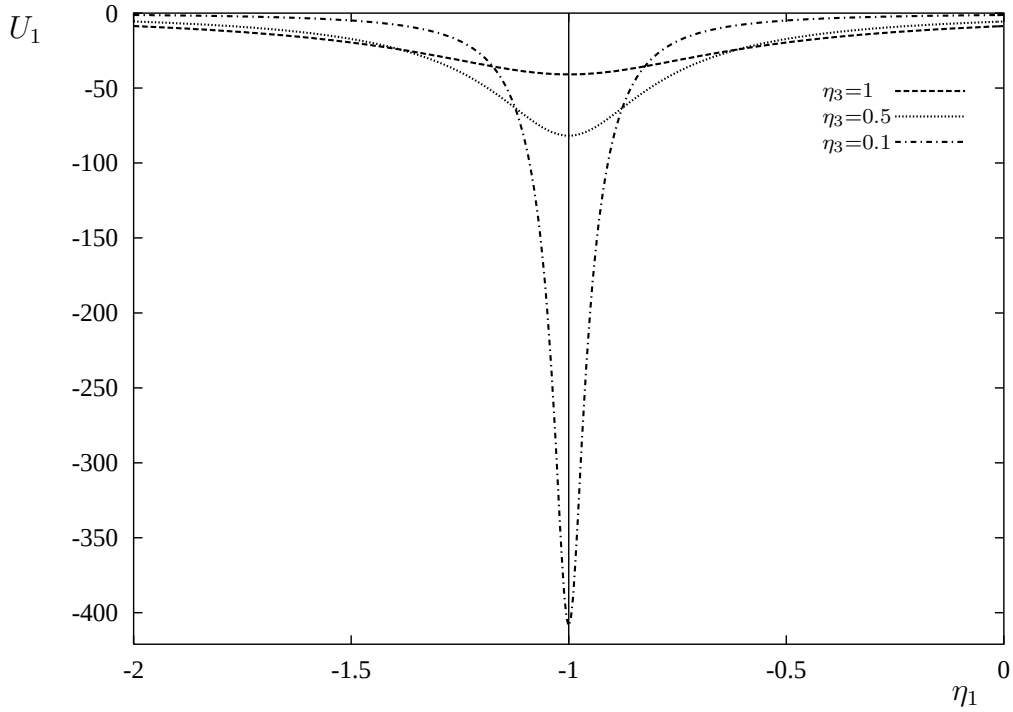

Figure 31: The super-Rayleigh diplacement U_1 vs. η_1 at $|\eta_2| = 1$ and $\eta_3 = 1, 0.5, 0.1$.

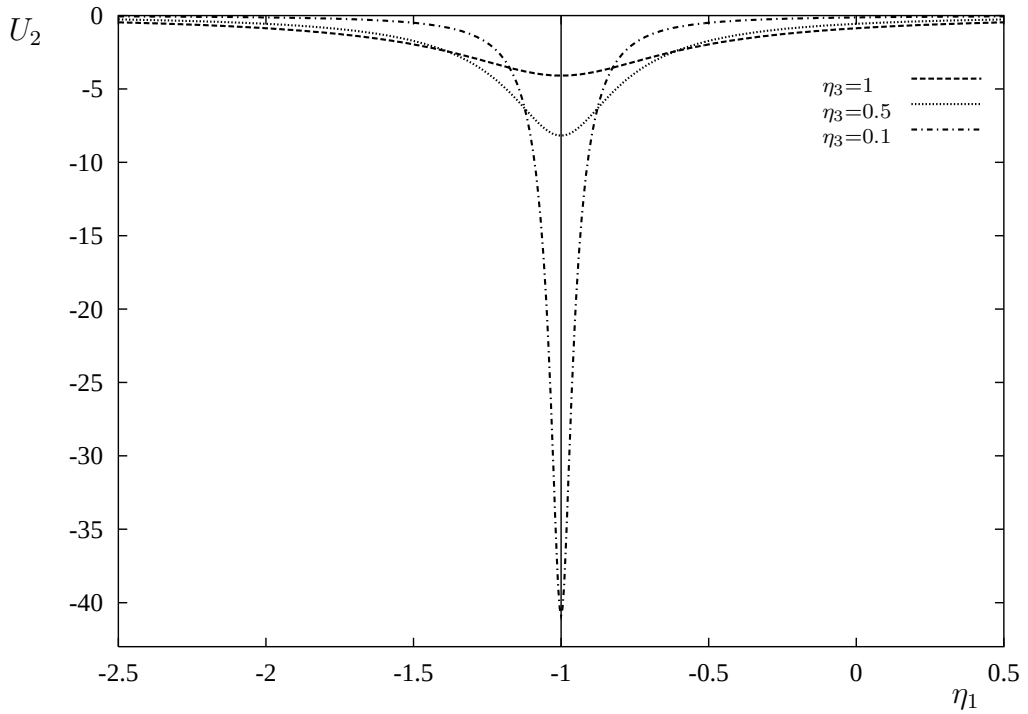

Figure 32: The super-Rayleigh diplacement U_2 vs. η_1 at $|\eta_2| = 1$ and $\eta_3 = 1, 0.5, 0.1$.

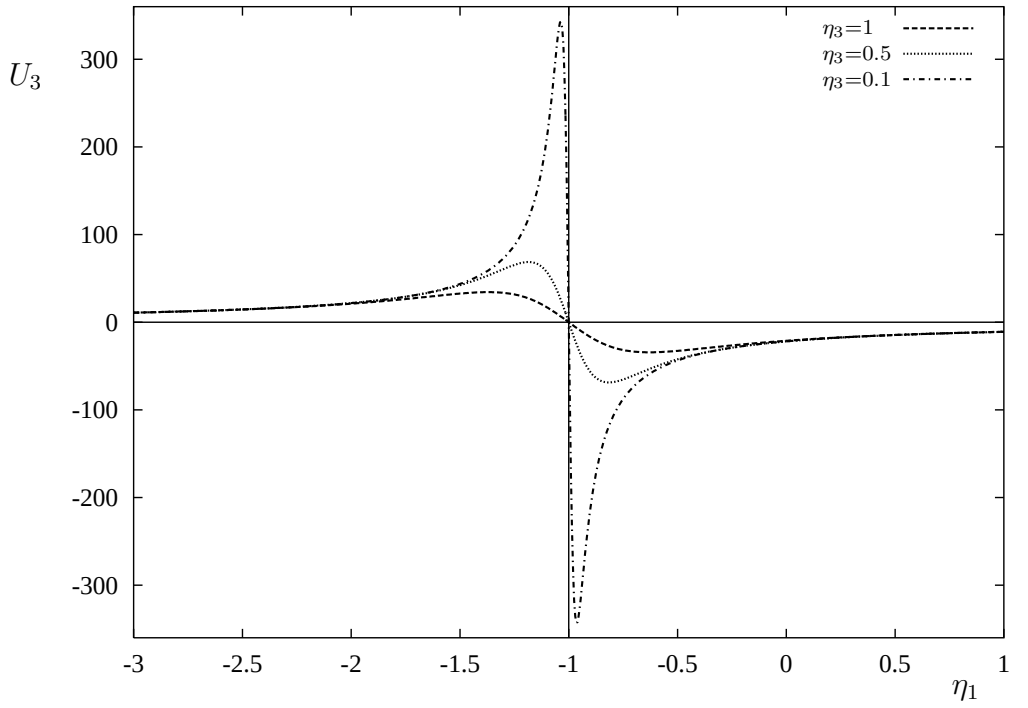

Figure 33: The super-Rayleigh diplacement U_3 vs. η_1 at $|\eta_2| = 1$ and $\eta_3 = 1.0, 0.5, 0.1$.

6.4 3D steady-state problem for a coated half-space

Let us extend the consideration of the previous subsection to an elastic half-space $\mathcal{H}_3^+$ coated by a thin layer occupying the domain $-h \le x_3 \le 0$, subject to the moving point force $P = P_0\delta(x_1 - ct)\delta(x_2)$, see Fig. 34. The statement of the problem includes now a pseudo-

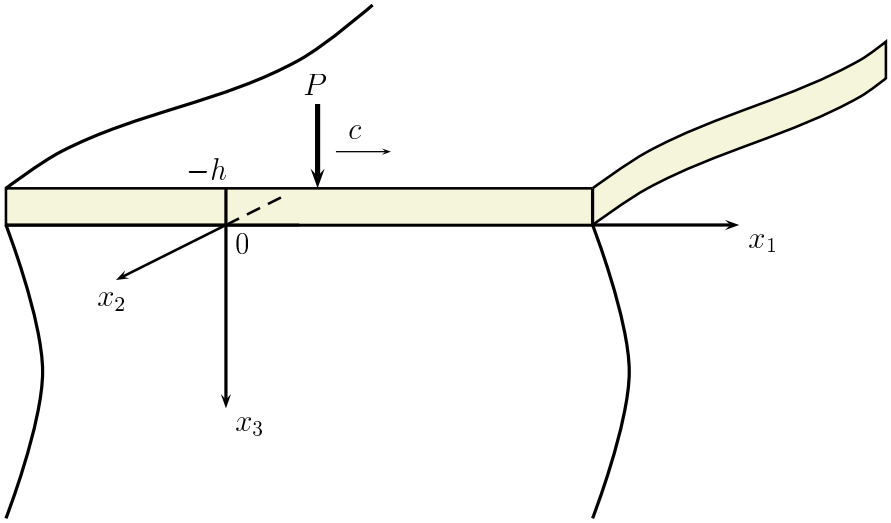

Figure 34: A moving point load on a coated half-space.

differential equation at $x_3 = 0$, see (5.6), which may be written as

$$\phi_{,22} + \left(1 - \frac{c^2}{c_R^2}\right)\phi_{,ss} - bh\sqrt{-(\partial_{,ss} + \partial_{,22})}\,(\phi_{,ss} + \phi_{,22}) = \frac{(1+\beta_R^2)P_0}{2\mu B}\,\delta(s)\delta(x_2), \tag{6.52}$$

where, as previously, $s = x_1 - ct$ is a moving coordinate. The formulated problem has two small parameters, including $\epsilon \ll 1$ defined by (6.32), and $h/L \ll 1$ over the long-wave domain, see subsection 5.1. The degenerations at $\epsilon = 0$ and $h = 0$ correspond to the critical speed of the load coinciding with the Rayleigh wave speed and a homogeneous half-space, respectively. These observations motivate the scaling

$$\xi = \frac{\epsilon^2 s}{bh}, \qquad \eta = \frac{\epsilon^3 s}{bh}, \tag{6.53}$$

for more detail throughout this subsection see Erbaş et al. (2014). Then, (6.52) takes the form of

$$\phi_{,\xi\xi} + \phi_{,\eta\eta} - \sqrt{-\partial_{,\xi\xi}}\,\phi_{,\xi\xi} = \frac{(1+\beta_R^2)P_0}{2\mu B\epsilon}\,\delta(\xi)\,\delta(\eta) \tag{6.54}$$

or

$$\phi_{,\xi\xi} - \phi_{,\eta\eta} - \sqrt{-\partial_{,\xi\xi}}\,\phi_{,\xi\xi} = \frac{(1+\beta_R^2)P_0}{2\mu B\epsilon}\,\delta(\xi)\,\delta(\eta) \tag{6.55}$$

for the sub-Rayleigh and super-Rayleigh regimes, respectively.

First, we investigate the sub-Rayleigh case. On applying the Fourier transform in (6.54), we have

$$\phi^F_{,\eta\eta} - k^2(1-|k|)\phi^F = \frac{(1+\beta_R^2)P_0}{2\mu B\epsilon}\delta(\eta), \tag{6.56}$$

where

$$\phi^F(k,\eta,0) = \int_{-\infty}^{\infty} \phi(\xi,\eta,0)\, e^{-ik\xi} d\xi. \tag{6.57}$$

The solution of this equation is piecewise-defined in the parameter $|k|$. Due to symmetry in η along with decay at infinity, it may be written as

$$\phi^F(k,\eta,0) = \begin{cases} -\dfrac{(1+\beta_R^2)P_0}{2\mu B\epsilon}\dfrac{e^{-|k|\sqrt{1-|k|}|\eta|}}{|k|\sqrt{1-|k|}}, & |k|<1; \\ \\ \dfrac{(1+\beta_R^2)P_0}{2\mu B\epsilon}\dfrac{\sin\left(|k|\sqrt{|k|-1}|\eta|\right)}{|k|\sqrt{|k|-1}}, & |k|>1. \end{cases} \tag{6.58}$$

Therefore, using (4.54), we have for the horizontal displacement u_1 along the plane $x_3 = 0$

$$u_1(\xi,\eta,0) = \frac{(1+\beta_R^2)P_0\varepsilon c_R^2 \mathrm{sgn}(\xi)}{4\pi\mu B c_2^2 bh}\left[\int_0^1 \frac{e^{-k\sqrt{1-k}|\xi|m}}{\sqrt{1-k}}\sin(k|\xi|)\,dk - \int_1^{\infty}\frac{\sin\left(k\sqrt{k-1}|\xi|m\right)}{\sqrt{k-1}}\sin(k|\xi|)\,dk\right], \tag{6.59}$$

where $m = \left|\dfrac{\eta}{\xi}\right|$.

Let us study the far-field approximation $|\xi| \gg 1$. It can be shown that the leading order asymptotic behaviour of u_1 is given by the contribution of the stationary points arising from the second integral in (6.59). Changing the variable k to $t = \sqrt{k-1}$, this integral takes the form

$$\int_1^{\infty}\frac{\sin\left(k\sqrt{k-1}|\eta|\right)}{\sqrt{k-1}}\sin(k|\xi|)\,dk = \sum_{n=1}^{2} G_n(|\xi|,m), \tag{6.60}$$

where

$$G_n(|\xi|,m) = (-1)^{n+1}\int_0^{\infty}\cos\left[|\xi|(t^2+1)(tm+(-1)^n)\right]dt. \tag{6.61}$$

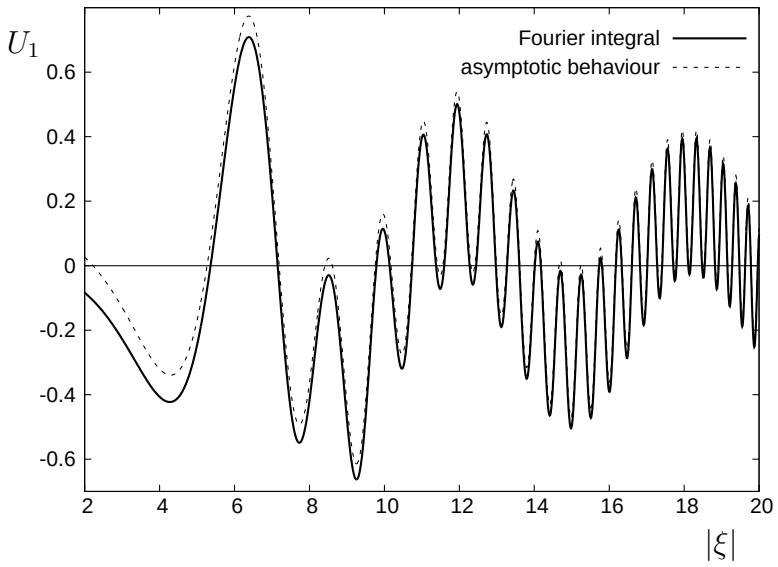

Figure 35: The longitudinal cross-section of the sub-Rayleigh horizontal displacement U_1 at $|\eta| = 3$.

It may be shown that only the intergrand in G_1 possesses stationary points, namely

$$t_* = \frac{1 \pm \sqrt{1 - 3m^2}}{3m}, \qquad 0 < m \leq \frac{1}{\sqrt{3}}, \tag{6.62}$$

which coincide along the line $|\xi| = \sqrt{3}|\eta|$. In this case the uniform stationary phase method, see e.g. Borovikov (1994), yields

$$G_1\left(|\xi|, m\right) = \frac{2\pi}{\sqrt[3]{3m|\xi|}} \cos\left(p_1|\xi|\right) \mathrm{Ai}\left(p_2|\xi|^{2/3}\right), \tag{6.63}$$

where

$$\mathrm{Ai}(z) = \frac{1}{\pi} \int_0^\infty \cos\left(\frac{t^3}{3} + zt\right) dt \tag{6.64}$$

is the Airy function, see Abramowitz & Stegun (2012), with

$$p_1 = \frac{2(9m^2 + 1)}{27}, \qquad p_2 = \frac{3m^2 - 1}{(3m)^{4/3}}. \tag{6.65}$$

The resulting far-field approximation for the displacement u_1 is given by

$$u_1 \sim -\frac{\left(1 + \beta_R^2\right) P_0 c_R^2 \mathrm{sgn}(\xi)}{2\mu B c_2^2 bh \sqrt[3]{3|\xi|m}} \cos\left(p_1|\xi|\right) \mathrm{Ai}\left(p_2|\xi|^{2/3}\right). \tag{6.66}$$

The numerical illustrations in Figs. 35 and 36 demonstrate comparisons of the solution (6.59) with its far-field asymptotic approximation (6.66) depicted by the solid and dotted lines, respectively. Fig. 35 shows the variation of the scaled displacement

$$U_1 = \frac{2bh\mu B c_2^2}{(1 + \beta_R^2) P_0 c_R^2 \epsilon} u_1, \tag{6.67}$$

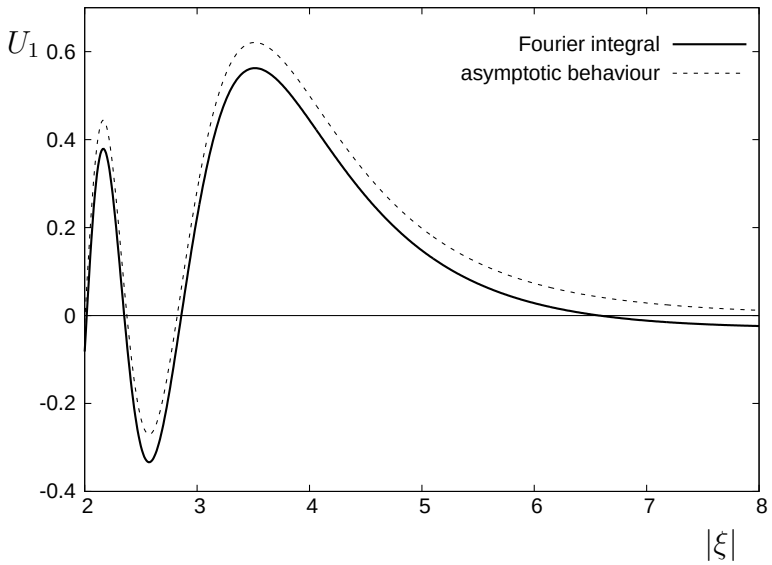

Figure 36: The transverse cross-section of the displacement profile U_1 at $|\xi| = 7$.

over ξ for the fixed value of $|\eta| = 3$, whereas Fig. 36 presents the perpendicular cross-section of U_1 at $|\xi| = 7$. It may be observed from Figs. 35 and 36 that even though there is no Mach cone for the sub-Rayleigh regime, there is still a region of oscillations associated with $m < \frac{1}{\sqrt{3}}$. The period of these oscillations decreases as $m \to 0$. The analysed profiles suggest an exponential decay over the region $m > \frac{1}{\sqrt{3}}$. Next, we plot a 3D graph of the scaled displacement U_1 corresponding to (6.59), over the region $-4 \leq \xi \leq 0$ and $0 \leq \eta \leq 4$, see Fig. 37.

The super-Rayleigh case is treated similarly. The pseudo-differential equation (6.55) becomes

$$\phi^F_{,\eta\eta} + k^2(1 + |k|)\phi^F = \frac{(1 + \beta_R^2)P_0}{2\mu B\epsilon}\,\delta(\eta), \tag{6.68}$$

from which

$$\phi(\xi, \eta, 0) = \frac{(1 + \beta_R^2)P_0}{2\pi\mu B\epsilon} \int_0^\infty \frac{\sin\left(k\sqrt{1+k}|\eta|\right)\cos\left(k\xi\right)}{k\sqrt{1+k}} dk. \tag{6.69}$$

The displacement u_1 is then given by

$$u_1(\xi, \eta, 0) = \frac{(1 + \beta_R^2)P_0 c_R^2 \epsilon}{8\pi\mu B c_2^2 bh} \sum_{n=1}^{2} I_n(\xi, \eta), \tag{6.70}$$

where

$$I_n(\xi, \eta) = \mathrm{sgn}(\xi) \int_0^\infty \frac{\cos\left(|\xi| f_n(k)\right)}{g(k)} dk, \qquad n = 1, 2, \tag{6.71}$$

with

$$f_n(k) = k\left[g(k)m + (-1)^{n+1}\right], \qquad g(k) = \sqrt{1+k},$$

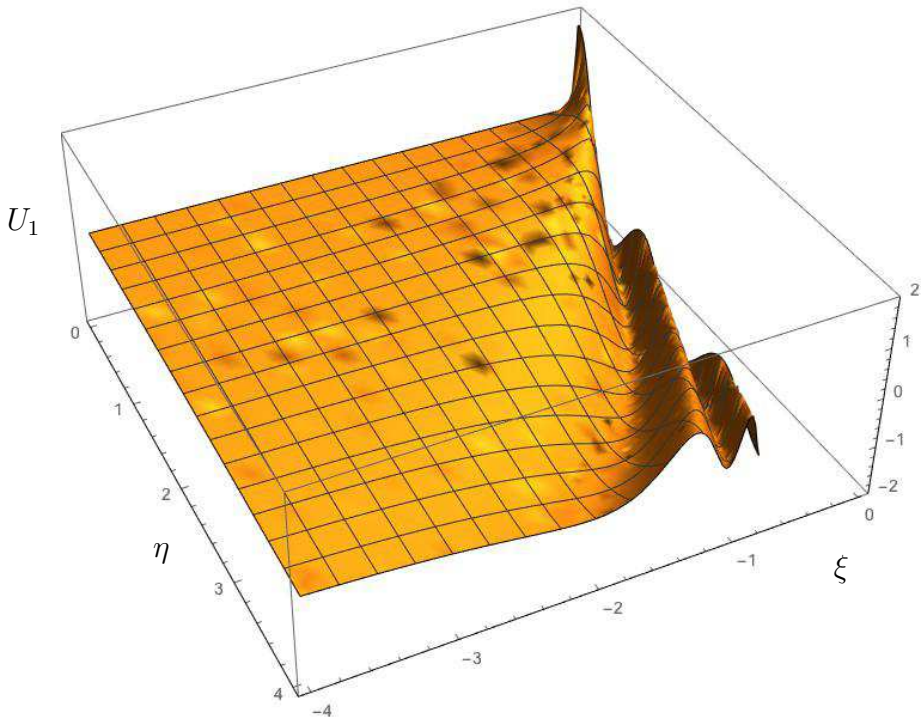

Figure 37: A 3D profile of the longitudinal sub-Rayleigh displacement U_1.

and, as previously, $m = \left|\dfrac{\eta}{\xi}\right|$.

The far-field asymptotic behaviour of the oscillating integrals (6.71) as $|\xi| \gg 1$, assuming $m \sim 1$, may now be studied. It appears that the effect of the first integral I_1 is asymptotically minor, whereas I_2 is dominated by the contribution of the stationary point

$$k_* = \frac{2\left(1 - 3m^2 + \sqrt{3m^2+1}\right)}{9m^2} \tag{6.72}$$

of the function $f_2(k)$.

The Mach cone observed in subsection 6.3.2, corresponds to the limit $h \to 0$, and is defined by $|\xi| = |\eta|$ or $m = 1$. Moreover, on the contour of the Mach cone, when $m = 1$, the stationary point k_* coincides with the lower limit of the integral I_2. Therefore, we again apply the uniform stationary phase method, leading to

$$I_2 \sim \mathrm{Re}\left[\frac{e^{i|\xi|f_*}}{g_*}\int_0^\infty e^{\frac{1}{2}i|\xi|f_2''(k_*)(k-k_*)^2}dk\right], \tag{6.73}$$

where

$$f_* = f_2(k_*) = \frac{2\left(1 - 3m^2 + \sqrt{3m^2+1}\right)\left(\sqrt{3m^2+1} - 2\right)}{27m^2}, \tag{6.74}$$

and

$$g_* = g(k_*) = \frac{1+\sqrt{3m^2+1}}{3m}. \tag{6.75}$$

The displacement u_1 becomes

$$u_1 \sim \frac{(1+\beta_R^2)P_0\varepsilon c_R^2 k_*}{16\pi\mu B c_2^2 bh g_* a}\frac{\mathrm{sgn}(\xi)}{|\xi|^{1/2}}F(|\xi|,m), \tag{6.76}$$

where

$$F(|\xi|,m) = \cos\left[f_*|\xi|\right]\left\{1-2\mathrm{C}\left(a\sqrt{|\xi|}\right)\right\} - \sin\left[f_*|\xi|\right]\left\{1-2\mathrm{S}\left(a\sqrt{|\xi|}\right)\right\}, \tag{6.77}$$

with

$$a = -k_*\sqrt{\frac{h''(k_*)}{\pi}} = \sqrt{\frac{2}{\pi}}\frac{\left[3m^2-1-\sqrt{3m^2+1}\right]\sqrt[4]{3m^2+1}}{3m\left[1+\sqrt{3m^2+1}\right]}, \tag{6.78}$$

and $S(x)$ and $C(x)$ are the Fresnel functions (5.24). It is evident that the derived uniform asymptotic formula is also valid at $m>1$ when $k_*<0$ and a takes imaginary values.

The interpretation of the formulae in this subsection, written in terms of $|\xi|$ and $|\eta|$, relies on the implementation of the causality principle, see also Erbaş & Şahin (2016). In absence of a coating, when $h=0$, the equation (6.55) degenerates into the wave equation. Hence, it seems to be logical to deal with the Mach cone behind the load, i.e. for $\xi b>0$, see Fig 38. In the presence of a coating, we have to expect decay of the solution outside the interior of

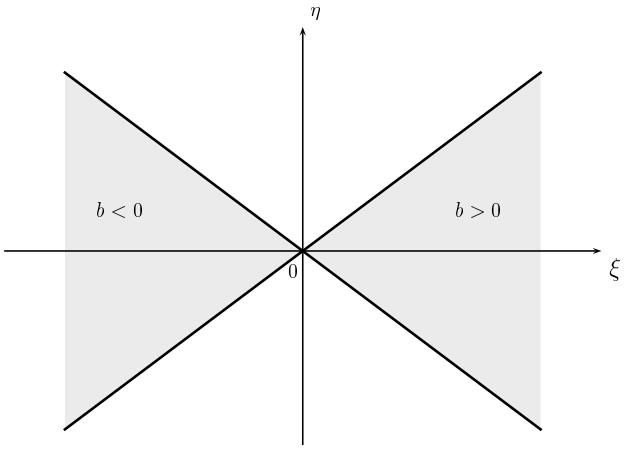

Figure 38: A Mach cone

the Mach cones predicted by the related degenerate non-dispersive equation. The asymptotic behaviours of the Fresnel functions in (6.77) at the large imaginary values of the argument show that the function (6.77) is exponentially small at $m-1 \gg |\xi|^{-1}$.

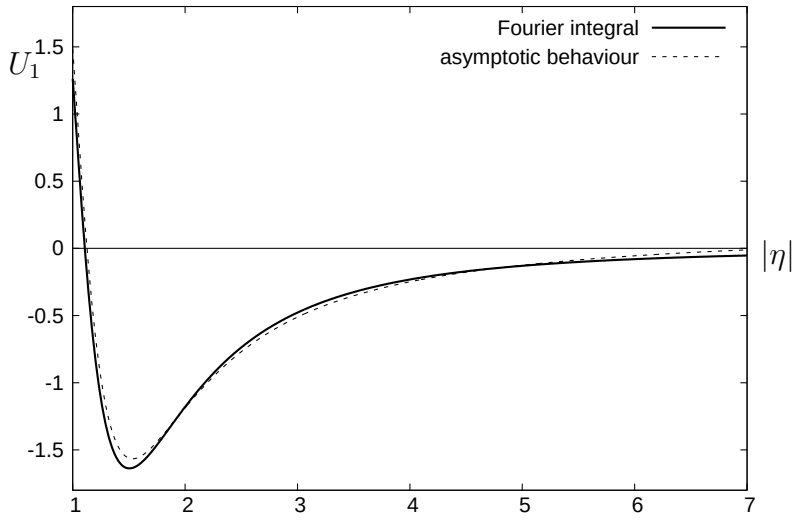

Figure 39: The super-Rayleigh displacement U_1 at $|\xi| = 3$.

Similarly to the sub-Rayleigh case, we analyse the longitudinal and transverse cross-sections of the scaled horizontal displacement

$$U_1 = \frac{8\mu\pi B c_2^2 bh}{(1+\beta_R^2)P_0 c_R^2 \epsilon} u_1, \tag{6.79}$$

see Figs. 39 and 40. The results of numerical integration in (6.70) are depicted by the solid line, with the dotted line corresponding to the far-field approximation (6.76). Fig. 39 displays dependence of U_1 on the transverse variable $|\eta|$ at $|\xi| = 3$. Fig. 40 mirrors Fig. 39, showing the variation of U_1 vs. $|\xi|$ at $|\eta| = 3$.

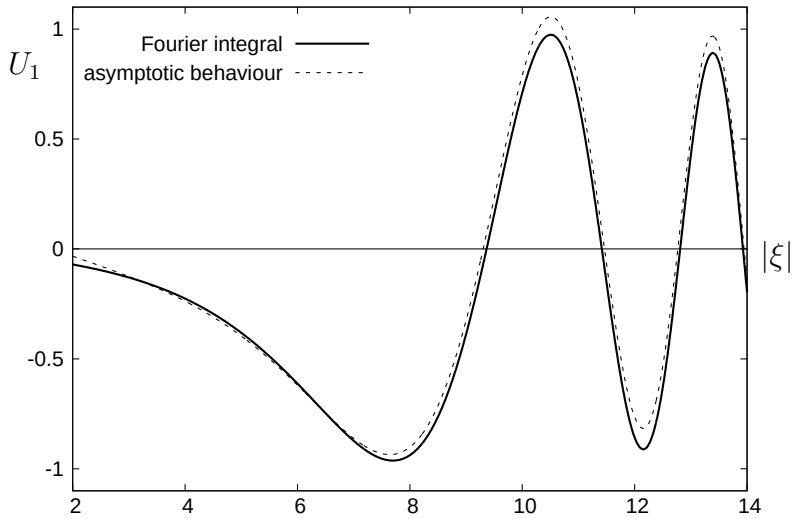

Figure 40: The super-Rayleigh displacement U_1 at $|\eta| = 3$.

It is clearly seen from both Figs. 39 and 40 that the dispersive effect of a coating leads to smoothing of the discontinuities along the contours of the Mach cone $|\xi| = |\eta|$, arising in a homogeneous half-space, see subsection 6.3. The oscillations occurring inside the Mach cone decay outside of it. The period of the oscillations diminishes in both graphs as $m \to 0$, due to $f_* \to \infty$, as may be noticed from (6.74). Finally, we present a 3D graph of the scaled displacement profile corresponding to the integral solution (6.70), over the region $-4 \leq \xi \leq 0$ and $0 \leq \eta \leq 6$ see Fig. 41.

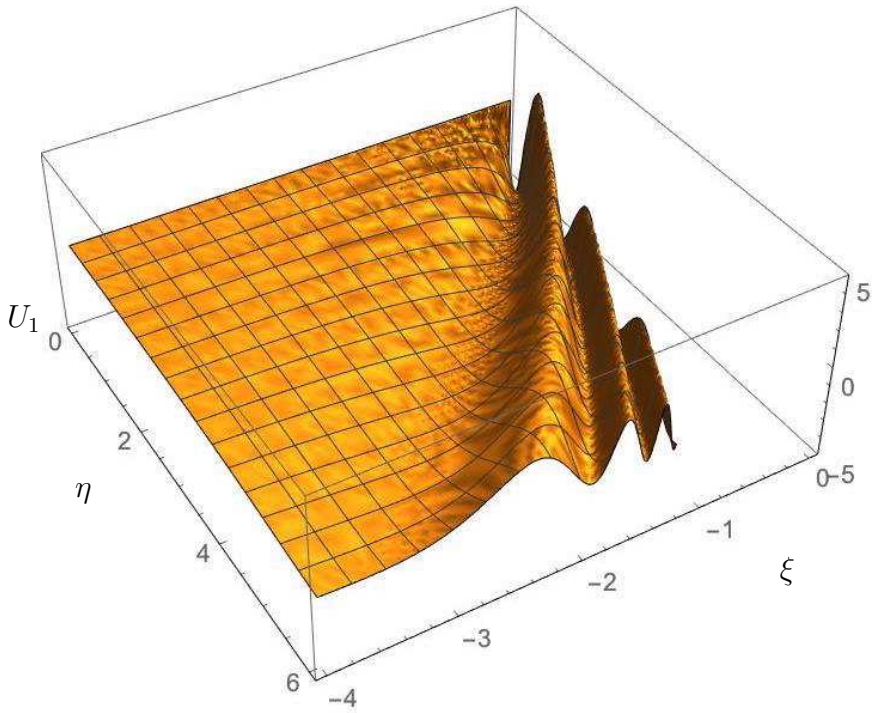

Figure 41: A 3D profile of the horizontal super-Rayleigh displacement U_1.

7 Parabolic-elliptic model for a bending edge wave on a thin plate

In this section we derive an asymptotic formulation for the bending edge wave introduced in subsection 3.3, complementing the hyperbolic-elliptic models for surface and interfacial waves considered in sections 4 and 5.

7.1 Bending edge wave of arbitrary profile

We begin with an eigensolution generalizing that of a sinusoidal profile, see (3.21). Throughout this section we operate with the dimensionless variables

$$\xi = \frac{x_1}{h}, \qquad \eta = \frac{x_2}{h}, \qquad \tau = \frac{t}{h}\left(\frac{E}{3\rho(1-\nu^2)}\right)^{1/2}. \tag{7.1}$$

Then, (3.18) becomes

$$\Delta^2 W + W_{,\tau\tau} = 0, \tag{7.2}$$

where Δ now denotes the 2D Laplace operator in the variables ξ and η.

Next, we proceed with the *implicit ansatz*

$$\gamma_e^4 \frac{\partial^4 W}{\partial \xi^4} + \frac{\partial^2 W}{\partial \tau^2} = 0, \tag{7.3}$$

where γ_e is defined by (3.25). The latter is in fact a counterpart of the implicit travelling wave ansatz (2.43) for the Rayleigh wave. It is clear that the sinusoidal solution (3.21) satisfies (7.3), leading to the dispersion relation (3.24). At the same time, in contrast to (2.43), (7.3) does not allow a functionally invariant travelling wave solution.

Now, using (7.3), we eliminate the time derivative in (7.2), arriving, as in subsection 2.2, at the pseudo-static equation

$$\left(1-\gamma_e^4\right)\frac{\partial^4 W}{\partial \xi^4} + 2\frac{\partial^4 W}{\partial \xi^2 \partial \eta^2} + \frac{\partial^4 W}{\partial \eta^4} = 0, \tag{7.4}$$

which may be rewritten in an operator form as

$$\Delta_1 \Delta_2 W = 0, \tag{7.5}$$

where

$$\Delta_j = \partial_{\eta\eta} + \gamma_j^2 \partial_{\xi\xi}, \qquad j = 1, 2 \tag{7.6}$$

and

$$\gamma_j^2 = 1 + (-1)^j \gamma_e^2. \tag{7.7}$$

The equation (7.5) is elliptic, since γ_j^2 are both positive at $0 < \gamma_e < 1$. Its general solution is therefore given by the sum of two arbitrary plane harmonic functions in the variables ξ and $\gamma_j \eta$, i.e.

$$W = \sum_{j=1}^{2} W_j \left(\xi, \gamma_j \eta, \tau\right). \tag{7.8}$$

On substituting (7.8) into the homogeneous edge boundary conditions (3.20), rewritten in terms of the dimensionless variables and employing the Cauchy-Riemann identities, we obtain

$$\begin{aligned} &\left(\nu - \gamma_1^2\right) W_{1,\xi\xi} + \left(\nu - \gamma_2^2\right) W_{2,\xi\xi} = 0, \\ &\gamma_1 \left(\gamma_1^2 - 2 + \nu\right) W^*_{1,\xi\xi\xi} + \gamma_2 \left(\gamma_2^2 - 2 + \nu\right) W^*_{2,\xi\xi\xi} = 0, \end{aligned} \tag{7.9}$$

with the asterisk, as previously, denoting a harmonic conjugate. These conditions imply

$$\gamma_1^2 \gamma_2^2 + 2(1 - \nu)\gamma_1 \gamma_2 - \nu^2 = 0, \tag{7.10}$$

which coincides with the dispersion relation (3.24).

Hence, on using (7.9), the representation for the bending edge wave through a single plane harmonic function is now established in the form

$$W\left(x, y, t\right) = W_j\left(x, \gamma_j y, t\right) - \frac{\nu - \gamma_j^2}{\nu - \gamma_n^2} W_j\left(x, \gamma_n y, t\right), \qquad 1 \le j \ne n \le 2, \tag{7.11}$$

which is similar to (2.40) for the Rayleigh wave. On the edge $\eta = 0$ the last formula reduces to

$$W\left(x, 0, t\right) = \frac{\gamma_j^2 - \gamma_n^2}{\nu - \gamma_n^2} W_j\left(x, 0, t\right), \qquad 1 \le j \ne n \le 2. \tag{7.12}$$

As an example, we construct a non-time-harmonic eigensolution for the bending edge wave mirroring that considered in subsection 2.2. The sought for functions W_j, $j = 1, 2$, should satisfy the ansatz (7.3) along with the elliptic equations

$$W_{j,\eta\eta} + \gamma_j^2 W_{j,\xi\xi} = 0. \tag{7.13}$$

Let us specify the initial conditions

$$W_j\big|_{\tau=0} = A_j(\xi, \gamma_j\eta), \qquad W_{j,\tau}\big|_{\tau=0} = B_j(\xi, \gamma_j\eta), \tag{7.14}$$

where A_j and B_j are plane harmonic functions. Then, (7.11) implies

$$\begin{aligned} W\big|_{\tau=0} &= A_j(\xi, \gamma_j\eta) - \frac{\nu-\gamma_j^2}{\nu-\gamma_n^2} A_j(\xi, \gamma_n\eta), \\ W_{,\tau}\big|_{\tau=0} &= B_j(\xi, \gamma_j\eta) - \frac{\nu-\gamma_j^2}{\nu-\gamma_n^2} B_j(\xi, \gamma_n\eta), \end{aligned} \tag{7.15}$$

The Fourier transforms of the functions W_j are given by

$$W_j^F = w_j(k,\tau) e^{-\gamma_j|k|\eta}, \tag{7.16}$$

with the initial conditions for the quantities w_j

$$w_j\big|_{\tau=0} = A_j^F(k,0), \quad w_{j,\tau}\big|_{\tau=0} = B_j^F(k,0), \tag{7.17}$$

where k is the Fourier transform parameter. Hence, the functions W_j satisfying (7.3) are

$$W_j = \frac{1}{2\pi} \int\limits_{-\infty}^{\infty} \left[\frac{B_j^F(k,0)}{\gamma_e^2 k^2} \sin\left(\gamma_e^2 k^2 \tau\right) + A_j^F(k,0) \cos\left(\gamma_e^2 k^2 \tau\right) \right] e^{-\gamma_j|k|\eta + i\xi k} dk, \tag{7.18}$$

with the edge deflection following from (7.11).

Consider, for example, the functions $A_j(\xi, \gamma_j\eta)$ and $B_j(\xi, \gamma_j\eta)$ specified as

$$A_j(\xi, \gamma_j\eta) = \frac{\gamma_j\,(\eta + a)}{\pi\left(\gamma_j^2\,(\eta+a)^2 + \xi^2\right)}, \qquad B_j(\xi, \gamma_j\eta) = 0, \tag{7.19}$$

where a is a positive constant corresponding to a distributed delta-like initial profile at the edge $\eta = 0$; at the limit $a \to 0$ we get $W_j(\xi, 0, 0) = \delta(\xi)$. On inserting the Fourier transforms of (7.19) into (7.18), we arrive at

$$W(\xi, \eta, \tau) = \frac{1}{\pi} \sum_{j=1}^{2} \int\limits_{0}^{+\infty} \cos\left(\gamma_e^2 k^2 \tau\right) \cos(\xi k) e^{-\gamma_j k(\eta + a)} dk, \tag{7.20}$$

decaying away from the edge $\eta = 0$. The integrals in (7.20) may be evaluated with the help of the formula, e.g. see Prudnikov et al. (1986)

$$I(p,q) = \int\limits_{0}^{+\infty} e^{-p^2 k - qk} dk = \frac{1}{2}\sqrt{\frac{\pi}{p}}\, f\left(\frac{q}{2\sqrt{p}}\right), \tag{7.21}$$

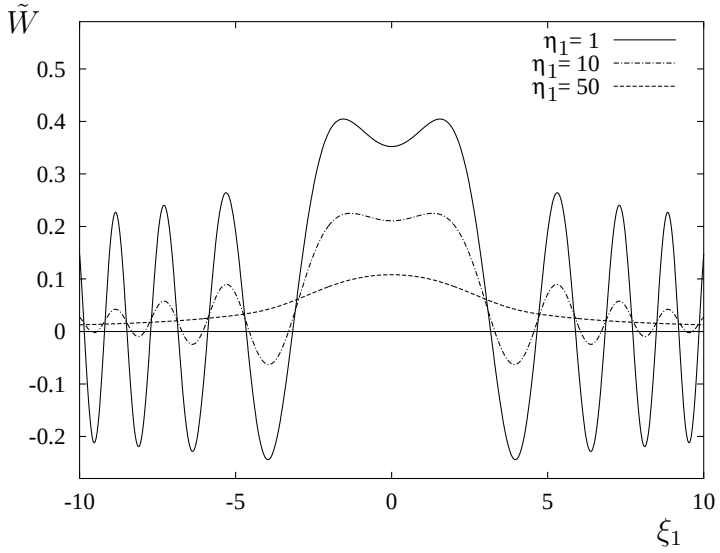

Figure 42: The scaled deflection $\tilde{W}$ vs. ξ_1 at $\nu = 1/3$.

where $f(z) = e^{z^2} erfc(z)$, $\mathrm{R}e(p) = 0$, $\mathrm{I}m(p) \neq 0$, $\mathrm{R}e(q) \geq 0$, with

$$erfc(z) = \frac{2}{\sqrt{\pi}} \int_z^{+\infty} e^{-t^2} dt \tag{7.22}$$

denoting the complementary error function, see Abramowitz & Stegun (2012).

As a result, (7.20) is expressed in terms of the quantities $\xi_1 = \dfrac{\xi}{\sqrt{\tau}}$ and $\eta_1 = \dfrac{\eta + a}{\sqrt{\tau}}$ as

$$W(\xi, \eta, \tau) = \tau^{-0.5}\, \tilde{W}(\xi_1, \eta_1), \tag{7.23}$$

where

$$\tilde{W}(\xi_1, \eta_1) = \frac{1}{4\gamma_e \sqrt{\pi}} \sum_{j=1}^{2} \mathrm{R}e \left[e^{i\pi/4} \sum_{m=1}^{2} f(\zeta_{jm}) \right], \tag{7.24}$$

with $\zeta_{jm} = \dfrac{e^{i\pi/4} \left(\gamma_j \eta_1 + (-1)^m i \xi_1\right)}{2\gamma_e}$.

A numerical illustration of (7.24) is given in Fig. 42 for the Poisson's ratio $\nu = 1/3$. As might be expected, the amplitudes of the propagating disturbances decay away from the edge $\eta_1 = 0$.

7.2 Bending edge wave induced by prescribed moments and shear forces

Once the eigensolution is established, we proceed with the development of an explicit model for the bending edge wave, aiming at extracting its contribution to the overall dynamic response in a manner similar to that presented in section 4 for the Rayleigh wave.

Throughout this subsection we study bending edge waves induced by prescribed bending moment M_0 and shear force N_0. The boundary conditions along the edge $x_2 = 0$ are therefore given by

$$\begin{aligned} W_{,22} + \nu W_{,11} &= -\frac{M_0}{D}, \\ W_{,222} + (2-\nu)\, W_{,112} &= -\frac{N_0}{D}. \end{aligned} \tag{7.25}$$

As before, we start from a multiple scale procedure, adapting it for plate bending. Accordingly, the slow time $\tau_s = \varepsilon\tau$ is introduced along with the fast time $\tau_f = \tau$, where $\varepsilon \ll 1$ is a small parameter, characteristic of a near-resonant edge excitation, see subsection 7.4.2 and also Kaplunov et al. (2016).

First, we rewrite (7.2) in the form

$$\Delta^2 W + W_{,\tau_f\tau_f} + 2\varepsilon W_{,\tau_f\tau_s} + \varepsilon^2 W_{,\tau_s\tau_s} = 0. \tag{7.26}$$

Then, the deflection W can be expanded into asymptotic series as

$$W = \frac{h^2 P}{\varepsilon D}\left(W^{(0)} + \varepsilon W^{(1)} + ...\right). \tag{7.27}$$

Here and below in this subsection

$$P = \max_{x,t}\left[M_0(x,t), hN_0(x,t)\right]. \tag{7.28}$$

On substituting (7.27) into (7.26), we have at leading order

$$\Delta^2 W^{(0)} + W^{(0)}_{,\tau_f\tau_f} = 0. \tag{7.29}$$

In view of the ansatz (7.3), the last equation is transformed to the elliptic equation

$$W^{(0)}_{,\eta\eta\eta\eta} + 2W^{(0)}_{,\xi\xi\eta\eta} + \left(1-\gamma_e^4\right) W^{(0)}_{,\xi\xi\xi\xi} = 0, \tag{7.30}$$

leading to

$$W^{(0)} = \sum_{j=1}^{2} W_j^{(0)} \left(\xi, \gamma_j \eta, \tau_f, \tau_s\right), \tag{7.31}$$

with the scaling factors $\gamma_j,\ \ j = 1, 2$, defined by (7.7).

At next order, we obtain from (7.26)

$$\Delta^2 W^{(1)} + W^{(1)}_{,\tau_f \tau_f} + 2W^{(0)}_{,\tau_f \tau_s} = 0. \tag{7.32}$$

In view of the assumption (7.3) along with the superposition principle, the equation (7.32) may be re-written as

$$\Delta_1 \Delta_2 W_j^{(1)} = -2W^{(0)}_{,\tau_f \tau_s} \qquad (j = 1, 2), \tag{7.33}$$

with $W^{(1)} = W_1^{(1)} + W_2^{(1)}$.

Let us first study $W_1^{(1)}$. On employing the basic properties of harmonic functions, we have

$$\Delta_2 W_1^{(0)} = (\gamma_2^2 - \gamma_1^2) W^{(0)}_{1,\xi\xi} = 2\gamma_e^2 W^{(0)}_{1,\xi\xi}. \tag{7.34}$$

Then, due to (7.33) and (7.34), we infer

$$\Delta_1 \Delta_2 W^{(1)}_{1,\xi\xi} = -\frac{1}{\gamma_e^2} \Delta_2 W^{(0)}_{1,\tau_f \tau_s}, \tag{7.35}$$

from which

$$\Delta_1 W^{(1)}_{1,\xi\xi\eta} = -\frac{1}{\gamma_e^2} W^{(0)}_{1,\tau_f \tau_s \eta}. \tag{7.36}$$

The solution of (7.35) is found in the form

$$W^{(1)}_{1,\xi\xi\eta} = \Phi^{(1,0)}_{1,\xi\xi\eta} - \frac{\eta}{2\gamma_e^2} W^{(0)}_{1,\tau_f \tau_s}, \tag{7.37}$$

where $\Phi_1 = \Phi_1\left(\xi, \gamma_1 \eta, \tau_f, \tau_s\right)$ is an arbitrary plane harmonic function in the first two arguments.

Similar derivations for $W_2^{(1)}$ yield

$$W^{(1)}_{2,\xi\xi\eta} = \Phi^{(1,0)}_{2,\xi\xi\eta} + \frac{\eta}{2\gamma_e^2} W^{(0)}_{2,\tau_f \tau_s}, \tag{7.38}$$

where $\Phi_2 = \Phi_2\left(\xi, \lambda_2 \eta, \tau_f, \tau_s\right)$ is also a plane harmonic function.

Thus, we obtain the following two-term asymptotic expansion

$$\begin{aligned} W_{,\xi\xi\eta} = \frac{h^2 P}{D} \Big[\varepsilon^{-1} \left(W^{(0)}_{1,\xi\xi\eta} + W^{(0)}_{2,\xi\xi\eta} \right) + \Phi^{(1,0)}_{1,\xi\xi\eta} + \Phi^{(1,0)}_{2,\xi\xi\eta} \\ - \frac{\eta}{2\gamma_e^2} \left(W^{(0)}_{1,\tau_f \tau_s} - W^{(0)}_{2,\tau_f \tau_s} \right) + \ldots \Big]. \end{aligned} \tag{7.39}$$

Now, we proceed further with analysis of the non-homogeneous edge boundary conditions (7.25), beginning with a prescribed bending moment ($M_0 \neq 0, N_0 = 0$). On rewriting (2.9) in terms of the dimensionless variables ξ and η, we get

$$\begin{aligned} W_{,\eta\eta} + \nu W_{,\xi\xi} &= -\frac{h^2}{D} M_0, \\ W_{,\eta\eta\eta} + (2-\nu)\, W_{,\xi\xi\eta} &= 0. \end{aligned} \tag{7.40}$$

Then, we insert the asymptotic expansion (7.39) into (7.40), having at leading order

$$\begin{aligned} &(\nu - \gamma_1^2)\, W^{(0)}_{1,\xi\xi} + (\nu - \gamma_2^2)\, W^{(0)}_{2,\xi\xi} = 0, \\ &\gamma_1 (\gamma_1^2 - 2 + \nu)\, W^{(0)}_{1,\xi\xi\xi} + \gamma_2 (\gamma_2^2 - 2 + \nu)\, W^{(0)}_{1,\xi\xi\xi} = 0. \end{aligned} \tag{7.41}$$

It can be easily verified that these equations imply the dispersion relation (7.10).

At next order, after straightforward transformations involving (7.35), the boundary conditions (7.40) yield

$$\begin{aligned} &\left(1 - \frac{\nu}{\gamma_1^2}\right) W^{(1)}_{1,\xi\xi\eta\eta} + \left(1 - \frac{\nu}{\gamma_2^2}\right) W^{(1)}_{2,\xi\xi\eta\eta} - \frac{\nu}{\gamma_e^2 \gamma_1^2}\, W^{(0)}_{1,\tau_f\tau_s} \\ &\qquad + \frac{\nu}{\gamma_e^2 \gamma_2^2}\, W^{(0)}_{2,\tau_f\tau_s} = -\frac{1}{P}\, M_{0,\xi\xi}, \\ &W^{(1)}_{1,\xi\xi\eta\eta\eta} + W^{(1)}_{2,\xi\xi\eta\eta\eta} + (2-\nu)\, W^{(1)}_{1,\xi\xi\xi\xi\eta} + (2-\nu)\, W^{(1)}_{2,\xi\xi\xi\xi\eta} = 0. \end{aligned} \tag{7.42}$$

On substituting (7.39) into (7.42), using the Cauchy-Riemann identities, taking the harmonic conjugate of the second equation, and integrating with respect to ξ, the analysed boundary conditions may be rearranged to

$$\begin{aligned} &(\nu - \gamma_1^2)\, \Phi^{(1,0)}_{1,\xi\xi\xi\xi} + (\nu - \gamma_2^2)\, \Phi^{(1,0)}_{2,\xi\xi\xi\xi} = \frac{1}{2\gamma_e^2} \left(1 + \frac{\nu}{\gamma_1^2}\right) W^{(0)}_{1,\tau_f\tau_s} \\ &\qquad - \frac{1}{2\gamma_e^2} \left(1 + \frac{\nu}{\gamma_2^2}\right) W^{(0)}_{2,\tau_f\tau_s} - \frac{1}{P}\, M_{0,\xi\xi}, \\ &\gamma_1 (\nu - \gamma_2^2)\, \Phi^{(1,0)}_{1,\xi\xi\xi\xi} + \gamma_2 (\nu - \gamma_1^2)\, \Phi^{(1,0)}_{2,\xi\xi\xi\xi} = \frac{\gamma_2}{\gamma_e^2}\, W^{(0)}_{2,\tau_f\tau_s} - \frac{\gamma_1}{\gamma_e^2}\, W^{(0)}_{1,\tau_f\tau_s}. \end{aligned} \tag{7.43}$$

In contrast to (7.41), the equations (7.43) are non-homogeneous, with the determinant vanishing due to (7.10). Then, the compatibility condition necessitates

$$\begin{aligned} &\left[\gamma_1(\nu - \gamma_2^2) - \frac{\gamma_2(\nu^2 - \gamma_1^4)}{2\gamma_1^2}\right] W^{(0)}_{1,\tau_f\tau_s} \\ &+ \left[\gamma_2(\nu - \gamma_2^2) + \frac{(\nu - \gamma_1^2)(\nu + \gamma_2^2)}{2\gamma_2}\right] W^{(0)}_{2,\tau_f\tau_s} = -\frac{\gamma_e^2 \gamma_2 (\nu - \gamma_1^2)}{P}\, M_{0,\xi\xi}. \end{aligned} \tag{7.44}$$

In view of (7.11), it is possible to express $W_1^{(0)}$ and $W_2^{(0)}$ through $W^{(0)}$ on the edge $\eta = 0$, leading to

$$W^{(0)}_{,\tau_f\tau_s} = \frac{B_K}{2P}\, M_{0,\xi\xi}, \tag{7.45}$$

where

$$B_K = -\frac{4\gamma_e^4\gamma_2(\nu-\gamma_1^2)}{a_{1K}(\nu-\gamma_1^2)+a_{2K}(\nu-\gamma_2^2)}, \tag{7.46}$$

with

$$a_{1K} = \frac{(\nu+\gamma_2^2)(\nu-\gamma_1^2)}{2\gamma_2} + \gamma_2(\nu-\gamma_2^2), \quad a_{2K} = \frac{\gamma_2(\nu^2-\gamma_1^4)}{2\gamma_1^2} + \gamma_1(\nu-\gamma_2^2).$$

After some rather tedious but straightforward algebra, (7.46) can be reduced to

$$B_K = \frac{\sqrt{1-\gamma_e^4}\left(\nu+\sqrt{1-\gamma_e^4}\right)}{1-\nu+\sqrt{1-\gamma_e^4}}, \tag{7.47}$$

depending on the Poisson's ratio only. Fig. 43 reveals a monotonic increase of B_K in ν.

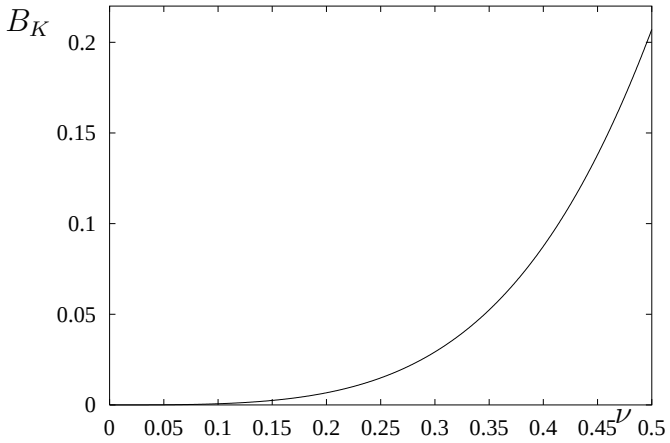

Figure 43: The coefficient B_K vs. ν

Finally, on employing the leading order approximation

$$W = \frac{h^2P}{\varepsilon D}W^{(0)}, \tag{7.48}$$

we present (7.45) as

$$2\varepsilon W_{,\tau_f\tau_s} = \frac{3B_K(1-\nu^2)}{2Eh}\, M_{0,\xi\xi}. \tag{7.49}$$

Then, due to the ansatz (7.3), this equation becomes

$$\gamma_e^4 W_{,\xi\xi\xi\xi} + W_{,\tau_f\tau_f} + 2\varepsilon W_{,\tau_f\tau_s} = \frac{3B_K(1-\nu^2)}{2Eh}\, M_{0,\xi\xi}, \tag{7.50}$$

or, in the original variables to within the error $O(\varepsilon^2)$

$$D\gamma_e^4 W_{,1111} + 2\rho h W_{,tt} = B_K\, M_{0,11}. \tag{7.51}$$

In this case the behaviour over the interior is described by the elliptic equations

$$W_{j,22} + \gamma_j^2 W_{j,11} = 0, \tag{7.52}$$

which should be solved in conjunction with the deduced parabolic equation (7.51) and the relation (7.11). Thus, the solution of the dynamic equation (7.51) is used together with (7.12) as a boundary condition for the pseudo-static equations (7.52). The obtained plane harmonic function is then substituted into (7.11) in order to restore the deflection of the plate.

Similarly to the Rayleigh wave, it may be shown that the derived parabolic-elliptic formulation provides a correct evaluation of the edge wave contribution to the overall response arising from an arbitrary edge moment M_0. This is not surprising, since the developed procedure is, in fact, aimed at accounting for edge wave poles, see subsection 7.4.1 below.

A parabolic-elliptic formulation may also be established for a *shear force* excitation, having $N_0 \neq 0, M_0 = 0$. However, instead of the deflection W, the parabolic equation is now obtained in respect of the rotation angle $\theta_K = W_{,2}$ evaluated at the edge $x_2 = 0$. It is

$$D\gamma_e^4 \theta_{K,1111} + 2\rho h \theta_{K,tt} = -B_K N_{0,11}, \tag{7.53}$$

with the constant B_K defined by (7.47). In this case the parabolic-elliptic model also contains the elliptic equations

$$\theta_{Kj,22} + \gamma_j^2 \theta_{Kj,11} = 0, \tag{7.54}$$

which are to be solved together with (7.53) and (7.11).

7.3 Plate on elastic foundation

Bending edge waves in plates on elastic foundations have recently been investigated in Kaplunov et al. (2014), Kaplunov & Nobili (2015), and Kaplunov et al. (2016). In this subsection we briefly address several peculiarities of the bending edge wave on a thin Kirchhoff plate resting on a Winkler foundation. In this case an additional term arises in the governing equation (3.18), namely

$$D\Delta^2 W + 2\rho h W_{,tt} + \beta_W W = 0, \tag{7.55}$$

where β_W is the Winkler foundation modulus. The related dispersion relation is

$$Dk^4\gamma_e^4 + \beta_W = 2\rho h\omega^2. \tag{7.56}$$

The latter may be simplified to

$$K^4 = \Omega^2 - 1, \tag{7.57}$$

where

$$K = k\gamma_e \left(D/\beta_W\right)^{1/4}, \qquad \Omega = \omega \left(2\rho h/\beta_W\right)^{1/2}. \tag{7.58}$$

The presence of a Winkler foundation leads to the cut-off frequency $\Omega_0 = 1$, see Fig. 44. Another remarkable feature caused by a foundation is the local minimum of the phase velocity

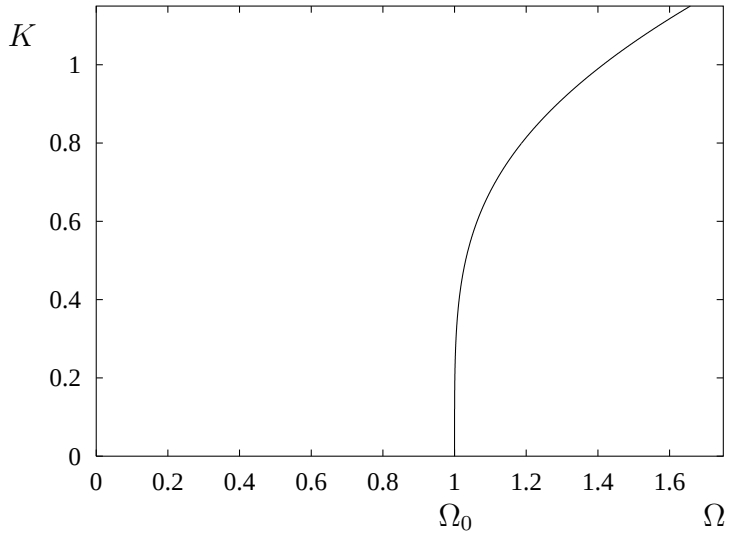

Figure 44: The dispersion curve (7.57).

$$V^{ph} = \frac{\Omega}{K} = \frac{\Omega}{\left(\Omega^2 - 1\right)^{1/4}} \tag{7.59}$$

$V^{ph} = \sqrt{2}$, occurring at $\Omega = \sqrt{2}$ or $K = 1$, see Fig. 45. Moreover, at this point V^{ph} coincides with the group velocity

$$V^g = \frac{d\Omega}{dK} = \frac{2}{\Omega}\left(\Omega^2 - 1\right)^{3/4}. \tag{7.60}$$

It is also worth mentioning that the minimal value of the phase velocity $V^{ph} = V^g = \sqrt{2}$, similar to that shown in Fig. 45, corresponds to the critical speed of a moving load in the steady-state problem for a beam supported by a Winkler foundation, e.g. see the well-known

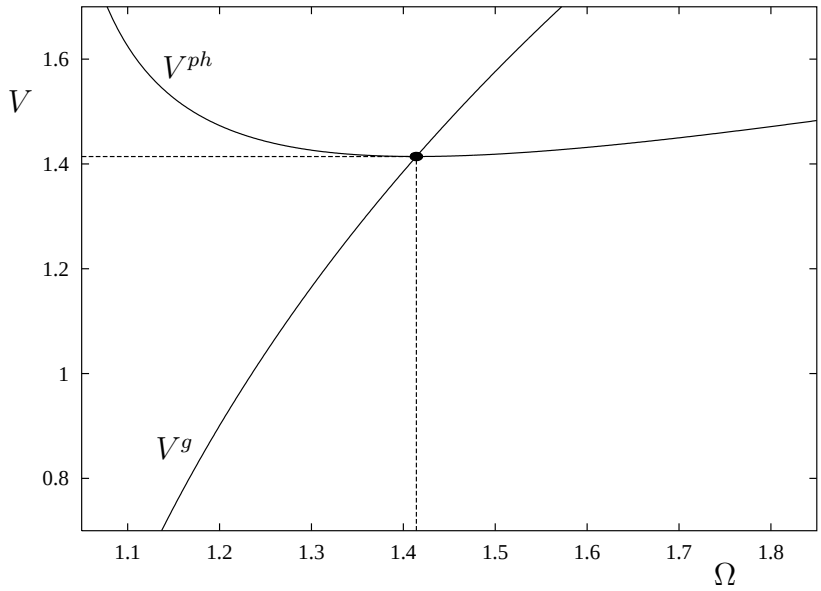

Figure 45: The phase and group velocities according to (7.59) and (7.60).

contribution of Timoshenko (1927). Therefore, the same resonant effect may be expected for a moving load on the edge of an elastically supported plate.

Finally, we present the parabolic-elliptic formulation for a plate on a Winkler foundation, which may be derived in the same manner as in the previous subsection 7.2, see also Kaplunov et al. (2016). The ansatz generalising (7.3) is now written as

$$\gamma_e^4 W_{,\xi\xi\xi\xi} + W_{,\tau\tau} + \frac{\beta_W h^4}{D} W = 0. \tag{7.61}$$

As a result, we arrive at the pseudo-static elliptic equation (7.52), subject to a boundary condition on the edge $x_2 = 0$ given by the dynamic parabolic equation

$$D\gamma_e^4 W_{,1111} + 2\rho h W_{,tt} + \beta_W W = B_K\, M_{0,11}, \tag{7.62}$$

or the similar equation (7.54) with the boundary condition

$$D\gamma_e^4 \theta_{K,1111} + 2\rho h \theta_{K,tt} + \beta_W \theta_K = -B_K N_{0,11}. \tag{7.63}$$

7.4 Examples

Consider now examples demonstrating the implementation of the formulation developed in subsection 7.2.

7.4.1 Comparison with exact solution

Let us apply the Laplace transform in time τ and the Fourier transform in the longitudinal coordinate ξ in (7.2). Then, the transformed deflection W^{FL} satisfies the equation

$$W^{FL}_{,\eta\eta\eta\eta} - 2k^2 W^{FL}_{,\eta\eta} + \left(k^4 + p^2\right) W^{FL} = 0, \tag{7.64}$$

where k and p, as above, denote the parameters of the Fourier and Laplace transforms, respectively. The solution of this equation is

$$W^{FL} = C_1 e^{-g_1\eta} + C_2 e^{-g_2\eta}, \tag{7.65}$$

where $C_n(k,p)$, $n = 1, 2$, are arbitrary functions and

$$g_{1,2} = k^2 \pm ip. \tag{7.66}$$

Consider an arbitrary bending moment M_0 applied at the edge $\eta = 0$. In this case the boundary conditions (7.40) are transformed to

$$\begin{aligned} W^{FL}_{,\eta\eta} - \nu k^2 W^{FL} &= -\frac{h^2}{D} M_0^{FL}, \\ W^{FL}_{,\eta\eta\eta} - (2-\nu)\, k^2 W^{FL}_{,\eta} &= 0, \end{aligned} \tag{7.67}$$

where M_0^{FL} is the transformed moment M_0. On substituting (7.65) into (7.67), we determine C_n, having

$$W^{FL} = \frac{1}{G}\left(G_1 e^{-g_1\eta} + G_2\, e^{-g_2\eta}\right), \tag{7.68}$$

where

$$\begin{aligned} G_j &= (-1)^j g_j \left[g_j^2 - (2-\nu)k^2\right] \frac{h^2 M_0^{FL}}{D}, \qquad (j = 1, 2) \\ G &= (g_1 - g_2)\left[g_1^2 g_2^2 + 2g_1 g_2 (1-\nu)k^2 - \nu^2 k^4\right]. \end{aligned} \tag{7.69}$$

Next, we note that the term in square brackets in the expression for G may be rewritten as

$$k^4 + p^2 + 2(1-\nu)k^2\sqrt{k^4 + p^2} - \nu^2 k^4. \tag{7.70}$$

The poles

$$p^2 = -\gamma_e^4 k^4, \tag{7.71}$$

correspond to those of the dispersion relation (7.10). It is worth mentioning that at the poles (7.71) the equation (7.64) is identical to the tranformed elliptic equation (7.5) (or (7.52)), while (7.68) is related to the parabolic equation (7.51) at the edge $\eta = 0$. In particular, on taking into account (7.69), we deduce from (7.68)

$$W^{FL}\big|_{\eta=0} = -\frac{h^2 M_0^{FL}\left(\sqrt{k^4+p^2}+\nu k^2\right)}{D\left(k^4+p^2+2(1-\nu)k^2\sqrt{k^4+p^2}-\nu^2k^4\right)}. \tag{7.72}$$

Near the poles (7.71) the latter becomes

$$W^{FL}\big|_{\eta=0} \approx -\frac{h^2 M_0^{FL} p^2\sqrt{1-\gamma_e^4}\left(\sqrt{1-\gamma_e^4}+\nu\right)}{D\left(\sqrt{1-\gamma_e^4}+1-\nu\right)\left(\gamma_e^4k^4+p^2\right)}, \tag{7.73}$$

which is indeed the transformed solution of the equation (7.51) expressed in the variables ξ and τ. Thus, the formulation (7.51) and (7.52) captures the contribution of the poles of the bending edge wave induced by a moment of a general shape.

7.4.2 Near-resonant excitation

Let a prescribed bending edge moment be

$$M_0 = Ae^{i(kx-\omega t)}, \tag{7.74}$$

with no shear edge force assumed. Then, the solution of the plate bending equation (3.18), subject to the non-homogeneous boundary conditions (7.40), can be written as

$$W(x,y,t) = V(y)e^{i(kx-\omega t)}. \tag{7.75}$$

As a result, (3.18) becomes

$$\frac{d^4V}{dy^4} - 2k^2\frac{d^2V}{dy^2} + \left(k^4 - \frac{2\rho h\omega^2}{D}\right)V = 0, \tag{7.76}$$

leading to

$$W(x,y,t) = \sum_{n=1}^{2} C_n e^{i(kx-\omega t)-k\chi_n y}, \tag{7.77}$$

with

$$\chi_1^2+\chi_1^2 = 2, \qquad \chi_1^2\chi_2^2 = 1 - \frac{2\rho h\omega^2}{Dk^4}. \tag{7.78}$$

It is easily verified that the attenuation orders χ_n, $n = 1, 2$, coincide with γ_n defined by (7.7), provided that the frequency ω and the wave number k satisfy the dispersion relation (3.24). The constants C_n may be determined from the boundary conditions (7.40). The exact solution at the edge is then given by

$$W(x,0,t) = -\frac{A}{Dk^2}\,\frac{\chi_1\chi_2+\nu}{\chi_1^2\chi_2^2+2(1-\nu)\chi_1\chi_2-\nu^2}\,e^{i(kx-\omega t)}. \tag{7.79}$$

Compare this formula with that obtained from the approximate formulation derived in subsection 7.2 and given by the solution of (7.51). The latter is

$$W(x,0,t) = -\frac{AB_Kk^2}{Dk^4\gamma_e^4-2\rho h\omega^2}\,e^{i(kx-\omega t)}, \tag{7.80}$$

with B_K defined by (7.47). It may be observed that both (7.79) and (7.80) exhibit a resonant behaviour when the frequency ω and the wave number k satisfy the dispersion relation (3.24).

Let the excitation frequency be close to that of the bending edge wave, i.e.

$$\omega = \omega_0 + \varepsilon\omega_1, \qquad |\varepsilon| \ll 1, \tag{7.81}$$

where $\omega_0 = \sqrt{\dfrac{D\gamma_e^2k^4}{2\rho h}}$, see (3.24). This is exactly the setup of bending edge motion evolving in the slow time $\tau_s \sim \varepsilon t$, which is in line with the asymptotic theory developed in subsection 7.2.

First, we obtain

$$\chi_1\chi_2 \approx \gamma_1\gamma_2 - \frac{2\rho h}{Dk^4}\,\frac{\varepsilon\omega_0\omega_1}{\gamma_1\gamma_2}. \tag{7.82}$$

On substituting the latter into (7.79) and making use of (7.10), we arrive at

$$\begin{aligned} W(x,0,t) \approx -\frac{A}{Dk^2}\frac{(\gamma_1\gamma_2+\nu)\,e^{i(kx-\omega t)}}{[\gamma_1^2\gamma_2^2+2(1-\nu)\gamma_1\gamma_2-\nu^2]-\dfrac{4\rho h\varepsilon\omega_0\omega_1}{Dk^4}\left(1+\dfrac{1-\nu}{\gamma_1\gamma_2}\right)} \\ = \frac{AB_Kk^2e^{i(kx-\omega t)}}{4\rho h\varepsilon\omega_0\omega_1}. \end{aligned} \tag{7.83}$$

This expression coincides with the leading order behaviour of (7.80). Indeed, on inserting (7.81), we have

$$W(x,0,t) \approx -\frac{AB_Kk^2\,e^{i(kx-\omega t)}}{[Dk^4\gamma_e^4+\beta-2\rho h\omega_0^2]-4\rho h\varepsilon\omega_0\omega_1} = \frac{AB_Kk^2e^{i(kx-\omega t)}}{4\rho h\varepsilon\omega_0\omega_1}, \tag{7.84}$$

which coincides with (7.83).

8 Conclusion

Explicit hyperbolic-elliptic and parabolic-elliptic models drastically simplify treatment and understanding of dynamic phenomena involving Rayleigh and Rayleigh-type waves. In particular, they enable a straightforward insight into various impact and moving load problems, including surprisingly simple asymptotic formulae for the 3D displacement fields caused by a point moving load. Another important advantage of these models is the separation of the original exact formulations into two parts, namely hyperbolic or parabolic dynamic problems along the surface or edge together with pseudo-static elliptic problems over the interior. The solutions of dynamic problems provide boundary conditions for pseudo-static ones; in doing so, sometimes it is enough to restrict ourselves to the dynamic problems only. In addition, the possibility of dealing with elliptic equations over the interior instead of hyperbolic ones appears to be very useful for optimising numerical computations.

The developed methodology allows a number of extensions. Among them, we mention finite and curved bodies as well as half-spaces with a more general vertical inhomogeneity. Modelling of the surface wave induced by internal sources is also of obvious interest. Another important area is concerned with interaction of surface and bulk waves. This may occur when an elastic structure, e.g. a rod, is attached to the surface or in the case of a rigid stamp. Also, the well-known phenomenon of the conversion of plate bending and extensional waves into surface ones at a short-wavelength limit may open new prospects for deriving refined plate theories. Analysis of some of the aforementioned problems is already in progress.

Appendix A. Near-resonant behaviour of a single degree of freedom linear oscillator

Consider forced vibrations of a single degree of freedom linear oscillator governed by

$$\frac{d^2x}{dt^2} + \omega_0^2 x = F(\tau)e^{-i\omega_0 t}, \tag{A.1}$$

where ω_0 is the natural frequency, and $\tau = \varepsilon t$ is the slow time. Here the parameter $\varepsilon \ll 1$ is associated with a small deviation of the excitation frequency from the natural one. For example, the forcing $F(\tau) = e^{-i\omega_1 \tau}$ prescribes the excitation frequency of $\omega = \omega_0 + \varepsilon\omega_1$.

Let us now develop a multiple scale perturbation procedure, see e.g. Cole (1968) and Nayfeh (2000), expanding

$$x(t,\tau) = \varepsilon^{-1}\left(x_0(t,\tau) + \varepsilon x_1(t,\tau) + \dots\right), \tag{A.2}$$

and making use of the symbolic identity

$$\frac{d^2}{dt^2} = \frac{\partial^2}{\partial t^2} + 2\varepsilon\frac{\partial^2}{\partial t\partial\tau} + \varepsilon^2\frac{\partial^2}{\partial\tau^2}. \tag{A.3}$$

Then, on substituting (A.2) into (A.1), we have at leading order

$$x_{0,tt} + \omega_0^2 x_0 = 0. \tag{A.4}$$

As before, the comma in the subscript denotes a partial derivative. Therefore

$$x_0 = A(\tau)e^{-i\omega_0 t}. \tag{A.5}$$

At next order we obtain

$$x_{1,tt} + \omega_0^2 x_1 + 2x_{0,t\tau} = F(\tau)e^{-i\omega_0 t}, \tag{A.5}$$

or

$$x_{1,tt} + \omega_0^2 x_1 = \left(F(\tau) + 2iA'(\tau)\right)e^{-i\omega_0 t}. \tag{A.6}$$

In order to exclude a secular term, we impose

$$F(\tau) + 2iA'(\tau) = 0. \tag{A.7}$$

Then the sought for leading order solution becomes

$$x_0(t,\tau) = \frac{ie^{-i\omega_0 t}}{2}\int F(\tau)d\tau. \tag{A.8}$$

Appendix B. Exact analysis of plane moving load problems

In this appendix we discuss steady-state problems for a vertical force or stamp moving along the surface of an elastic half-plane.

First, we study dynamic response of the elastic half-plane $\mathcal{H}_2^+$, see (2.25), subject to a vertical distributed force P, moving steadily at a constant speed c. The boundary conditions at $x_3 = 0$ are specified as

$$\sigma_{13} = 0, \qquad \sigma_{33} = P(s), \tag{B.1}$$

where, as previously, s is a moving coordinate, i.e. $s = x_1 - ct$. The governing equations for the elastic potentials written in the moving coordinate frame (s, x_3), become

$$\begin{aligned} \phi_{,33} + \left(1 - \frac{c^2}{c_1^2}\right)\phi_{,ss} = 0, \\ \psi_{,33} + \left(1 - \frac{c^2}{c_2^2}\right)\psi_{,ss} = 0. \end{aligned} \tag{B.2}$$

Then, the boundary conditions (B.1) take the form

$$\begin{aligned} 2\phi_{,s3} + \psi_{,ss} - \psi_{,33} = 0, \\ (\kappa^2 - 2)\phi_{,ss} + \kappa^2\phi_{,33} + 2\psi_{,s3} = \frac{P(s)}{\mu}. \end{aligned} \tag{B.3}$$

Let us focus on the subsonic regime ($c < c_2 < c_1$), when the equations (B.2) are elliptic. In this case the solution is expressed through plane harmonic functions in line with the consideration in subsection 2.2. Thus,

$$\phi = \phi(s, \alpha x_3), \qquad \psi = \psi(s, \beta x_3), \tag{B.4}$$

with α and β defined by (2.14). The only difference of solution (B.4) from (2.31) is that, instead of the phase speed, c now denotes the speed of a moving load.

Not surprisingly, the elastic potentials ϕ and ψ may be related to each other using the first homogeneous boundary condition (B.3) along with the Cauchy-Riemann identities, resulting in

$$\psi = \frac{2\alpha}{\beta^2 + 1}\phi^*. \tag{B.5}$$

Hence, the displacement components are expressed in terms of a single plane harmonic function, similarly to subsection 2.2, as

$$\begin{aligned} u_1(s,x_3) &= \phi_{,s}\left(s,\alpha x_3\right) - \frac{2\alpha\beta}{1+\beta^2}\,\phi_{,\xi}\left(\xi,\beta x_3\right), \\ u_3(s,x_3) &= \phi_{,3}\left(s,\alpha x_3\right) - \frac{2}{1+\beta^2}\,\phi_{,3}\left(s,\beta x_3\right). \end{aligned} \tag{B.6}$$

Also, using (B.5), the second boundary condition (B.3) becomes

$$\phi_{,ss}\big|_{x_3=0} = -\frac{(1+\beta^2)\,P(s)}{\mu R(c)}, \tag{B.7}$$

where $R(c)$ is defined by (4.77).

Let us assume that $P(s) = P_0\dfrac{dp}{ds}$. Then, on employing the Poisson formula, see e.g. Courant & Hilbert (1989), the derivative $\phi_{,s}$ is given by

$$\phi_{,s}(s,\alpha x_3) = -\frac{(1+\beta^2)\,P_0}{\pi\mu R(c)}\int\limits_{-\infty}^{\infty}\frac{\alpha x_3 p(r)}{(r-s)^2+\alpha^2 x_3^2}\,dr, \tag{B.8}$$

enabling a straightforward calculation of the displacement field through (B.6). For example, for the point load $P(s) = P_0\delta(s)$, e.g. see the well-known paper of Cole & Huth (1958), integration in (B.7) gives

$$\phi_{,s}\big|_{x_3=0} = -\frac{(1+\beta^2)\,P_0}{\mu R(c)}\left[H(s)-\frac{1}{2}\right]. \tag{B.9}$$

This solution is determined to within an arbitrary constant, which cannot be found from the steady-state formulation. The value $\frac{1}{2}$ in (B.9) is chosen in order to have symmetry.

On satisfying the boundary condition (B.9), the harmonic function $\phi_{,s}(s,\alpha x_3)$ is obtained as

$$\phi_{,s}(s,\alpha x_3) = -\frac{(1+\beta^2)\,P_0}{\pi\mu R(c)}\,\tan^{-1}\frac{s}{\alpha x_3}. \tag{B.10}$$

Finally, the sought for displacements are given by

$$\begin{aligned} u_1(s,x_3) &= -\frac{(1+\beta^2)\,P_0}{\pi\mu R(c)}\left[\tan^{-1}\frac{s}{\alpha x_3} - \frac{2\alpha\beta}{1+\beta^2}\,\tan^{-1}\frac{s}{\beta x_3}\right], \\ u_3(s,x_3) &= \frac{\alpha(1+\beta^2)\,P_0}{2\pi\mu R(c)}\left[\ln\left(s^2+\alpha^2x_3^2\right) - \frac{2}{1+\beta^2}\ln\left(s^2+\beta^2x_3^2\right)\right]. \end{aligned} \tag{B.11}$$

This result is identical to that presented in the aforementioned paper by Cole & Huth (1958), up to a rigid body motion component of the horizontal displacement.

The same methodology may be applied to mixed boundary value problems. In particular, consider the steady-state problem for a rigid stamp moving along the boundary of the elastic half-plane $\mathcal{H}_2^+$ at a constant speed $c < c_2$. The equations of motion in the moving coordinate frame (s, x_3) are again taken in the form (B.2), whereas now the boundary conditions along the surface $x_3 = 0$ become

$$\begin{aligned} \sigma_{33} &= 0, \qquad s \in S_1; \\ u_3 &= f(s), \qquad s \in S_2; \\ \sigma_{s3} &= 0, \qquad s \in \mathbb{R}, \end{aligned} \tag{B.12}$$

where $S_1 \cup S_2 = \mathbb{R}$. Due to the last condition, the relation (B.5) holds true. On introducing the auxiliary function

$$\phi_1 = \frac{\beta^2 - 1}{\beta^2 + 1}\,\phi_{,3} \tag{B.13}$$

and also the scaling $z = \alpha x_3$, it is possible to reduce the first equation of (B.2) with the boundary condition (B.12) to a conventional mixed boundary value problem for the Laplace equation. Thus, we have

$$\phi_{1,zz} + \phi_{1,ss} = 0 \tag{B.14}$$

subject to

$$\begin{aligned} \phi_1 &= f(s), \qquad \xi \in S_2; \\ \phi_{1,s} &= 0, \qquad \xi \in S_1, \end{aligned} \tag{B.15}$$

along the surface $z = 0$.

References

References

Abramowitz, M., & Stegun I.A. (2012). *Handbook of Mathematical Functions: with Formulas, Graphs, and Mathematical Tables*. Dover Publications, New York.

Achenbach, J.D. (1973). *Wave propagation in elastic solids*. North-Holland, Amsterdam, the Netherlands.

Achenbach, J.D. (1998). Explicit solutions for carrier waves supporting surface waves and plate waves, *Wave Motion*, **28**, 89–97.

Agarwal, V.K. (1978). On surface waves in general thermoelasticity. *Journal of Elasticity*, **8**, 171–177.

Alenitsyn, A.G. (1963). Rayleigh waves in a nonhomogeneous elastic half-space. *Journal of Applied Mathematics and Mechanics*, **27(3)**, 816–822.

Babich, V.M., & Kiselev, A.P. (2014) *Elastic waves. High-frequency theory*. BHV, Saint-Petersburg. (in Russian)

Barnett, D.M., & Lothe, J. (1974). Consideration of the existence of surface wave (Rayleigh wave) solutions in anisotropic elastic crystals. *Journal of Physics F*, **4**, 671-686.

Barnett, D.M., Lothe, J., Gavazza, S.D., & Musgrave, M.J.P. (1985). Considerations of the existence of interfacial (Stoneley) waves in bonded anisotropic half-spaces. *Proceedings of the Royal Society London Series A*, **402**, 153-166.

Bleustein, J. L. (1968). A new surface wave in piezoelectric materials. *Applied Physics Letters*, **13**, 412–413.

Borovikov, V.A. (1994). *Uniform stationary phase method*. IEE electromagnetic wave series, 40, London.

Brulé, S., Javelaud, E.H., Enoch, S., & Guenneau, S. (2014). Experiments on seismic metamaterials: molding surface waves. *Physical Review Letters* **112**, 133901.

Campbell, C.K. (1998). *Surface acoustic wave devices for mobile and wireless communications.* Academic Press, San Diego.

Cao, Y., Xia, H., & Li, Z. (2012). A semi-analytical/FEM model for predicting ground vibrations induced by high-speed train through continuous girder bridge. *Journal of Mechanical Science and Technology* **26**, 2485–2496.

Chadwick, P. (1976). The existence of pure surface modes in elastic materials with orthorhombic symmetry. *Journal of Sound and Vibration*, **47**, 39–52.

Chadwick, P. (1976). Surface and interfacial waves of arbitrary form in isotropic elastic media. *Journal of Elasticity*, **6**, 73–80.

Cherednichenko, K. (2007) An asymptotic expansion of the boundary-layer type for bending waves along the curved edge of a Kirchhoff-Love elastic plate. *Journal of Mathematical Sciences*, **142**, 2682-2688.

Chouet, B.(1985). Excitation of a buried magmatic pipe: A seismic source model for volcanic tremor. *Journal of Geophysical Research*, **90**, No. B2, 1881–1893.

Cole, J. D. (1968) *Perturbation methods in applied mathematics.* Blaisdell Publishing Company, Waltham Massachusetts.

Cole, J., & Huth, J. (1958). Stresses produced in a half plane by moving loads. *Journal of Applied Mechanics*, **25**, 433-436.

Colombi, A., Colquitt, D., Roux, P., Guenneau, S., & Craster, R. V. (2016). A seismic metamaterial: The resonant metawedge. *Scientific reports*, **6**, 27717.

Courant, R., & Hilbert, D. (1989). *Methods of Mathematical Physics. Vol. 2.* John Wiley & Sons, New York.

Dai, H.-H., Kaplunov, J., & Prikazchikov, D.A. (2010). A long-wave model for the surface elastic wave in a coated half-space. *Proceedings of the Royal Society London Series A*, **466**, 3097-3116.

De Hoop A.T. (2002). The moving-load problem in soil dynamics the vertical displacement approximation. *Wave Motion*, **36**, 335–346.

Destrade, M. (2004). Surface acoustic waves in rotating orthorhombic crystals. *Proceedings of the Royal Society London Series A*, **460**, 653-665.

Destrade, M. (2007). Seismic Rayleigh waves on an exponentially graded, orthotropic half-space. *Proceedings of the Royal Society London Series A*, **463**, 495-502.

Destrade, M., & Fu, Y.B. (2006). The speed of interfacial waves polarized in a symmetry plane. *International Journal of Engineering Science*, **44**, 26–36.

Destrade, M., Fu, Y.B., & Nobili, A. (2016). Edge wrinkling in elastically supported pre-stressed incompressible isotropic plates. *Proceedings of the Royal Society of London A: Mathematical, Physical and Engineering Sciences*, **472**, 20160410.

Dieterman H.A., Metrikine A. (1996). The equivalent stiffness of a half-space interacting with a beam. Critical velocities of a moving load along the beam. *European Journal of Mechanics, A/Solids*, **15**, 67–90.

Dockrey, J.A., Lockyear, M.J., Berry, S.J., Horsley, S.A.R., Sambles, J.R., & Hibbins A.P. (2013). Thin metamaterial Luneburg lens for surface waves. *Physical Review B*, **87**, 125137.

Dowaikh, M.A., & Ogden, R.W. (1990). On surface waves and deformations in a pre-stressed incompressible elastic solid. *IMA Journal of Applied Mathematics*, **44**, 261–284.

Dowaikh, M.A., & Ogden, R.W. (1991). Interfacial waves and deformations in pre-stressed elastic media. *Proceedings of the Royal Society London Series A*, **433**, 313–328.

Ege, N., Erbas, B., & Prikazchikov, D.A.(2015). On the 3D Rayleigh wave field on an elastic half-space subject to tangential surface loads. *Zeitschrift für Angewandte Mathematik und Mechanik*, **95**, 1558-1565.

Erbaş, B., Kaplunov, J., & Prikazchikov, D.A. (2013). The Rayleigh wave field in mixed problems for a half-plane. *IMA Journal of Applied Mathematics*, **78**, 1078–1086.

Erbaş, B., Kaplunov, J., Prikazchikov, D.A., & Şahin, O. (2014). The near-resonant regimes of a moving load in a 3D problem for a coated elastic half space. *Mathematics and Mechanics of Solids*, doi: 10.1177/1081286514555451.

Erbaş, B., & Şahin, O. (2016). On causality of the Rayleigh wave. *Journal of Mechanics of Materials and Structures*, **11(4)**, 449–461.

Erdelyi, A., Magnus, W., Oberhettinger, F., & Tricomi, F. G. (1954). *Table of Integral Transforms, Vol. II.* McGraw-Hill, New York.

Eshelby, J. D. (1949). Uniformly moving dislocations. *Proceedings of the Physical Society. Section A*, **62**(5), 307–314.

Fu, Y.B. (2003). Existence and uniqueness of edge waves in a generally anisotropic elastic plate. *Quarterly Journal of Mechanics and Applied Mathematics*, **56**, 605–616.

Fu, Y.B., & Mielke, A. (2002). A new identity for the surface-impedance matrix and its application to the determination of surface-wave speeds. *Proceedings of the Royal Society London Series A*, **458**, 2523-2543.

Freund, L.B. (1990). *Dynamic fracture mechanics*. Cambridge University Press, Cambridge.

Friedlander, F.G. (1948). On the total reflection of plane waves. *Quarterly Journal of Mechanics and Applied Mathematics*, **1**, 376–384.

Georgiadis H.G., Lykotrafitis G. (2001). A method based on the Radon transform for three-dimensional elastodynamic problems of moving loads. *Journal of Elasticity*, **65**, 87-129.

Goda, M.A.A. (1992). The effect of inhomogeneity and anisotropy on Stoneley waves. *Acta Mechanica*, **93**, 89–98.

Gogoladze, V.G. (1948). Rayleigh waves on the interface between a compressible fluid medium and a solid elastic half-space. *Trudy Seismologicheskogo Instituta Academii Nauk USSR*, **127**, 27–32.

Goldstein R.V. (1965). Rayleigh waves and resonance phenomena in elastic bodies. *Journal of Applied Mathematics and Mechanics (PMM)* **29**, 516–525.

Gudra, T., & Stawiski, B. (2000). Non-destructive strength characterization of concrete using surface waves. *NDT&E International*, **33**, 1–6.

Gulyaev, Y.V. (1969). Electroacoustic surface waves in solids. *JETP Letters*, **9**, 37–38.

Hayes, M.A., & Rivlin, R.S. (1961). Surface waves in deformed elastic materials. *Archive for Rational Mechanics and Analysis*, **8**, 358–380.

Ishlinsky, A.Yu. (1954). A particular limit transition in the theory of the stability of rectangular elastic plates. *Doklady AN USSR*, **95**, 477–479.

Ivanov, T.P. (1988). On the propagation of thermoelastic Rayleigh waves. *Wave Motion*, **10**, 73–82.

Kamotskii, I.V., & Kiselev, A.P. (2009). An energy approach to the proof of the existence of Rayleigh waves in an anisotropic elastic half-space. *Journal of Applied Mathematics and Mechanics*, **73(4)**, 464–470.

Kaplunov J. (1986). *Transient dynamics of an elastic half-plane subject to a moving load.* Preprint No. 277, Institute for Problems in Mechanics. Moscow.

Kaplunov, J.D. & Kossovich, L.Y. (2004) Asymptotic model of Rayleigh waves in the far-field zone in an elastic half-plane. *Doklady Physics*, **49**, 234–236.

Kaplunov, J.D., Kossovich, L.Y., Nolde, E.V. (1998). *Dynamics of thin walled elastic bodies.* Academic Press, San-Diego.

Kaplunov, J., Kossovich, L., & Zakharov, A. (2004). An explicit asymptotic model for the Bleustein-Gulyaev wave. *Comptes Rendus Mecanique*, **332**, 487492.

Kaplunov, J., & Nobili, A. (2015). The edge waves on a Kirchhoff plate bilaterally supported by a two-parameter elastic foundation. *Journal of Vibration and Control*, 1077546315606838.

Kaplunov J., Nolde E., Prikazchikov D.A.(2010). A revisit to the moving load problem using an asymptotic model for the Rayleigh wave. *Wave Motion*, **47**, 440–451.

Kaplunov, J.D., Nolde, E.V., Rogerson, G.A. (2000). A low-frequency model for dynamic motion in pre-stressed incompressible elastic structures. *Proceedings of the Royal Society London Series A*, **456**, 2589–2610.

Kaplunov, J., & Prikazchikov, D.A.(2013). Explicit models for surface, interfacial and edge waves in elastic solids. In *Dynamic localization phenomena in elasticity, acoustics and electromagnetism* (Eds. R.V. Craster & J. Kaplunov) *CISM International Centre for Mechanical Sciences*, **547**, 73–114, Springer-Verlag Wien.

Kaplunov, J., Prikazchikov, D.A., Erbaş, B., & Şahin, O. (2013). On a 3D moving load problem for an elastic half-space. *Wave Motion*, **50**, 1229–1238.

Kaplunov, J., Prikazchikov, D.A., & Rogerson, G.A. (2005). On three-dimensional edge waves in semi-infinite isotropic plates subject to mixed face boundary conditions. *Journal of Acoustical Society of America*, **118**, 2975–2983.

Kaplunov, J., Prikazchikov, D.A., & Rogerson, G.A. (2016). Edge bending wave on a thin elastic plate resting on a Winkler foundation. *Proceedings of the Royal Society of London A: Mathematical, Physical and Engineering Sciences*, **472**, 20160178.

Kaplunov, J., Prikazchikov, D.A., Rogerson, G.A., & Lashab, M.I. (2014). The edge wave on an elastically supported Kirchhoff plate. *Journal of the Acoustical Society of America*, **136**, 1487-1490.

Kaplunov, J., Prikazchikov, D.A., & Zakharov, A. (2006). Explicit models for elastic and piezoelastic surface waves. *IMA Journal of Applied Mathematics*, **71**, 768–782.

Kiselev, A.P. (2004). Rayleigh wave with transverse structure. *Proceedings of the Royal Society London Series A*, **460**, 3059–3064.

Kiselev, A.P. (2015). General surface waves in layered anisotropic elastic structures. *Zapiski Nauchnyh Seminarov POMI*, **438**, 133–137.

Kiselev, A.P., & Parker, D.F. (2010). Omni-directional Rayleigh, Stoneley and Scholte waves with general time dependence. *Proceedings of the Royal Society London Series A*, **466**, 2241-2258.

Kiselev, A.P., & Rogerson, G.A. (2009). Laterally dependent surface waves in an elastic medium with a general depth dependence. *Wave Motion*, **46**, 539-547.

Konenkov, Yu.K. (1960) A Rayleigh-type flexural wave. *Soviet Physics Acoustics* **6**, 122-123.

Kossovich E. (2011). Explicit models for flexural edge and interfacial waves in thin elastic plates. *PhD thesis, Brunel University, UK.*

Kryshynska, A.A. (2011). Flexural edge waves in semi-infinite elastic plates. *Journal of Sound and Vibration*, **330**, 1964–1976.

Lamb, H. (1904). On the propagation of tremors over the surface of an elastic solid. *Philosophical Transactions of the Royal Society of London. Series A*, **203**, 1–42.

Lawrie, J.B., & Kaplunov, J. (2012). Edge waves and resonance on elastic structures: an overview. *Mathematics and Mechanics of Solids*, **17**, 4–16.

Lord Rayleigh (1885). On waves propagated along the plane surface of an elastic solid. *Proceedings of the London Mathematical Society*, **17**, 4–11.

Madshus C., Kaynia A.M. (2000). High-speed railway lines on soft ground: dynamic behaviour at critical train speed. *Journal of Sound and Vibration*, **231**, 689–701.

Malischewsky, P. (2000). Comment to 'A new formula for velocity of Rayleigh waves' by D. Nkemzi [Wave Motion 26 (1997) 199-205]. *Wave Motion*, **31**, 93-96.

Miklowitz, J. (1978). *Elastic waves and waveguides.* North-Holland, Amsterdam, the Netherlands.

Morrissey, J. W., & Rice, J. R. (1998). Crack front waves. *Journal of the Mechanics and Physics of Solids*, **46**(3), 467–487.

Nayfeh, A.H. (2000). *Perturbation methods.* John Wiley & Sons, New York.

Norris, A.N. (1994). Bending edge waves. *Journal of Sound and Vibration*, **174**, 571–573.

Norris, A. N., & Abrahams, I. D. (2007). A multiple-scales approach to crack-front waves. *Journal of Engineering Mathematics*, **59**(4), 399-417.

Norris, A.N., Krylov, V.V., & Abrahams, I.D. (2000). Bending edge waves and comments on 'A new bending wave solution for the classical plate equation'. *Journal of the Acoustical Society of America*, **107**, 1781-1784.

Parker, D.F. & Kiselev, A.P. (2009). Rayleigh waves having generalised lateral dependence. *Quarterly Journal of Mechanics and Applied Mathematics*, **62**, 19–29.

Parker, D.F. (2012). Evanescent Schölte waves of arbitrary profile and direction. *European Journal of Applied Mathematics*, **23**, 267–287.

Parker, D.F. (2013). The Stroh formalism for elastic surface waves of general profile. *Proceedings of the Royal Society London Series A*, **469**, 20130301.

Pichugin, A.V., & Rogerson, G.A. (2012). Extensional edge waves in pre-stressed incompressible plates. *Mathematics and Mechanics of Solids*, **17**, 27–42

Polyanin, A.D. (2002). *Handbook of linear partial differential equations for engineers and scientists.* CRC Press, Boca Raton London.

Prikazchikov, D.A. (2013). Rayleigh waves of arbitrary profile in anisotropic media. *Mechanics Research Communications*, **50**, 83–86.

Prudnikov, A.P., Brichkov, Y.A., & Marichev, O.I. (1986). *Integrals and series.* New York, Gordon & Breach.

Rogerson, G.A. (1998). On the existence of surface waves and the propagation of plate waves in pre-stressed fibre-reinforced composites. *Journal of Mechanics and Physics of Solids*, **46**, 1581-1612.

Rousseau, M., & Maugin, G.A. (2011). Rayleigh surface waves and their canonically associated quasi-particles. *Proceedings of the Royal Society London Series A*, **467**, 495-507.

Royer, D., Dieulesaint, E. (1996). *Elastic waves in solids. Volume II.* Springer, Berlin.

Schölte, J.G. (1947). The range of existence of Rayleigh and Stoneley waves. *Geophysical Journal International* **5**, 120–126.

Schölte, J.G. (1949). On true and pseudo Rayleigh waves. *Proceedings of Koninklijke Nederlandse Akademie van Wetenschappen Series-B*, **52**, 652–653.

Steigmann, D.J., & Ogden, R.W. (2007). Surface waves supported by thin-film/substrate interactions. *IMA Journal of Applied Mathematics*, **72**, 730-747.

Stoneley, R. (1924). Elastic waves at the surface of separation of two solids. *Proceedings of the Royal Society London Series A*, **106**, 416-428.

Sobolev, S. L. (1937). Some problems in wave propagation. In *Differential and integral equations of mathematical physics*, (Eds. Frank P., von Mises R.). ONTI, Moscow-Leningrad, 468–617. (in Russian)

Sveshnikov, A. G. & Tikhonov, A. N. (2005). *The theory of functions of a complex variable.* Phyzmatlit, Moscow, Russia.

Thompson, I., Abrahams, I.D., & Norris, A.N. (2002). On the existence of flexural edge waves on thin orthotropic plates. *Journal of the Acoustical Society of America*, **112**, 1756-1765.

Timoshenko, S.P. (1927). Method of analysis of statical and dynamical stresses in rail. *Proceedings of the Second International Congress of Applied Mechanics, Zurich, September 1926*, Orell Fössli Verlag, 1–12.

Titchmarch, E.C. (1939). *The theory of functions.* Oxford University Press, Oxford, UK.

Viktorov, I.A. (1981). *Surface acoustic waves in solids.* Nauka, Moscow (in Russian).

Vinh, C.V., Anh, V.T.N., & Thanh, V.P. (2014). Rayleigh waves in an isotropic elastic halfspace coated by a thin isotropic elastic layer with smooth contact. *Wave Motion*, **51**, 496-504.

Vinh, C.V., & Ogden, R.W. (2004). On formulas for the Rayleigh wave speed. *Wave Motion*, **39**, 191-197.

Vinh, C.V., & Seriani, G. (2010). Explicit secular equations of Stoneley waves in a non-homogeneous orthotropic elastic medium under the influence of gravity. *Applied Mathematics and Computation*, **215**, 3515–3525.

Willis, J. R., & Movchan, A. B. (1995). Dynamic weight functions for a moving crack. I. Mode I loading. *Journal of the Mechanics and Physics of Solids*, **43**(3), 319–341.

Yoffe, E. H. (1951). LXXV. The moving Griffith crack. *The London, Edinburgh, and Dublin Philosophical Magazine and Journal of Science*, **42**(330), 739–750.

Zakharov, D.D. (2004). Analysis of the acoustical edge bending mode in a plate using refined asymptotics. *Journal of the Acoustical Society of America*, **116**, 872–878.

Zernov, V., & Kaplunov, J. (2008). Three dimensional edge-waves in plates. *Proceedings of the Royal Society London A*, **464**, 301–318.

Zhu, J., Popovics, J.S., & Schubert, F. (2004). Leaky Rayleigh and Schölte waves at the fluidsolid interface subjected to transient point loading. *Journal of the Acoustical Society of America*, **116**, 2101-2110.